Progress in Polymer Science 122 (2021) 101451

Contents lists available at ScienceDirect

Progress in Polymer Science

journal homepage: www.elsevier.com/locate/progpolymsci

Polyamide desalination membranes: Formation, structure, and properties

Viatcheslav Freger[a,c,1,*], Guy Z. Ramon[a,b,c,2]

[a] Wolfson Department of Chemical Engineering, Technion – Israel Institute of Technology, Haifa, Israel
[b] Department of Civil and Environmental Engineering, Technion – Israel Institute of Technology, Haifa, Israel
[c] Grand Water Research Institute, Technion - Israel Institute of Technology, Haifa, Israel

ARTICLE INFO

Article history:
Received 31 December 2020
Revised 17 May 2021
Accepted 27 August 2021
Available online 5 September 2021

Keywords:
Polyamide desalination membranes
Interfacial polymerization
Thin-film formation
Polyamide morphology
Structure-performance relations
Fully aromatic and semiaromatic membranes

ABSTRACT

Empirical discovery, four decades ago, of polyamide membranes made by interfacial polymerization revolutionized large-scale desalination and has made desalinated water affordable to millions of people worldwide. The path to better understanding of the exceptional performance exhibited by these polymeric films, critical for rational membrane design and the search for alternative materials, begins from understanding their formation and the resultantmolecular and nanostructure and has posed numerous questions. The self-limited, ultra-small thickness, irregular multiscale nanostructure, and the need for polyamide films to be formed on a support rather than in a bulk process pose formidable challenges for structural characterization and molecular modeling. Further challenges arise from insufficient understanding of the relations between polymer chemistry, multi-scale structure, and their impact on transport and mechanical characteristics. Extensive research conducted over the last decades, using dedicated experimental and theoretical approaches, have highlighted many remarkable features of polyamide thin films, and yet many questions still await conclusive answers.

The present paper reviews the current state of understanding of polyamide thin films, and, in particular, fully and semi-aromatic "winner" chemistries used for membrane separation, based on recent advances in the nanoscale characterization and theoretical investigations of their formation, chemistry, structure, morphology and barrier characteristics down to the molecular scale. These are reviewed in light of the recent developments in understanding of the interfacial polymerization process, reaction, packing and crosslinking of polymeric building blocks, formation and distribution of charge groups, and interaction of the resultant polymer network with water and ions. The proposed unified picture that links the emerging picture of the multiscale nano- and molecular structure of polyamide thin films with macro-scale characteristics, enables a consistent rationalization of their superior barrier characteristics. Furthermore, such a framework provides insight on inherent weaknesses of polyamides and the challenges of overcoming these limitations and developing viable alternatives. With membranes fast becoming the choice for a growing number of challenging separations, and with the need to replace current materials with sustainable, environmentally benign alternatives, drawing on established knowledge will provide a solid foundation from which better controlled, tunable membranes can be fabricated from next-generation building blocks.

1. Introduction and problem statement

1.1. Thin-film composites prepared by IP: a key breakthrough in membrane desalination

Since their inception in the late 70s, polyamide membranes prepared by interfacial polymerization (IP) have been a key factor in the rapid growth of desalination technology [1,2]. The invention of thin-film composite (TFC) membranes and the discovery of the unique performance of fully-aromatic polyamide by Cadotte and coworkers brought about a major breakthrough that achieved

* Corresponding author.
E-mail addresses: vfreger@technion.ac.il (V. Freger), ramong@technion.ac.il (G.Z. Ramon).
[1] OCRCID for: 0000-0001-8067-052X.
[2] ORCID for: 0000-0002-0711-0654.

https://doi.org/10.1016/j.progpolymsci.2021.101451
0079-6700/

List of symbols and abbreviations

ATR	attenuated total reflection
AFM	atomic force spectroscopy
BW	brackish-water
DMSO	dimethylsulfoxide
EDS	energy dispersive spectroscopy
EELS	electron energy loss spectroscopy
EIS	electro-chemical Impedance Spectroscopy
FTIR	fourier-transformed infra-red
HAADF	high-angle annular dark-field
IP	interfacial polymerization
MD	molecular dynamics
MPD	*m*-phenylene diamine
NF	nanofiltration
OCT	optical coherence tomography
PALS	positron annihilation spectroscopy
QCM	quartz-crystal microbalance
QENS	quasi elastic neutron scattering
RBS	Rutherford back-scattering
RMS	root-mean squared
RO	reverse osmosis
SEM	scanning electron microscopy
STEM	scanning transmission electron microscopy
SW	seawater
TEM	transmission electron microscopy
TFC	thin-film composite
TMC	trimesoyl chloride
XPS	X-ray photoelectron spectroscopy

Latin letters

A	membrane water permeance [m/s·Pa]
b	geometric prefactor
B	membrane salt permeance [m/s]
C	concentration [mol/m^3]
D	diffusion coefficient [m^2/s]
G	Aerial conductivity
h	solution layer thickness
ΔH	Enthalpy of reaction [J/mol]
J	molar flux [mol/m^{2}s]
k	reaction rate constant [1/s]
L	boundary layer thickness [m]
L_p	membrane water permeance [m/s·Pa]
Ma	Marangoni number [-]
r_p	pore radius
R	universal gas constant [J/mol·K]
V_M	molecular volume [m^3]
V_w	water molar volume [m^3]
t	time [s]
T	Temperature [$^\circ$C]

Greek letters

α	tortuosity [-]
δ	thickness (membrane, film) [m]
ε	strain [-]
ϕ	porosity [-]
Φ	water fraction [-]
λ	wavelength [m]
μ	viscosity [Pa·s]
σ	surface tension [N/m]

Sub- and super-scripts

0	bulk or initial value
c	concentration dependent coefficient
T	temperature dependent coefficient

>99% salt rejection in seawater (SW) desalination by reverse osmosis (RO) and concluded a two decade-long effort to surpass the cellulosic membranes introduced in the late 50s by Loeb and Sourirajan [2,3]. While cellulosic membranes were so-called 'integrally-skinned' asymmetric membranes, fabricated using a single phase-inversion step, TFC membranes comprised a selective layer added on top of a separately fabricated porous support [4], as schematically shown in Fig. 1. The immense success of polyamide TFC membranes is partly due to the very concept of a composite – offering the potential to separately optimize each layer – but mostly due to the serendipitous ability to form robust, ultra-thin films of polyamide via IP. Owing to the exceptional performance, along with facile and readily up-scalable manufacturing, polyamide composites rapidly surpassed their cellulosic counterparts in most RO applications [3,5,6], while also demonstrating great potential for other applications such as organic molecule separations [7,8] and gas separation [9].

Following the success of fully-aromatic polyamide membranes came the early realization that the complete removal of all salts is not necessary in all applications. For example, water softening or removal of humic substances or colors mainly require high water permeability and hardness retention, while NaCl rejection may be low. These applications paved the way for the development of another family of polyamide composites - semi-aromatic nanofiltration (NF) membranes that offer an order-of-magnitude higher water permeability, but much lower salt rejection [3,4,11].

To date, several industrial companies have successfully developed a line of polyamide-based products with a wide range of separation capabilities, normally defined by two parameters: the water permeance A (or L_p) and the salt (NaCl) rejection. The latter is an operational parameter, a combination of the permeate flux and the solute permeance B (or ω_s) and so the membrane is better characterized by its selectivity, A/B, i.e., the ratio of solvent and solute permeances [4,12–14]. These properties vary widely, from NF membranes with ~20% NaCl rejection (but often with high rejection, >98%, of di-valent anions) and ultra-high permeance, $A > 2 \times 10^{-11}$ m s^{-1} Pa^{-1}, up to the tightest SW RO grades (rejection >99.7% and permeance of $<7 \times 10^{-12}$ m s^{-1} Pa^{-1}), as well as intermediate brackish-water (BW) and energy-saving (low-pressure) RO grades [6,14].

1.2. IP-based membranes and their chemistry: inception and development

The remarkable breakthrough achieved by Cadotte and co-workers was both preceded and followed by numerous efforts to prepare membranes via the IP process, which was first conceived by Morgan and Kwolek [15,16]. The IP process may involve various condensation chemistries, most commonly polyamides, polyureas, polyurethanes, polyesters, polycarbonates, and polysulfonamides; interfacial synthesis using addition polymers is also possible [15,17,18]. Fig. 2 shows several representative chemistries explored as candidate membrane materials. We note that the use of IP for the fabrication of thin barriers is not limited to separation membranes and has been used extensively for encapsulating drugs, biochemicals, food products, and catalysts [18–21]. For making membranes or selective films in general, IP is a viable alternative to other coating methods, offering several truly remarkable features, such as [1,3,22]:

(1) self-limiting kinetics, which considerably slow down the growth of film thickness in a self-controlled manner, yielding ultra-thin films;
(2) self-healing nature of the process that tends to direct the reaction to the most permeable spots (potential defects), seal-

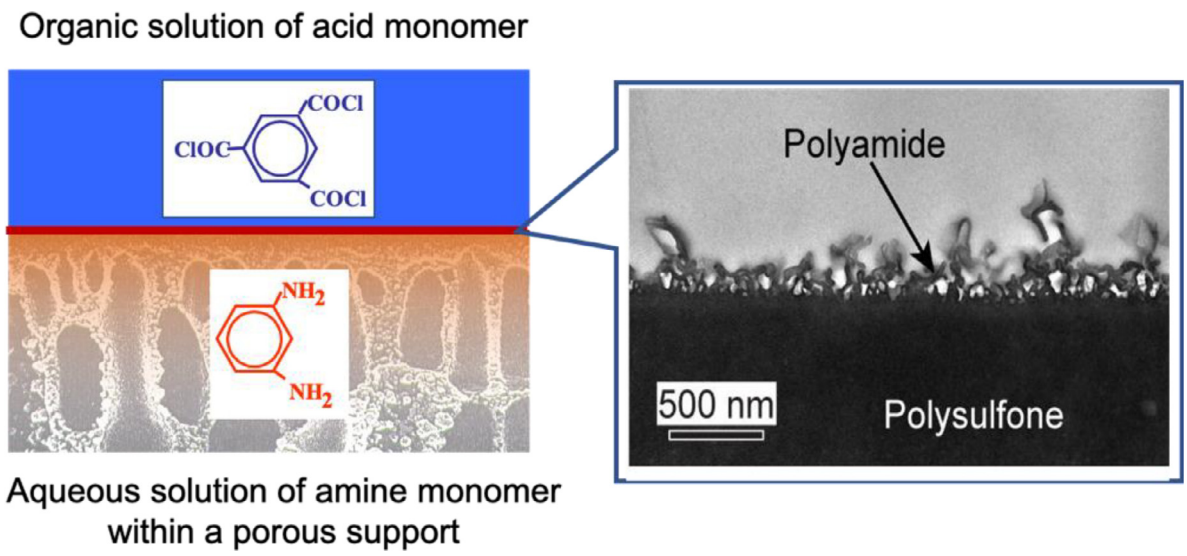

Fig. 1. *A schematic view of thin film composites membranes prepared via interfacial polymerization and a TEM cross-section image showing the morphology of a polyamide active layer on top of a porous polysulfone support. TEM image.* [10]*, Copyright 2010. Adapted with permission from Elsevier Science Ltd.*

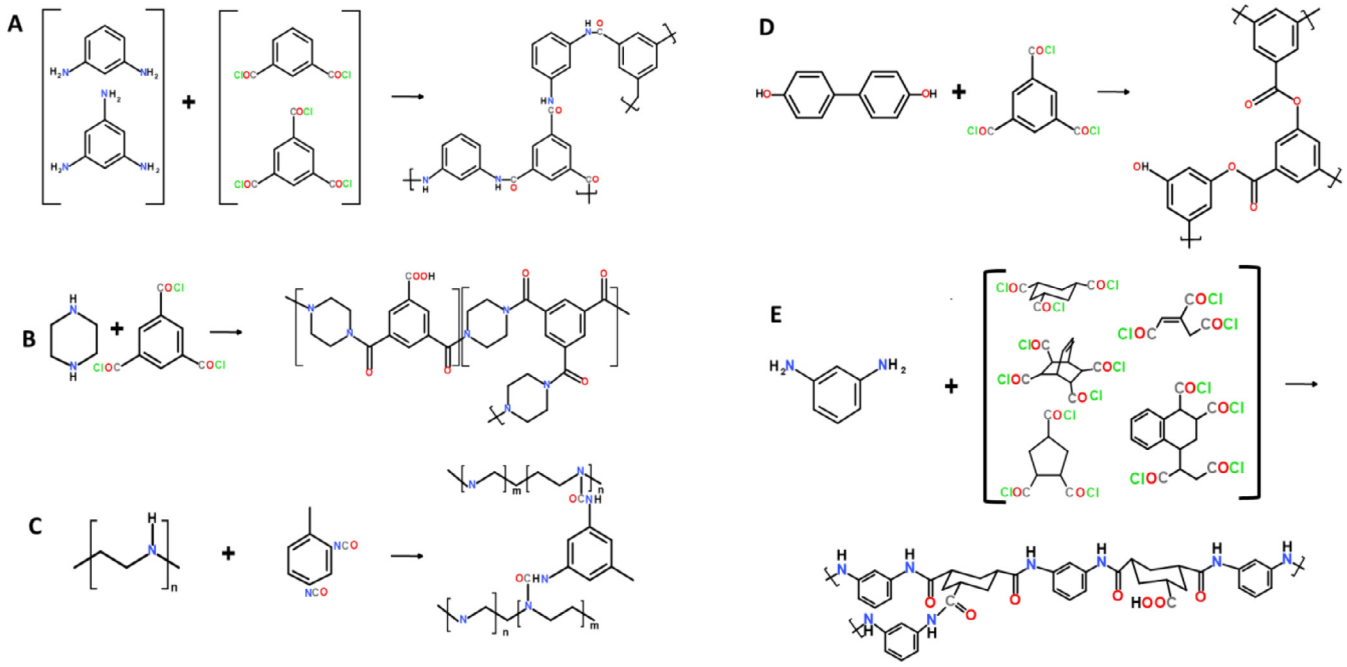

Fig. 2. *Representative IP chemistries of TFC membranes: (A) Fully-aromatic polyamide employed in most commercial RO membranes; (B) Semi-aromatic polyamides employed in many commercial NF membranes; (C) Interfacial poly(ethylene imine) cross-linking with a diisocyanate* [24]*; (D) Interfacial polycondensation yielding a polyester membrane* [25]*; (E) Alternative semi-aromatic polyamides reported by Arthur et al.* [26,27] *and by Hirose* [28]*. The shown resulting polymer is obtained from the first triacid monomer in brackets, cyclohexane tricarboxylic acid chloride.*

ing them and producing films with an exceptionally low defect rate;

(3) *in-situ* polymer crosslinking through use of multifunctional monomers, resulting in mechanically robust films with tunable barrier properties.

Excellent accounts of early membrane development, given by Petersen [3] as well as by Linder and Kedem [23], present numerous examples of IP-based chemistries examined as candidates for making RO and NF membranes. A substantial part of these candidate systems employed di- or tri-functional amines (see Fig. 2A,B and E) and polyamine (Fig. 2C) precursors such as poly(ethylene imine), poly(vinyl amine) or polyepiamine, which were interfacially cross-linked with di-isocynates or diacid chlorides to yield, respectively, polyurea or polyamide films. Polyester chemistries were also considered, where poly (vinyl alcohol) was used or blended with polyamines for interfacial reactions. Aromatic polyester, in which diphenols replaced alcohol monomers (Fig. 2D), as well as polyurea (Fig. 2C) and other chemistries were revisited much later [24,25]; however, from quite early on, the majority of research focused on polyamides as the most promising candidates. Another line of examined systems employed polyamides based on different monomeric acid precursors with three or more acid chloride groups (Fig. 2E). Many such examples, predominantly coming from industrial research in the pre-80s era, are presented in Petersen's review [3]. Papers by Arthur et al. [26,27] and by Hirose [28] offer a further glimpse into research directions pursued by major

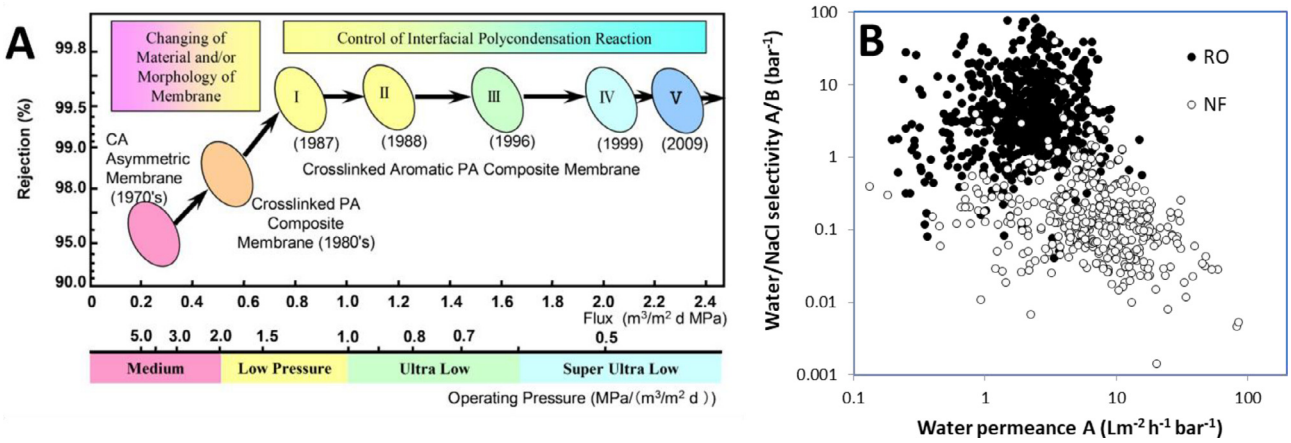

Fig. 3. *(A) Timeline of commercial membrane development and different classes of RO membranes based on permeance and salt rejection, after Kurihara and Sasaki [6], Copyright 2017. Reproduced with permission from Farnood Institute of Membrane Technology (FIMTEC) and Membrane Processes Research Laboratory (MPRL); (B) The correlation between reported water permeability and water/salt selectivity for commercial RO and NF polyamide membranes, from Yang et al. [14], Copyright 2019. Reproduced with permission from Elsevier Science Ltd. Data are kindly provided by Chuyang Tang.*

industrial players DuPont and Nitto Denko in the 80s and 90s. These accounts tell a fascinating story of trials-and-errors and rationales, e.g., considerations of molecular architecture, functionality and packing, that gradually emerged from this largely empirical effort. It seems, however, that following the widespread adoption of fully aromatic and semi-aromatic polyamide chemistries (Fig. 2A and B, see the next section), the membrane industry downscaled the search for new materials and approaches and, at present, these efforts continue mainly as academic research.

1.3. Fully aromatic and semi-aromatic polyamides: the "winner" chemistries

The first "winner" chemistry discovered by Cadotte and coworkers was based on interfacial condensation of aromatic trimesoyl chloride (TMC) and *m*-phenylene diamine (MPD), yielding fully aromatic polyamide membranes [2] (Fig. 2A). Notwithstanding an element of serendipity, this discovery was a logical outcome of a long and extensive effort that included not only scouting across a host of possible IP reactions, but also development of other technological components, such as supporting asymmetric porous polysulfone membranes and spiral-wound elements [4]. The resulting prototypes - culminating in Filmtec's celebrated FT-30 membrane - reached the performance that eventually led to commercially viable SW RO technology that became a global success within the next two decades.

Notably, at the time of invention, the membrane's performance was not exceptional and some previously invented candidates showed commensurate and even superior fluxes and selectivity; yet - except for chlorine resistance - the new membrane was remarkably robust, stable and easy to prepare and upscale [3]. Over the past four decades, its superiority in seawater desalination has remained unchallenged and subsequent improvements were mainly achieved through optimization and tuning of the manufacturing procedures and synthesis conditions to specific needs, e.g., for treating low salinity and brackish waters [5,6,29]. Fig. 3A illustrates the progress and growing diversity of desalination membranes during the last five decades [6].

Cadotte's group also developed another important IP-based system, in which MPD was replaced with an aliphatic diamine, piperazine, and reacted with TMC or a mixture of TMC with its difunctional analogue isophthaloyl chloride, yielding a film with markedly different characteristics [30] (Fig. 2B). The salt rejection of this semi-aromatic membrane was too low for SW RO desalination, which was the primary target, therefore its application potential was only realized years later, with the emergence of NF as another commercially viable process. The key factor was the high water permeance of NF membranes that allowed purification of low-salinity streams (e.g., softening and decoloring of drinking water) at significantly reduced cost and energy consumption, compared to RO membranes [3,11].

The two "winner" chemistries mentioned above, with some modifications, make up the majority of today's commercial RO and NF products, in which they form either the selective top layer or the key sublayer, when the membranes include extra layers, e.g., an antifouling coating [31]. However, despite their widespread industrial use, and following decades of extensive research, these membranes still pose a number of challenging questions, keeping them at the focus of ongoing research. For example, one of the key questions revolves around the unrivaled performance of fully-aromatic polyamides, its relation to molecular structure and nanoscale morphology as well as formation and manipulation via synthesis conditions and post-treatment [32]. Fig. 3B displays the reported performance characteristics for hundreds of polyamide membranes, of nominally the same chemistry. The data suggest a certain average permeability and selectivity (defined as ratio of water and salt permeabilities A/B), as well as a possible upper bound of selectivity-permeability tradeoff [14]. However, the large observed variations and the lack of overall correlation between permeability and selectivity indicate a vast playground for further tuning performance via subtle and poorly understood differences in the membrane structure and chemistry. Fig. 3B shows a fairly similar situation for NF membranes.

Various modern microscopic and spectroscopic tools, as well as theoretical modeling of the IP process, reveal a formidably complex picture and hierarchy of structures spanning molecular to micron scales. It is generally agreed that in-depth understanding of these points, which goes in parallel with the effort to unravel the physics of solute selectivity in RO and NF, is critical for further development of desalination and water purification technologies. This is also expected to facilitate the development of alternative materials, which would overcome inherent weaknesses of polyamides, such as low resistance to chlorine and insufficient rejection of certain micropollutants such as boron or persistent organic molecules. This review presents the current level of understanding of polyamide membranes, in which different pieces gradually come together towards completing this fascinating puzzle.

2. Polymerization mechanism and thin-film formation: theory and experiments

2.1. IP process: effect of parameters and chemistry on film characteristics

The IP process is most commonly based on a polycondensation reaction of two polyfunctional monomers, separately dissolved in immiscible solvents, thereby the reaction occurs at the interface between the two liquid phases (see schematic drawing in Fig. 1). Among many other types of reactions amenable to interfacial polycondensation and polymerization (polyesters, polyureas, polyurethanes etc. [17,18]), formation of polyamide (Nylon) films is by far the best known, typically involving a difunctional, hydrophobic acyl chloride and a hydrophilic diamine or analogous monomers of higher functionality (see examples in Fig. 2). The amine is placed in an aqueous solution, whereas acyl chloride is dissolved in a hydrophobic organic solvent such as hexane, immiscible with water.

In the conventional preparation of polyamide TFC membranes, the aqueous phase is soaked into a porous support (a UF-like membrane typically made of polysulfone or polyethersulfone, see schematic in Fig. 1) and subsequently contacted with the organic phase, such that the film is fabricated in a way that intrinsically provides it mechanical support. The reaction may also be carried out without a supporting membrane, at the interface between free aqueous and organic liquid layers. This configuration, used in Morgan's original demonstration, produces free-standing films that proved useful in some recent studies (see, for example, [33]). For research purposes, IP has also been carried out at a stabilized liquid-liquid interface, e.g. a single droplet of one of the phases surrounded by the other phase, in a pendant-drop goniometer or a microfluidic setup [34–39]. Such configurations allow fast optical and/or mechanical monitoring of the film formation, useful for studying IP kinetics (see Section 2.2 for a more in-depth discussion of these aspects). Finally, outside of the realm of separation membranes, IP can be carried out around dispersed droplets in emulsified two-phase systems, resulting in shell-like structures employed for encapsulation and controlled release of drugs, agrochemicals, enzymes, bacterial cells, etc. [19,20,40–42].

In order to diffuse and react with its counterpart, a monomer first has to partition into the opposite phase. Since the solubility of the two monomers in the opposite phases is usually asymmetric, the reaction occurs in the phase that more readily dissolves both monomers. For example, in Nylon synthesis, diamines more readily partition into hexane than diacyl chlorides do in in water, thereby the reaction occurs and the film forms at the organic side of the interface [15,22,43]. There are some exceptions to this rule; for example, polymeric amine reactants, such as poly (ethylene imine) (Fig. 2C), are hardly soluble in the hydrophobic organic solvents, thereby the reaction occurs in close vicinity of the interface, possibly, at the aqueous side [42,44].

An important requirement for successful film formation via IP is that the reaction between the monomers occurs rapidly and irreversibly, otherwise it would not be limited to the interfacial region and the polymer would form a homogeneous solution or dispersion rather than a thin film [22]. Faster-reacting monomers tends to produce thinner films; for example, poly(piperazine amide) membranes have the thinnest active layer of all commercial polyamide TFCs, only 15–20 nm thick [45], consistent with the exceptionally high reactivity of piperazine with acyl chlorides, $\sim 10^4$-10^6 L mol^{-1} s^{-1} [46].

Apart from polymer chemistry, IP synthesis offers many other pathways for optimizing film characteristics and film thickness via manipulation of monomer transport and reaction. One variable is the monomer concentrations in the two phases. The overall effect appears to be fairly complex, since increasing concentration may either increase or decrease film thickness. Larger concentrations drive faster diffusion across the film and so faster film growth, however, this also increases the reaction rate which reduces the initial film thickness (see Section 2.3). For example, when preparing aromatic polyamide membranes using the TMC-MPD reaction, the optimal composition was found to be about 0.1% of TMC in hexane and 2% MPD in water [1]. It must be stressed that the higher concentration of MPD in the aqueous phase is not indicative of the actual TMC:MPD ratio in the IP reaction, which takes place in the hexane phase, where the MPD concentration is much lower (see Section 2.3).

The nature of the solvent also plays an important role in controlling the film characteristics, as it affects monomer solubility, diffusivity, and reaction rates. For polyamide synthesis, a more polar organic solvent usually increases both amine solubility and reactivity. Accordingly, adding chloroform, a more polar solvent, to the hydrocarbon solvent phase for encapsulation was shown t to increase film permeability [41]. Although chloroform addition would not suit TFC membranes, as this would damage the polysulfone support, other additives have been proposed in the context of aromatic polyamide RO membranes. Addition of water-soluble co-solvents such as acetone or dimethylsulfoxide (DMSO) was found to steadily increase the membrane permeance. Remarkably, they may be added to either phase with a similar effect [29,47,48]. Presumably, the co-solvent diffusing to the organic phase along with diamine enhances its solubility and accelerates its reaction with acyl chloride, which should modify film morphology and thus its effective thickness or permeation area. The solvent viscosity may also significantly affect the ultimate film characteristics, since higher viscosity is expected to slow down the monomer diffusion. Thus, replacing hexane with isopar G (five times more viscous) substantially increased the membrane permeance [49].

Monomer functionality was identified as another key factor in controlling film characteristics. Thus, difunctional amine and diacid chloride should form a linear, non-crosslinked polymer that may pack or crystallize more readily and form a uniform, dense film. However, in absence of a cross-linker, such a film would also swell substantially, which may reduce its selectivity and, moreover, allow easier monomer diffusion and faster growth during IP , resulting in a thicker film with a lower permeance [50]. Increasing monomer functionality is a facile way to induce *in-situ* crosslinking in the polymer and thus modify its barrier characteristics. Hence, polyamide membranes are usually prepared through the reaction of a diamine, MPD or piperazine, and a *tri*functional acyl chloride, TMC. Curiously, the acid functionality does not need to increase all the way from 2 to 3, as a fractional functionality, obtained by mixing 25–75% diacid chloride (isophthaloyl chloride) with TMC, produces films with characteristics nearly identical to 100% TMC [51].

Table 1 summarizes the major synthesis variables and their effect on the reaction, diffusion and solution thermodynamics that control the IP process and resultantant polyamide film characteristics. These effects and corresponding changes in permeability point to systematic morphological changes, whose nature we will clarify below. The model presented in Section 2.3 offers a simplified picture that facilitates understanding of the above-mentioned and other effects, quantitative relations between different parameters as well as experimentally observed IP kinetics (Section 2.2). Subsequently, this picture is extended to include more complex effects, particularly various inherent instabilities responsible for the observed irregular and diverse morphology of the polyamide layer.

Table 1
The effects of synthesis parameters on the IP process and film formation, with some representative references of papers examining these effects (the reader is also referred to Yang et al. [14] for more examples).

Parameter variation	Effect	Example References
Monomer/polymer type	Reaction kinetics and enthalpy; monomer diffusivity; amine partitioning; monomer permeability in the polymer film	[52–59]
Monomer concentration	rate of reaction vs. rate of mass transfer (incipient thickness); mass transfer across the film (film growth above incipient thickness)	[58,60,61]
Solvent viscosity	Monomer diffusivity; mass transfer rate	[49]
Additive: co-solvent	Amine partitioning; reaction rate; interfacial tension;	[48,62–67]
Additive: surfactant	Interfacial tension; support wetting	[63,68–70]
Additive: acid/base	Increased reaction rate	[63,71,72]
Additive: polymer	Increased viscosity and reduced diffusivity	[73–75]

2.2. IP kinetics: experimental studies

While there is a multitude of literature focused on IP-formed polyamide films as affected by various synthesis and formation conditions, these studies have mostly taken an 'autopsy' approach, whereby the film is characterized post-fabrication. Relatively few experimental studies have been carried out with the focus on the actual formation process, *in-situ*. This is primarily due to the challenges associated with such an experiment, requiring high resolution for both the spatial and temporal scales involved – a very thin film, forming at a (potentially mobile) liquid-liquid interface, over time scales as short as fractions of a second but often extended to hundreds of seconds. Nevertheless, there have been several noteworthy attempts, using a variety of techniques, primarily optical, which provided valuable insight as well as an initial platform for further development.

The kinetic aspects of interfacial polymer growth were already mentioned by Morgan and Kwolek [16] as part of their seminal series of papers on the fundamentals of interfacial polycondensation. Several insightful observations were made concerning choices of monomers, their concentration and solvent. In particular, basic features of the polymerization process were established, namely, the predominant occurrence in the organic phase and the diffusion-limited character, in which the differentiation was made between limitations due to the acid-chloride or the amine monomer, at low concentrations of either one, respectively. Furthermore, it was noted that at very low amine concentrations, it might be possible for the reaction to proceed at the interface or within the aqueous phase. Finally, the extremely fast reaction rates and self-limiting character of the process were highlighted. The first attempt at directly measuring the polymer growth rate was made by Enkelmann and Wegner [76], who measured the polyamide film thickness vs. time using a microscope. The experimental data fit rather well to a simple model based on first-order growth kinetics, proceeding rapidly at short times and ultimately limited by the 'blocking' of the amine by hydrochloric acid generated in the reaction zone. Importantly, the long-time thickness was shown to scale as the square of the amine concentration. This preliminary study, while instrumental to the progress of such endeavors, can be viewed as qualitative since the accuracy of the thickness measurement is unknown; furthermore, short times were not accessible.

A more rigorous attempt to measure IP kinetics was made by Chai and Krantz [36], who pioneered both the use of direct imaging as well as, more importantly, the use of optical reflectometry. This method relies on the different optical properties of the polymer solutions vs. the solid phase and so was able to capture relatively short-time changes in the system, demonstrating the extremely fast growth of the polymer film, as affected by variations of the monomer concentrations. These measurements also highlighted the rapid early-time growth, followed by a significant tapering and self-limiting behavior, but were not able to resolve the first few seconds of the reaction. These time scales, however, were accessible using the direct imaging of a pendant drop of the aqueous phase immersed in the organic phase. This technique, known as pendant drop tensiometry, provided images of the drop shape from which the change in surface tension could be estimated. While it is not entirely clear what surface tension would physically represent in the polymerizing system, the change in droplet shape does reflect processes occurring at the interface, and as such are a good proxy for the polymerization kinetics.

What are the kinetics of film formation? Recent studies have been able to employ more elaborate methods and experimental setups to study film formation. Using diffuse reflectance, Matthews et al. [37] studied the formation of a polyamide film on top of a polysulfone support, representing a more industrially-relevant system. With this method, a reduction of reflectance is attributed

to increased absorption by the growing polymer film. The results showed a pronounced effect of altering the amine monomer at a constant concentration of TMC (0.1 wt%), with distinctively faster initial growth at higher MPD concentrations (1 and 2%). Meanwhile, although thicker films resulted from higher TMC concentrations (at 2% MPD), the general kinetic time-evolution appeared to be unaffected. In all cases, initial polymer growth was rapid, and was followed by a noticeable tapering with an apparent power-law behavior (particularly the constant MPD case). This is indicative of growth limited primarily by supply of the amine. Measurements were also carried out using Rutherford backscattering, which provides the areal density, from which thickness may be deduced. These measurements further established the very rapid formation of the polymer and, combined with the reflectance data, gave an estimate of 50% formation within the first 2s of the process, and up to 70% formed at lower MPD concentrations.

Use of microfluidic platforms has also provided recent advances in experimental monitoring of IP; this was first demonstrated by Zhang et al. [77], who created IP films in a co-flow microfluidic configuration, though kinetic information was not inferred from their visualization. Nevertheless, the ability to control the interface and provide a visualization platform has been used to provide spatial information on the distributions of monomer concentrations [38] and temperature [39]. Using multiple-beam reflectometry and an immobilized oil-water interface, trapped in a microfluidic cell, Nowbahar et al. [38] measured the MPD concentration profiles during IP (see Fig. 4A and B). These measurements were then used to infer the diffusive flux at the interface, and the total amine mass delivered to the polymerization.

Furthermore, measurements made with different initial concentrations of MPD and TMC enabled several insightful observations. The initial MPD flux varied linearly with its concentration, with a slope determined by the TMC concentration. It was further confirmed that the initial flux is proportional to the multiple of the MPD concentration and the square-root of the TMC concentration, with the slope of this curve revealing the rate constant for the initial stage of the reaction, before a significant obstruction is presented by the forming film. In these experiments, a high concentration of MPD was employed (2.5–10 wt%), for which the reaction is expected to be controlled by the availability of TMC, generating conditions that indeed conform with the picture of a reaction-diffusion boundary layer, so long as the TMC concentration is not too low [22]. Furthermore, the scaling of the inferred MPD flux vs. time showed a rapid decay after ~1 s, consistent with other reported trends of significant 'slow-down' of the reaction leading, presumably, to self-limiting behavior.

Is IP always self-limiting? This point appears to be widely agreed upon – the reaction is self-limiting. However, recent evidence shows that, while the reaction is indeed slowed down considerably as seen in practically all studies described herein, this is not necessarily an intrinsic property of the film-formation process. Rather, this can be attributed to the actual barrier posed by the forming film and, perhaps as importantly, to the availability of MPD. The second point was suggested in some earlier IP models [79] and was illustrated by Ukrainsky and Ramon [39], where films with thicknesses on the order of tens of microns were fabricated in a microfluidic channel, indicating that so long as MPD is supplied to the system, the IP process continues, albeit at a slower rate. In an industrial setting, the MPD is supplied from a solution contained primarily within the pores of a supporting structure. Under such a scenario, it is conceivable that the support itself will become the limiting factor in the supply of MPD, eventually becoming depleted and resulting in termination of the reaction. Indeed, typical support thickness and porosity suggest it contains an equivalent to a few tens of micrometers thick layer of 2% MPD solution, sufficient to form a polymer layer of the order of a tenth of a micrometer thick, which reasonably compares with the typical polyamide layer thickness in TFC membranes. Further evidence of this may be found in a recent study by Li et al. [78], who measured IP film formation using imaging based on low-coherence interferometry (optical coherence tomography - OCT), see Fig. 4C and D. In these experiments, an MPD-soaked support was fixed in an optically-accessible flowcell, into which the TMC-containing organic phase (hexane) was flowed. In experiments mimicking standard formulations (2 wt% MPD and 0.15 wt% TMC), the film thickness showed a marked two-stage process, with a rapid initial rate of formation, followed by a nearly constant rate which then drops to zero, after ~100 s. The first two stages closely resemble, in terms of timescales and qualitative slope variations, the measurements made by Ukrainsky and Ramon [39], based on the temperature evolution of the reaction zone (see Fig. 4E and F). This resemblance is remarkable, since the latter study measured the temperature at the interface as a proxy of film formation, which appears to be quite representative. However, the abrupt end of the process, as seen in Li et al.'s data [78], suggests that the reaction ended due to MPD depletion, rather than transport limitations presented by the forming film. In another study, the IP of piperazine and MPD was monitored using FT-IR spectroscopy [80], where the spectral response of C=O bond stretching was used as a proxy for film formation. In these experiments, the reaction was deliberately slowed down by introducing transport barriers in the aqueous phase, either as an intermediate film or via addition of long-chain polymers. An interesting aspect emerging from these transport modifications is the transition from typical kinetics that follow a fast initial rate followed by pronounced tapering, to a nearly constant rate of formation, manifested by a linear growth rate in time. This suggests that the rate of initial growth plays a major role in creating 'self-limiting' conditions.

In summary, the demonstration of new experimental techniques, as well as possible extension of older ones, presents interesting opportunities to further investigate IP kinetics, by creating well-controlled environments and measurement modalities – notably temperature and concentration profiles, at high temporal resolutions. The studies discussed herein provide a foundation for understanding the basic features of the process - the dependence on monomer transport and availability – but given the many other synthesis variables, much can still be learned through these direct measurements.

2.3. Continuum reaction-diffusion models

IP is a complex hierarchical process involving simultaneous and strongly coupled reaction and diffusion of a multitude of species - monomeric, oligomeric and polymeric. Condensation of two difunctional monomers results in a linear polymer; however, with a higher average functionality, e.g., condensation of di- and trifunctional monomers or interfacial crosslinking of a polymer, an infinite network is ultimately formed (in general, for condensation of monomers A and B of functionalities f_A and f_B, the mathematic condition for formation of an infinite network is $(f_A - 1)(f_B - 1) > 1$). The reaction is further complicated by side reactions, such as acid chloride hydrolysis, steric and topological constraints on reactant species and difficulty to assess relevant kinetic parameters. Rigorous modeling of IP kinetics is then a formidable task, further complicated by the challenge of experimentally measuring the required kinetic parameters. Hence, simplified approaches have proven to be most productive. Berezkin and Khokhlov reviewed models published prior to 2006 and defined three levels of IP modeling [81]:

- kinetic, viewing IP as a homogeneous polymerization reaction with appropriate reaction rate constants.

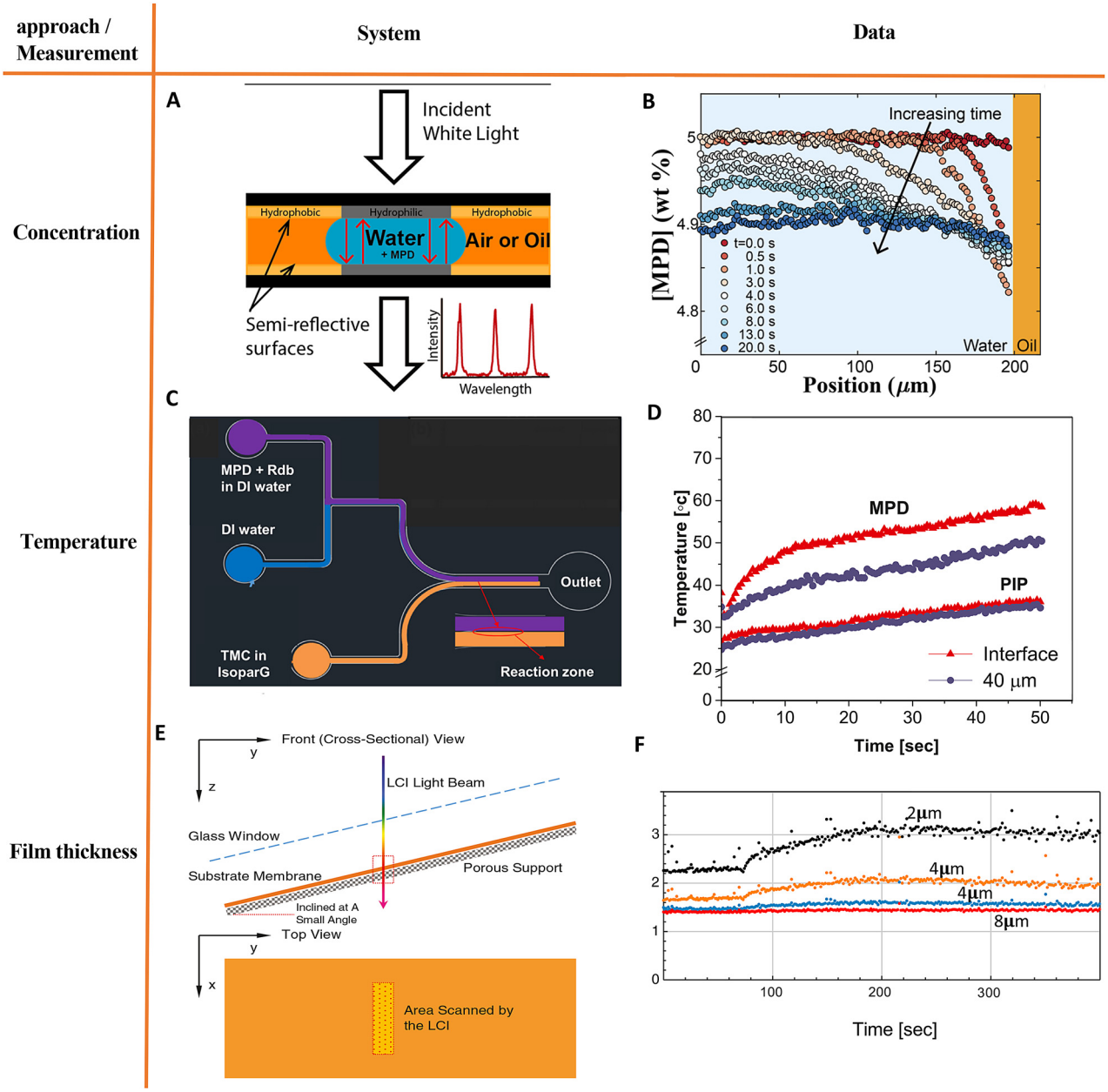

Fig. 4. *Experimental setups (left) and corresponding measurments (right) of IP kinetics. (A) Microfluidic chip designed with a hydrophobic patch, trapping an oil droplet. Incident white light is used for interferometric measurments of the MPD concentration in the adjacent aqueous phase. (B) The concentration profile of MPD, at different reaction times, measured near the oil-water interface. Adopted from [38], copyright 2018, Reproduced with permission the American Chemical Society. (C) Microfluidic contactor used to measure the temperature evolution during IP, based on the temperature-dependent fluorescent signal of Rhodamine-B. (D) Temperature measured during IP, at the interface and 40 microns away. Adopted from [39], copyright 2018, Reproduced with permission from Elsevier Science Ltd. (E) Low-coherence interferometry (also known as optical coherence tomography, OCT) setup used to measure the film thickness as it is being formed by IP in a flowcell. (F) Polyamide film thickness vs. time, measured by OCT. Labels indicate relative heights from base surface. [78], Copyright 2019. Adapted with permission from John Wiley & Sons, Inc.*

- local or microscopic, considering diffusion and reaction in a small volume and aimed at understanding the kinetics of local evolution of oligomeric and polymeric species.
- macroscopic, aimed at understanding the ultimate result of the process, e.g., formation of the film and evolution of its characteristics over time.

In the context of separation or encapsulation membranes, the latter has been of most interest. In this context, early models of IP considered the process to be diffusion-limited [76,79,82,83]. In this picture, the film, of zero thickness, is assumed to form immediately after the two solutions are brought in contact and its subsequent growth is determined by the quasi-steady-state diffusion of the amine monomer through the film. This model obviously assumes that the rate of reaction is very large and has no effect on the overall kinetics. If the film is further assumed to be uniformly dense, the monomer permeation rate and, ultimately, the rate of change of film thickness is inversely proportional to the film thickness, δ, and bulk concentration of the diffusing monomer, C_0, so that $d\delta/dt \sim C_0/\delta$. This relation predicts that the thickness increases approximately as the square root of elapsed reaction time,

$$\delta \sim (C_0 t)^{1/2}, \quad (1)$$

i.e., may reach any thickness when allowed to grow for a sufficiently long time. Such models showed reasonable agreement for some polyamides that exhibited a significant permeability to the

amine monomer and could grow to thicknesses as large as several tens of microns [76,82]. Later, more sophisticated reaction-diffusion models confirmed this generic relation and offered insight into fine structural details such as molecular weight distribution of evolving polymer species [83–85].

However, fully-aromatic polyamide films do not exhibit unlimited growth, contrary to what is predicted by Eq. (1). Usually, once formed, the nascent film may still grow in resistance with increasing reaction time, yet it does not show any visible change in morphology or superficial thickness [36,37,86]. Eq. (1) also predicts that, for a given reaction time, larger monomer concentrations would produce thicker films, which does not always agree with experimental observations. Finally, the model ignores the role of monomer reactivity, long known to be of critical importance for film formation [46]; furthermore, the solvent only affects the growth rate through its impact on polymer permeability.

Proposed mechanisms and stages of film formation. The above observations point to the existence of a termination mechanism, absent in the diffusion-limited growth. A few studies introduced such mechanisms in an *ad hoc* manner, e.g., by assuming a competing hydrolysis reaction [76] or limited supply of a monomer [79]. Such limitations may indeed occur in actual IP settings (see previous section), but, unfortunately, they alone cannot reconcile all experimental findings. The treatment reviewed here in more detail reveals termination or an abrupt slowdown as an inherent feature of simultaneous transport and reaction, particularly relevant during initial stages of IP, when diffusion may be very fast and possibly exceed the reaction rate [22,43,86]. This approach identifies three distinct, successive, kinetic stages during the course of the entire process, each with a different characteristic timescale [22,43], as highlighted in Fig. 5. In the first stage, initiated after the two solutions are brought in contact, monomer concentration profiles develop within the boundary layer, of thickness L, adjacent to the interface on the organic side. The profiles (dotted lines in Fig. 5) move until a quasi-stationary state (solid lines) is reached. The time required to reach such a quasi-steady-state is on the order of L^2/D_0, the monomer diffusion time-scale across the boundary layer, where D_0 is the monomer diffusivity - it is less than 0.1 s, assuming L is typically on the order of a few microns. The quasi-stationary profiles eventually ensure a stoichiometrically balanced influx of the monomers from opposite sides into a thin reaction zone of initial thickness δ_0, in which the monomers are fully consumed by the reaction.

Once the quasi-stationary profiles are established, a second stage - formation of a nascent film - begins, manifested as the filling of the reaction zone with the polymer at an approximately constant rate, equal to the rate of monomer diffusion into the reaction zone, which is determined by the diffusion resistance of the boundary layer, L/D_0, and monomer concentrations. The thickness of the nascent film is roughly the thickness of the reaction zone δ_0, which is related to the diffusivity and reactivity of the monomers (bimolecular rate constant, k) in the organic phase [22], via

$$\delta_0 \cong \left(\frac{D_0 L}{kC_0}\right)^{1/3}. \tag{2}$$

Here, the concentration C_0 is the sum of the amine and acid molar concentrations in the organic phase, each weighed by its functionality, with the amine concentration determined by equilibrium partitioning from the aqueous to the organic phase. Typically, the latter is on the order 10^{-2} – 10^{-1}, i.e., equilibrium amine concentration in the organic phase is 10–100 times smaller than in the aqueous phase. Depending on the permeability of the film, this stage proceeds up to the point when either the resistance of the nascent film exceeds that of the boundary layer or it reaches a completely dense state. The latter is reached approximately after a time

$$t_0 \cong \frac{\delta_0 L}{D_0 C_0 V_M}, \tag{3}$$

where V_M is the monomer molar volume, thereby $1/V_M$ is approximately the polymer molar density. For conditions typical of membrane preparation, this time is on the order of a few seconds.

The last stage, of diffusion-limited growth, may follow two different scenarios, depending on the permeability of the polymer to the amine monomer. If the nascent film reaches its maximal density but is still more permeable than the entire boundary layer, its growth continues at about the same rate, with the film resistance (thickness) increasing linearly with t until it exceeds the boundary layer resistance and crosses over to the classical $t^{1/2}$ regime limited by the monomer diffusion across the film, as predicted by Eq. (1). However, if the nascent film exceeds the boundary layer resistance before reaching its maximal density, the growth will slow down more abruptly and proceed in a different manner. In this distinct scenario, a dense ultrathin sublayer will possibly form within the nascent film, without any detectable change in the overall film morphology. The ultimate thickness of such a dense inner barrier, embedded within the nascent structure, is determined by a different combination of parameters, namely,

$$\delta \cong \left(\frac{D}{kC_0}\right)^{1/2}, \tag{4}$$

where $D << D_0$ is the monomer diffusivity (or, more accurately, permeability) in the polymer. Given sufficient time, this thin barrier would eventually increase in thickness via diffusion-limited growth, following the $t^{1/2}$ dependence dictated by Eq. (1).

How do different factors affect film thickness? The kinetic scheme shown in Fig. 5, along with Eqs. (2) and (4) seems to explain many experimental observations [22]. For instance, it rationalizes the importance of high reactivity for forming a thin self-limiting film rather than a homogeneous bulk solution or dispersion, as discussed in Section 2.1. The high reactivity ensures that the reaction zone remains within the boundary layer, i.e., $\delta_0 < L$. The effect of reactivity also partly explains why the more reactive piperazine forms thinner and more permeable NF membranes than MPD, which produces tighter films with RO selectivity [3]. The model also explains the permeability-enhancing effect of more polar solvents or additives such as DMSO or acetone [29,47,48]. Indeed, when added to the aqueous phase, these organic solvents rapidly partition into the organic phase and increase the solvent polarity within the boundary layer. This has a two-fold effect: increasing both reactivity (k, correlating with medium polarity [46]) and, through larger amine partitioning, C_0. Both factors act to reduce the nascent film thickness and increase permeability. Eqs. (2) and (4) also point to solvent viscosity as a means of reducing monomer diffusivity, resulting in decreased film thickness and increased membrane permeability; this effect was demonstrated experimentally for Isopar G versus the less viscous hexane [49]. Wang et al. explicitly confirmed an inverse relation between the diffusion rate and film thickness by varying amine diffusivity via addition of benzene to the hexane and performing *in-situ* measurements of the diffusion rate in the organic phase [74].

Most importantly, the model agrees with the existence of optimal monomer concentrations [2,3,36]. Indeed, Eqs. (2) and (4) both indicate that the nascent film thickness is inversely related to monomer concentration C_0. However, for excessively large concentrations, the thin nascent barrier will form fast, as predicted by Eq. (3), and the growth will cross over to the third regime, i.e., the barrier will begin to grow in thickness, following the diffusion-limited mechanism. Eq. (1) indicates that growth in this regime will proceed faster at larger C_0, so that the ultimate film thickness may increase with C_0 and membrane permeability will decrease.

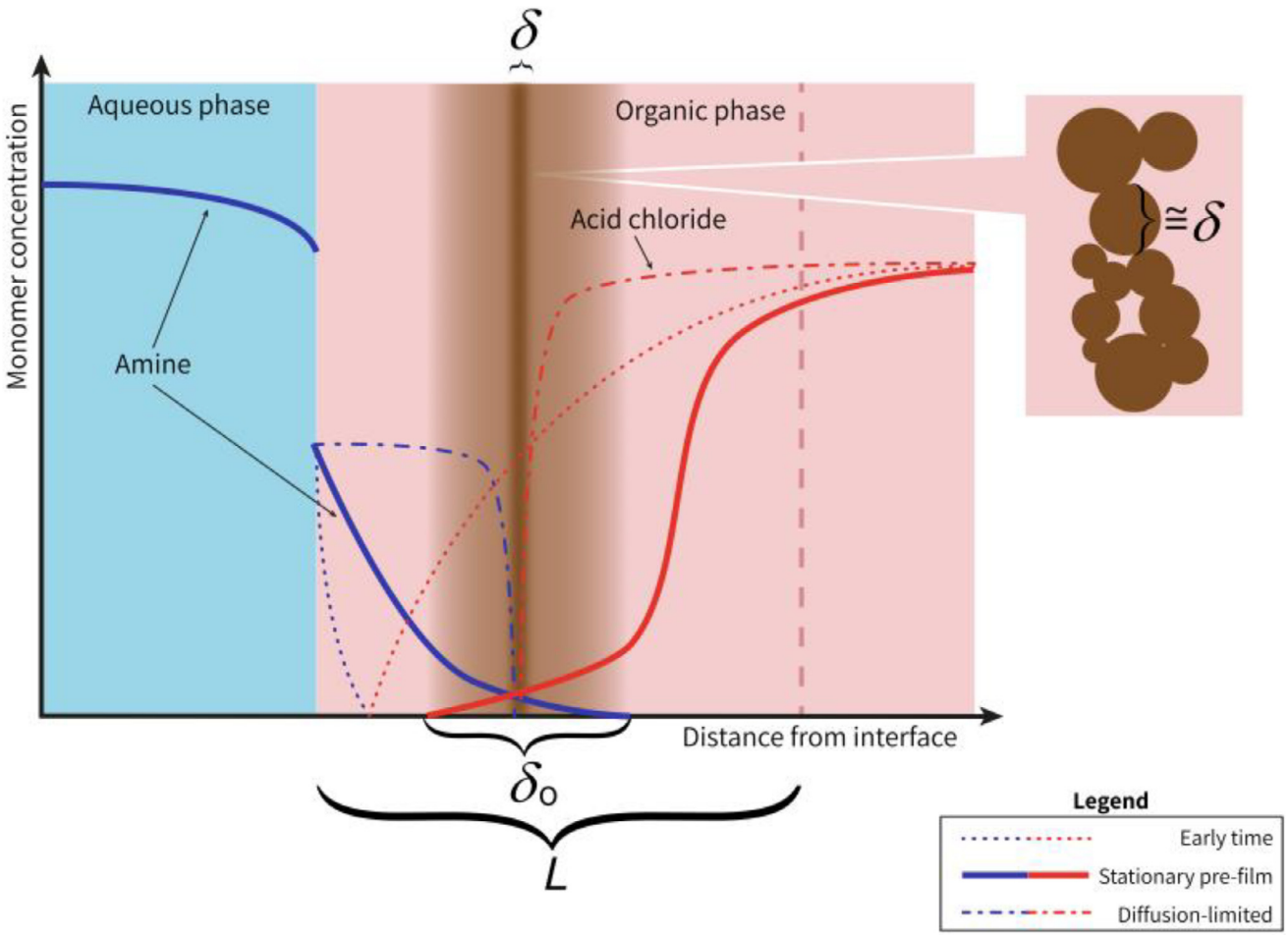

Fig. 5. Schematic representation of interfacial polycondensation of multifunctional amine and acid chloride and formation of a polyamide film, indicating the typical length scales L, δ_0w and δ. The red and blue lines, to the right and left of the reaction zone, respectively, illustrate acid chloride and amine concentration profiles evolving over time. Dotted lines represent the initial, transient, moving profiles; solid lines correspond to the quasi-steady state established around the reaction zone during incipient film formation; and dot-dashed lines represent a quasi-steady state around a thin, dense barrier within the incipient film when its diffusion resistance exceeds that of the boundary layer. The discontinuity of the amine profile across the interface is due to its partitioning between aqueous and organic phases. The zoom-in picture highlights polymer formation as the growth and fusion of reactive particles. (For interpretation of the references to color in this figure legend, the reader is referred to the web version of this article.)

Since C_0 affects the nascent (second) and diffusion-limited (third) growth regimes in opposing manners, for a fixed time of the IP reaction, their superposition is expected to yield a minimal thickness at some optimal concentration, as indeed observed in practice.

Model predictions of film morphology A closer inspection of the above reaction-diffusion mechanism reveals that the nanoscale film morphology may develop in an even more complex and non-uniform manner. Indeed, the picture presented in Fig. 5 may suggest that all concentrations vary only in one (thickness) dimension, ignoring fluctuations and lateral variations. However, such fluctuations are likely to be inherent and significant. When two monomers of functionality 2 react and form an amide bond, the reaction does not change the total number of reactive sites of the growing oligomer. The resulting linear polymer will tend to form a fairly uniform dense film [87]. However, when - on average - reacting monomers has a larger functionality, the number of reactive groups at the surface of growing oligomeric particles will increase exponentially, similar to the growth of dendrimers [88,89]. Due to the large surface density of reactive sites, the growing particles will actively scavenge free monomers at an increasing rate, at the expense of growth of smaller aggregates, as illustrated in the zoom-out in Fig. 5. The reactive particles may assume different shapes, e.g., be isotropic or sphere-like, when orientation of a newly and previously formed bonds is weakly correlated, or be lamella-like, when new and previous bonds tend to remain in the same plane, as in fully aromatic polyamides [28]. Regardless of the shape, such particles will eventually begin to coalesce, and the interstices will progressively fill, to the point where they and remaining reactive sites are no more accessible to free monomers. The resulting film morphology is then expected to resemble fused particle aggregates, with interstitial spaces filled with a looser polymer and some small residual voids. Remarkably, a simple analysis concludes that the characteristics particle size should be commensurate with film thickness, suggesting that small-scale surface roughness must be an inherent feature of films formed by IP of multifunctional monomers [22,45].

2.4. IP: the molecular scale picture

The reaction-diffusion model reviewed in the previous section considers concentration variations of the monomers, as well as the polymer and its reactive groups, over time, but - due to its continuum nature - it cannot address molecular-level structural details and thus shed light on the capability of different chemistries to form selective barriers. Before the wide adoption of molecular dynamics (MD) as a primary molecular simulation tool, Hirose et al. presented an interesting attempt to rationalize the effect of monomer structure on performance, based on simple packing con-

siderations of network subunits formed by the reaction of different diamine and triacid precursors [28]. All analyzed monomer systems (see Fig. 2E), except for MPD-TMC, were shown to form minimal-energy substructures with various degrees of bending and twisting that prevented efficient packing of network segments. Such inefficient packing would produce significant amounts of fractional free volume, with relatively large cavities, which is likely to reduce selectivity. The MPD-TMC system was unique in that it could form perfectly planar substructures, capable of tight and efficient packing, in a manner that resembles the packing of graphene sheets in graphite.

Molecular dynamics simulations of IP Over recent decades, MD simulations have become an important and common tool for *in-silico* polymer design and computation of various thermodynamic and kinetic characteristics, as well as structure. The first MD investigation of polyamide membranes was reported by Kotelyanskii et al. and mainly focused on understanding the transport properties of polyamide, rather than its structure [90,91]. This and many later MD studies adopted fairly crude approaches for constructing the polyamide structure, such as simple crosslinking of linear chains, somewhat downplaying the irregular nature of the actual polymerization process [92–97]. Other studies adopted a more realistic procedure to construct the polyamide structures, emulating the actual polymerization process as diffusion- or reaction-limited aggregation [93,98–103]. In this procedure, the model polymer is gradually formed by randomly adding monomers to the simulation volume, allowing them to connect to the growing oligomers and, ultimately, form a polymer network. Oligomeric species merge until possibilities for further monomer addition and bond formation are exhausted. Such growth may seem to ignore the macroscopic density variations inherent of the IP process highlighted in Fig. 5 but, as pointed out by Kolev and Freger [99], it may reasonably emulate the conditions encountered within the reaction zone, where composition gradients are minimal and where the densest part of the polyamide film (i.e., the actual barrier) forms.

A judicious choice of the time when such polymer "synthesis" is terminated is critical for obtaining a film with characteristics representative of genuine membranes. The rate of polymerization slows down considerably when the polymer approaches its maximal density. Early termination might then produce too open a structure, while denser structures may require excessively long computations, even when *ad hoc* modifications are applied to accelerate the process [93,102]. Many studies adopted an experimentally evaluated density of ~1.3 g/cm^3 for fully aromatic polyamide as the criterion to match, however, as it reflect average characteristics of the entire film including loose fringes, it may not represent the selective barrier part. A more appropriate termination criterion may be based on experimental RBS data that estimated the degree of cross-linking and amount of unreacted groups in genuine films [104,105]. Unfortunately, pioneering MD studies, performed before the publication of the first RBS data, settled for quite open structures with <80% crosslinking. This was improved by Kolev and Freger [99] who employed a much longer aggregation process, eventually reaching ~94% cross-linking, which reasonably agreed with the values obtained by RBS (94-96%). The resulting representative structure then offered insights into finer details of the molecular packing and pore space within the polyamide, yet even the structure obtained in this manner can be too open, underestimating the salt-rejecting properties compared with real membranes [100,106].

Polyamide structure emerging from MD simulations Fig. 6 highlights the main structural features of a polyamide molecule assembled via the above aggregation procedure [99]. Fig. 6A displays a network fragment containing a few tens of atoms, illustrating the propensity of fully aromatic polyamide to form planar subunits that tend to pack as dense lamella-like stacks containing very little free volume. However, along with dense fragments, simulated structures typically contain a significant void fraction, made up of network defects entrapped within the polymer. The defects are partly due to orientation mismatch and frustration at the boundaries between neighboring lamella stacks, as seen in Fig. 6A, and partly due to insufficiently long synthesis time, over which the dense matrix severely restricts monomer access to voids and prevents their filling. Fig. 6B shows the computed polymer density map for water-swollen polyamide, time-averaged over about 10 ns, which visualizes voids, colored dark blue, as a permanent and inherent feature of the polyamide structure. Notably, local polymer density may exceed 2 g/cm^3, significantly above the average density of dry polyamide, ~1.2-1.3 g/cm^3. Presumably, high density represents the most densely packed and thereby least permeable and most selective fragments. Time-averaging highlights another intriguing fact - over a time as long as 10 ns, most voids undergo only minor fluctuations and remain open. This behavior resembles that of a genuine porous solid and is quite unlike free volume cavities in soft solvent-swollen gels or rubbery polymers, which are highly dynamic and may significantly fluctuate in size and position, subject only to topological constraints imposed by crosslinks. The existence of permanently open voids is a manifestation of the exceptional rigidity of the aromatic polyamide network and strong topological constraints that greatly reduce the amplitude of fluctuations.

The water-filled void structure and spacing may be analyzed in a more quantitative manner using the computed radial correlation function $g(r)$ of water oxygens, presented as $\ln[g(r)\text{-}1)]$ in Fig. 6C. It displays two major features; a peak at the lower cut-off radius $r_{min} \sim 0.25$ nm and an exponential decay at $r > r_{min}$. The cut-off corresponds to the closest approach distance of water molecules, while the decay may be related to the void size or spacing distribution. Its exponential dependence is characteristic of a random porous material, with a widely distributed void size. Apparently, this feature is inherent to all parts of the film, including the densest part. However, the total free volume fraction might vary significantly, reflecting differences in monomer accessibility to the different parts of the film, which favors more complete filling for the middle, densest part of the film, as shown in Fig. 5.

What determines polyamide permeability and selectivity? Regardless of the exact structural details and free volume, it is the connectivity of the voids, i.e., the passages between the voids, rather than the voids themselves, which primarily determines the permeability and selectivity. Already in the first MD study, Kotelyanskii et al. concluded that transport of water and solutes in polyamide is controlled by fairly rare jumps between voids [91], which was confirmed in later MD simulations.

Viewing passages that control jumps between voids as resistances and using the well-known general percolation theory arguments [107,108], the overall permeability may be related to a so-called critical resistance [109]. The critical resistance is the one that just allows percolation across the entire film through a sub-network of passages, less resistant than the critical one. It is expected to be highly sensitive to the completeness of densification and cross-linking at the final stages of polymerization, which determines whether solutes may find a percolating path that goes entirely through the void space or have to traverse sections partly or fully blocked by the dense polymer. Evidently, the latter is expected to yield lower permeability yet a much larger selectivity.

Curiously, virtually all published MD simulations predict a similar water permeability, which compares reasonably well with that measured in polyamide membranes. However, different MD studies show large discrepancies in the value of salt permeability, which may exceed the measured salt permeability of polyamide membranes by as much as four orders of magnitude [100]. This sug-

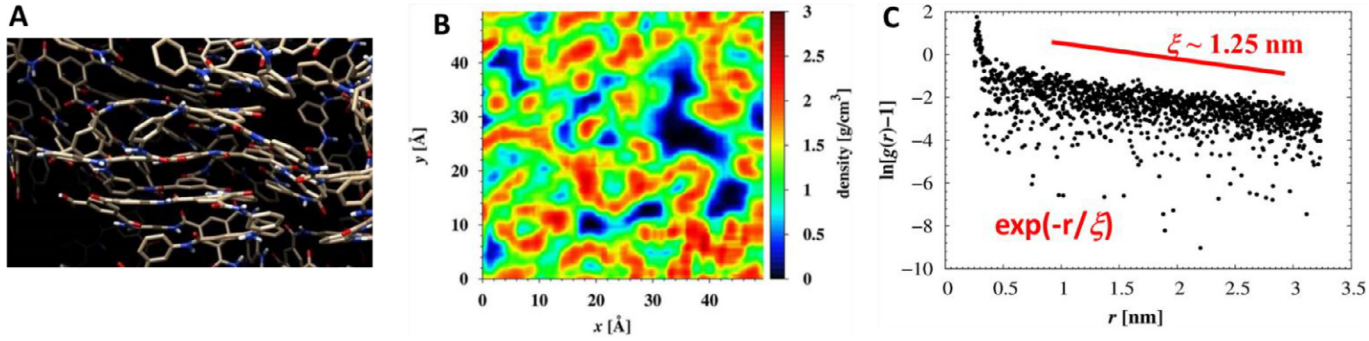

Fig. 6. *Molecular and nanoscale structure or polyamide revealed by MD simulations. (A) Simulated atomic structure of polyamide obtained by in silico synthesis, showing packing of planar segments of aromatic network. (B) Time-averaged map of polymer density highlighting presence of permanent cavities and dense fragments within polymer matrix. (C) MD-based pair correlation function of water oxygens within polyamide; the exponential slope is characteristic of a random porous material with a correlation length ξ = 1.25 nm. After Kolev and Freger.* [99]*, Copyright 2014, Adopted with permission from Elsevier Science Ltd.* (For interpretation of the references to color in this figure, the reader is referred to the web version of this article.)

gests that subtle differences in the overall polyamide density might affect the critical resistance to salt transport, more so than for water. This is reasonable and anticipated, since salt permeation is also affected by charge exclusion mechanisms, which are far more sensitive to the void or pore size than permeation of water or similarly-sized neutral molecules. This also suggests that even the densest structures simulated so far might be too open and do not adequately represent the transport properties of polyamide membranes, which may contain an ultra-thin yet nearly completely blocked barrier. In such a case, RBS may be unable to supply the information, as it mainly reflects average properties of the entire film. We return to this point in Section 3.4.

2.5. Inherent instabilities of IP process and their effect on morphology

As previously discussed, a seemingly inherent feature of polyamide films is their tendency to evolve into rough surfaces. One mechanism outlined in two previous sections is formation of the dense films via aggregation and fusion of reactive particles, whose remnants form asperities or nodules observed on the surfaces of semi-aromatic NF and probably some 'tight', fully-aromatic RO membranes [45,58]. However, for more open RO films, a vast amount of evidence highlights a very different, characteristic ridge-and-valley morphology. Evidently, this points to another cause, which we attribute to the destabilization of the initially formed planar nascent film, leading to extensive folding and crumpling, and resulting in a highly irregular and rough morphology. Indeed, detailed microscopic analysis reveals that polyamide surfaces can, in many cases, be described as a 'crumpled' ultra-thin film (where the 'real' thickness is O[10 nm]) [6,110–113]. Since recent studies demonstrated the capability of forming smooth PA films (notably Ref. [60]), a lingering question is: what are the possible causes of the transition from a smooth to crumpled morphology? Here, we speculate on several such 'instability' mechanisms, of varying origin – thermodynamic, kinetic, hydrodynamic, and elastic. A feature common to several of these instabilities is the temperature and chemical composition gradients in the reaction zone, as affected by the heat released and rapid chemical transformations during the reaction [39,60]. More specifically, the possibly non-uniform temperature and composition, due to spatially varying film growth rate, may be viewed as a trigger for an instability, manifesting itself as either a 'wavy' disturbance that propagates and grows in time, or a more 'violent' form of instability such as buckling, foaming or rupture.

Reaction-diffusion instabilities Non-linear reaction-diffusion systems are susceptible to inherent fluctuations, which shift the reaction front from uniformity towards spatially varying multi-dimensional profiles, whose characteristic dimensions are controlled by reactivities and diffusivities of reactants and products. The IP process shares features extensively studied in pattern formation observed for propagating reaction-precipitation fronts, which can evolve in time from a uniform initial distribution to form irregular patterns [114] (see illustration in Fig. 7). In the case considered here, of an IP reaction featuring two mobile reactants and a single immobile polyamide product, the relevant characteristic dimensions were identified as δ_0 and δ in Section 2.3. In more complex reaction-diffusion systems featuring a broken symmetry and certain kinetic feedbacks, e.g., when different products with disparate diffusivities act, respectively, as a promoter and an inhibitor, rich stationary patterns known as 'Turing structures' may arise [115–117]. It is unclear to what extent such conditions may be realized during IP. However, we mention an interesting, recent report of a semi-aromatic polyamide film, which is normally quite smooth, fabricated such that its roughness increased considerably, and also featured a transition from the usual nodular structure to a 'wrinkled' structure [73]. These patterns were attributed to a Turing-type instability. While there might be a superficial analogy to the IP process, it is not entirely clear how a Turing pattern, which would normally describe the spatial segregation of different products, applies to the polymerization case, where polyamide is the only product and polyamidation reaction (see Fig. 2) does not feature simultaneous promotor and inhibitor feedbacks that would potentially give rise to Turing patterns. Furthermore, a Turing pattern remains stationary only while the mass transfer rates are also stationary [115], and this is not the case in IP. We believe that, while certain parallels between IP and conditions leading to Turing patterns may be drawn, other instabilities discussed below are more likely to be involved in formation of the ridge-and-valley structures.

Thermo- and soluto-capillary instabilities Compositional fluctuations and differential heating of the interface between the two fluid phases during early-times of formation can trigger soluto- and thermo-capillary flows, driven by chemically or thermally induced gradients in surface tension, also known as Marangoni flow (see Fig. 7). These chemo-hydrodynamic instabilities have been studied in systems analogous to IP (usually with an acid-base neutralization reaction) [118–120]. The instability may be may be driven by buoyancy (Rayleigh-Benárd) and/or surface tension (Benárd-Marangoni) [121], where the latter case is far more likely to manifest over the spatial scales involved in IP. In these systems, patterns and plumes have been observed. In other cases, oscillatory flows have been shown to result from composition-induced variations of surface tension [122]. Notably, the formation of these patterns is suppressed, for example, when the initial concentration

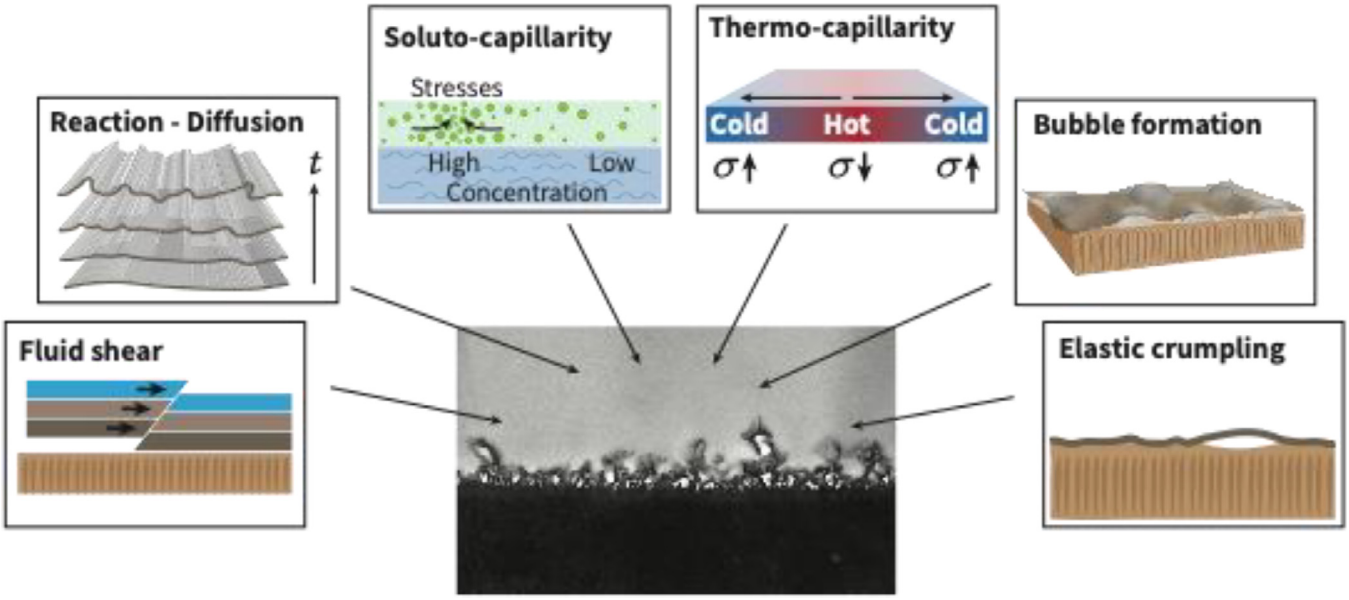

Fig. 7. Schematic illustration of hypothesized instability mechanisms leading to the rugose morphology of fully-aromatic polyamide films. (top) Fluctuations in the polymer formation rate result in non-uniform temperature and composition along the interface. Interfacial-tension variations drive flow and cause localized contraction. (right) Intense localized heat release can cause dissolved gas nucleation and growth into bubbles, as well as possible vaporization of the solvent. Differential thermal expansion at the interface between the formed film and underlying fluid/solid can result in crumpling. (left) Reaction-diffusion systems can evolve from uniform reaction fronts into random or periodic patterns, dependent on inherent disturbances and reaction kinetics. Fluid shear exerted through relative motion can result in interfacial waves and can amplify temperature and composition related instabilities.

of reactants is reduced [123], i.e., onset of instability requires a certain minimal (critical) driving force.

When considering the stability threshold, one asks what is the critical wavelength that may trigger an instability through an infinitesimal disturbance, which is always present due to thermal fluctuations. In this framework, the instability is defined by a clear boundary in the parameter space, embodied by a critical Marangoni number,

$$\mathrm{Ma} = \frac{h\Delta\sigma}{D\mu}, \tag{5}$$

which signifies the ratio of advective transport of mass or heat due to surface tension-driven flow and the respective rate of mass or heat diffusion. Here, $\Delta\sigma$ is the induced difference in surface tension, h is the solution layer thickness, D is the respective mass or thermal diffusivity, and μ is the solution viscosity. $\Delta\sigma$ is related to the respective perturbations in molar concentration ΔC or temperature ΔT, via the surface tension coefficients σ_C or σ_T, i.e., $\Delta\sigma = \sigma_C\Delta C$ or $\Delta\sigma = \sigma_T\Delta T$. In turn, ΔC or ΔT are related to the overall reaction rate, i.e., average molar flux of the reactants into the reaction zone J or respective heat generation, $J\Delta H$, where ΔH is the molar enthalpy of the reaction. In general, the reaction rate always increases with reactant concentration and so does Ma. At a critical Marangoni number, the instability is triggered from the random, thermal fluctuations that are always present, resulting in convection that will progressively distort the planar geometry of the nascent film.

Under moderate disturbances, the thin nascent film is expected to fold and crumple without rupturing, producing a highly permeable structure with a small effective thickness and a permeation area significantly larger than its footprint. Under more extreme conditions, fast flows may generate stresses sufficient for rupturing and fragmenting the film and inducing defects where a second-generation film, capping the defect, may form. Such second- or higher generation films were indeed observed in some IP studies at a free liquid-liquid interface [124] as well as for supported membranes [112] and are likely to yield films with a small effective thickness and significantly increased permeation area (see Section 3.1.2). With sufficient control and reproducibility, both scenarios should be beneficial for making high-flux energy-saving membranes.

Although transition from smooth to crumpled ridge-and-valley morphology above a certain limiting monomer concentration was demonstrated for IP carried out at the free interface between two solutions [60], the stability limit may be modified considerably in the case where inherent perturbations exist. In IP, such a disturbance may be manifested by the presence of the support structure – its roughness and the location of pores, which dictate regions of faster reaction and, hence, greater heat release or concentration fluctuations. These inherent disturbances manifest as geometrical features of the system or as boundary conditions and can generate different features compared with a 'base' state where these are absent; in fact, liquid film rupture has been shown to occur when the substrate is rough [120]. This instability mechanism will induce convective heat and mass transfer away from the hot regions, and so is expected to assist in speeding up the process.

Bubble-formation Several studies presented evidence that the IP reaction may produce "nanofoaming" or nanobubbles that, due to degassing or possibly even boiling of the solvents at the high temperatures generated in the reaction zone [39]. The bubbles may remain "frozen" within the nascent film structure and/or burst at later stages and thus favorably modify its morphology and transport characteristics [58,125] (see Fig. 7). Nanobubbles evolving between the support and nascent film may produce morphological changes similar to crumpling caused by surface tension-induced flow. Higher monomer concentration, mass transport enhanced using ultrasound, and certain additives, such as sodium bicarbonate, were all shown to presumably promote nanobubble formation. Notably, all these factors enhance reaction rate and thereby also cause a stronger heating of the reaction zone, compositional fluctuations and gas evolution. For example, bicarbonate may help generate CO_2 bubbles, yet it may also act as an acid scavenger that prevents protonation of amine and speeds up the IP reaction, promoting both interfacial instabilities and nanofoaming. Bubble for-

mation may then come along as another special form or a "by-product" of capillary instability, triggered when the reaction rate exceeds a certain limit. Regardless of whether nanofoaming may be categorized as such, it supplies an independent evidence of significant local overheating and destabilization within the reaction zone [39], as a general reason behind the characteristic rough morphology of polyamide membranes.

Hydrodynamic instabilities During a roll-to-roll IP process, another disturbance comes from the relative motion in the two-layer fluid system, namely the aqueous phase in the support, which moves with respect to the stationary, organic phase. In such a system, the film, once formed, will be subjected to a shear stress, which may be a source of instabilities of a different type. Considering the film to be a thin membrane or a finite-thickness elastic layer, it has been shown that shear can cause a fluid-solid instability that would lead to an initially flat film to become wavy and, possibly, folded and crumpled [126–128]. Alternatively, a viscosity difference between the two layers, which may be manifested during polymerization, can induce a similar instability. This instability is primarily triggered by the shear-induced stretching of the fluid-fluid interface or elastic film, in which case it is also enhanced by the presence of a second fluid on the other side [128]. The stability threshold is dependent on the shear rate and film thickness, but also very much on the viscosity ratio of the fluids and the elastic modulus of the film. Heating of the reaction zone can greatly modify the mechanical properties of the film and adjacent fluid, and it is conceivable that during early times, the film would be very soft and so more susceptible to this type of instability.

Elastic crumpling, wrinkling and buckling Finally, we briefly mention another mechanism that could potentially come into play - the wrinkling of the already-formed film (see Fig. 7). Several such 'buckling' instabilities have been studied in the context of thin solid films, at either solid-solid or solid-liquid interfaces [129–131]. Crumpling of ultra-thin, dimensionally confined films (such as graphene) due to such instabilities has also been reported [132]. Buckling and wrinkling instabilities may occur when there are transmitted stresses between layers with unevenly-matched elastic properties, as well as by diffusion-driven transport processes in thin, soft layers (e.g. [133,134]). Again, connected with the heat release during film formation in IP, the film may deform due to the varying thermal expansion coefficients and elasticity of the support, resulting in buckling and delamination.

3. Experimental insights on chemistry and structure of the polyamide layer

The plethora of possible scenarios and irregular structures that may evolve in an IP process (as discussed in Section 2) pose formidable challenges for characterization of polyamide membranes. The largest difficulties come from the submicron thickness of the polyamide layer and chemical and physical non-uniformities that span all scales from molecular to macroscopic. Features that control permeability and selectivity, such as the effective thickness, pore size, charge and dielectric characteristics, are of the greatest interest. Unfortunately, given the complexity of the IP reaction, its inherent propensity for fluctuations and instabilities, and the resulting irregular structure, even the thickness is non-trivial to define and determine. The required techniques must therefore possess the capability to differentiate and quantify the distribution of relevant chemical groups, with a nanoscale lateral and depth-resolution. The characterization methods that have so far supplied the most crucial inputs are TEM (morphology), positron annihilation life-time spectroscopy (PALS, molecular porosity), RBS, X-ray photoelectron spectroscopy (XPS) and ATR-FTIR (chemical composition and charge), AFM (roughness and swelling), and measurements of transport characteristics for charged and non-charged permeant molecules based on filtration and electro-chemical impedance spectroscopy (EIS) [135]. Recently, significant insight has been obtained on the nanostructure of polyamide thin films, using high-angle annular dark-field scanning-tunnelling electron microscopy (HAADF-STEM) imaging [136]. Nevertheless, many other techniques, including those specifically developed for studying ultrathin films and IP kinetics, have considerably helped put together different data into a unified picture. The following sections review the main results.

3.1. Film structure and morphology

3.1.1. Geometrical characteristics: thickness, porosity and pore size

How do we define film thickness? Film thickness is the primary structural characteristic of a membrane, as it has an inverse relation with permeance [4]. For the nanoporous films obtained in IP, thickness becomes poorly defined and non-trivial to measure. Compared to a dense film of the same overall thickness, pores and voids reduce transport resistance, i.e., effective thickness, by a factor that correlates with the porosity and pore connectivity [137]. Combining several types of measurements with thorough morphological investigation may help better understand the effective thickness and clarify its relation to porosity.

The superficial or *volumetric thickness* of polyamide films, i.e., the total volume of the film per footprint area, was evaluated by various imaging techniques. TEM and SEM are commonly employed to image cross-sections of composite membranes, either freeze-fractured for SEM or embedded in a resin, diced and microtomed for TEM [135,138,139]. The polyamide layer thickness measured in this way is typically in the range 100-300 nm for fully aromatic membranes and the films often appear as crumpled, folded films with voids, bubble-like features etc. (see Section 2.5) [6,31,58,140,141]. On the other hand, semi-aromatic films usually appear to be much thinner, 15–50 nm, and uniform down to the scale of a few nanometers, i.e., the smallest features observable in such films by TEM and SEM [10,43].

An important approach to high resolution characterization of nanoscopic features of polyamide is based on the separation of the polyamide layer from its support and subsequent transfer to a planar solid substrate, enabling thickness measurement using AFM or profilometry [45,60,109,142]. AFM is a convenient method to measure superficial thickness, e.g., by scratching the film down to the substrate and measuring the height of the formed step or, more accurately, by measuring the average height of a narrow strip. AFM is also well suited to quantify surface roughness (see next) and works under a liquid, which helps evaluate film swelling (see Section 3.2.2). Ellipsometry is another method that can evaluate volumetric thickness in air and liquid [143], but it requires optical modeling and is critically dependent on planarity and uniformity of the film and underlying substrate.

A major improvement in imaging the polyamide layer was achieved recently using TEM tomography, which revealed the spongey or crumpled morphologies of the aromatic polyamide, with voids ranging in size from a few to tens of nanometers [110,113,144,145]. Since some interpenetration of the polyamide and supporting layers obscures the boundary between them, representative average thickness of the entire polyamide layer may be difficult to evaluate [144]. Nevertheless, a thorough high-resolution 3D reconstruction combined with elemental mapping of adsorbed metal ions or nanoparticles, highlighted features that unequivocally indicate that the polyamide layer is a crumpled 10-20 nm thick parent film folded over, to varying degrees, to form a thicker structure [110], well in line with independent conclusions by STEM imaging combined with high-resolution elemental mapping [146,147] and other recent studies [6,32,111,112].

Another group of methods supply *mass thickness*, i.e., polyamide mass per unit area. Such measurements may utilize adsorption or scattering of radiation by specific chemical groups or atoms, which makes it far less sensitive to the presence of voids and the poorly defined polyamide-support boundary. Among these methods, perhaps the most successful one is the RBS approach developed at the University of Illinois Urbana-Champaign, which supplied extensive data on the thickness and structure of the polyamide layer of fully aromatic membranes [104,148,149]. The method is indirect and relies on sophisticated modeling for converting RBS spectra into atomic density profiles, but the fact that it may directly analyze polyamide layer within the composite membrane made the method highly attractive. The first data, presented by Mi et al., yielded mass densities equivalent to 85-200 nm, assuming 1.06 g/cm^3 density, in agreement with electron microscopy imaging [148]. More recently, Perry and Coronell employed quartz-crystal microbalance (QCM) to independently quantify the mass as well as small mass changes of an isolated polyamide layer, which showed good agreement with RBS data [150]. ATR-FTIR spectroscopy is another mass-sensitive method; due to its simplicity and specificity, it became a routine tool for analyzing coated membranes [139,151], and proved useful for studying the polyamide film both within the composite membranes as well as separately [109,143].

What is the film porosity? Combinations of different indicators offer insights into relations between structure and function of polyamide films. For example, the ratio of mass- and volume-based thicknesses of the same film directly yield its density, which may then be compared to that of the non-porous polymer (1.2–1.38 g/cm^3 for aromatic and about 1.1 g/cm^3 for semi-aromatic polyamides) to estimate film *porosity* or void fraction. Curiously, early attempts to obtain such estimates using AFM and ellipsometry (volumetric thickness) and EDS (mass thickness) measurements for polyamide films separated from commercial NF (semi-aromatic NF200 and NF270) and RO (fully aromatic tight SWC1 and open ESPA1) membranes suggested a fairly small void fraction [152]. While NF membranes indeed appear void-free in TEM, RO membranes clearly contain voids, as discussed above. Later, Karan et al. showed that a likely reason could be exposure to solvents used when dissolving the support, which "open up", i.e., swell and soften the polyamide matrix, possibly leading to collapse of the larger voids under capillary forces that arise during drying [60]. Curiously, despite void collapse, i.e., reduced overall porosity, solvent treatment was found to increase permeability, which suggests that mesoscopic voids have little to do with the overall transport, controlled by much smaller molecular pores (polymer free volume).

Due to possible pore collapse, correlating transport properties (see next) with mass thickness rather than volumetric thickness should be more appropriate, as was indeed found [153]. Such a comparison led Freger et al. to the conclusion that only a small fraction of the polyamide acts as an actual transport barrier, particularly in the more permeable RO membranes such as ESPA1 [32,109,154]. This conclusion is well in line with the IP mechanism, considering both inherent heterogeneity of the ultrathin nascent film (Section 2.3) and its subsequent destabilization and crumpling, resulting in a superficially thicker film (Section 2.5). Later studies demonstrated that this conclusion may be extended to the majority of fully-aromatic membranes, as discussed in Section 3.4.1. On the other hand, semi-aromatic NF membranes behave more akin to uniform, non-porous films, with permeability consistently described by correlations between thickness, swelling or mesh size, developed for such films [45,137].

Given that the total volume or even mass of the polyamide layer may not be a good representation of its transport properties, looking at transport characteristics may provide yet another route to estimating thickness, most relevant to the performance of polyamide membranes as selective barriers. One such characteristics maybe the hydraulic resistance or pure water permeability L_p (aka A) measured in regular filtration tests. Alternatively, diffusion permeability for various solutes and ions or electric conductivity of isolated films may be used. For example, L_p may be related to the thickness of a planar film as

$$L_p = \frac{b r_p^2 \phi}{\mu \alpha \delta}, \tag{6}$$

where $b = 1/8$ for straight or random pores, r_p is the pore radius, ϕ the porosity, identified as the volume fraction water or membrane swelling in the working conditions, α the tortuosity factor, usually correlated with ϕ, μ the solvent viscosity, and δ is the effective thickness. (We note that this is a potentially crude approximation, given the molecular scales involved and complex geometry. Nevertheless, this provides surprisingly well-correlated approximations). When porosity, i.e., polyamide swelling (see Section 3.2.2), and r_p are independently estimated, Eq. (6), along with the measured L_p may estimate the effective thickness δ. When ϕ and r_p are unknown but presumably similar for different membranes, L_p or other permeability characteristics may be a convenient indicator of differences in δ. Indeed, L_p and electric conductivity, were found to correlate well for different fully aromatic polyamide films (see also Section 3.4.1) [155], which suggests they are controlled by the same effective thickness, a few to a few tens of nanometers large and much smaller than the total thickness of the polyamide layer.

Evaluating pore size We should note that, at present, constantly improving high-resolution imaging allows identifying the effective barrier within an irregular polyamide structure and can supply independent estimates of its thickness (ca. 10–20 nm [110,112]), yet r_p stays still far below imaging resolution. It is then more common to use Eq. (6) for deducing from thickness the *pore size* r_p, which is the last and perhaps most critical geometric characteristic of the film, responsible for both its selectivity and permeability. Such estimates yield pore radii of the order 0.15–0.2 nm for fully aromatic polyamide and 0.2–0.4 nm for semi-aromatic NF membranes. Similar or slightly larger estimates may also be obtained from rejection of ions [156] or solutes of different sizes [157–159].

Alternative and somewhat more direct estimates of pore size may be obtained by PALS. Although the method relies on modeling pores as spherical cavities [47,160] and is not specific to the selective barrier, i.e., results are averaged over different parts of the film, it provides an analysis of the smallest pore sizes down to atomic dimensions and is relatively unaffected by large voids. Using PALS, Kim et al. discovered that molecular pores in fully aromatic polyamide have a bimodal distribution, featuring smaller "network" pores of radii 0.21–0.24 nm, assigned to the interior of dense crosslinked particles, and larger, 0.35–0.45 nm "aggregate" pores, presumably found in less cross-linked interstitial spaces [66,161]. This picture is consistent with the IP mechanism for the cross-linked nascent film, proceeding as growth and fusion of reactive particles (Section 2.3) as well as atomistic, coarse-grained and dissipative particle dynamics molecular simulations of IP [22,100,103,162]. The size of the smaller, network pores, agrees well with above estimates of r_p deduced from water permeance measurements. The larger aggregate pores, such as seen in Fig. 6B, may indeed be a "byproduct" of incomplete filling of the interstitial regions. However, they may also belong to looser polymer at the surface of the folded nascent film (cf. Fig. 5), sensed by PALS but less relevant to the barrier properties of polyamide. Note that a similar observation may apply to the two types of negatively charged groups with distinct pK_a values [163] (see Section 3.2.1), where lower pK_a groups assigned to aggregate pores may in fact be present mainly in the surface regions and have little effect on the

transport across the film, as was recently suggested by Ritt et al [164].

3.1.2. Morphology: nano-roughness, crumpling, and bubble-like features

As already discussed in previous sections, fully-aromatic polyamide films are notoriously rough, exhibiting a wide range of possible morphologies with roughness features reaching sizes of up to a few micrometers. The exact nature of these features has only recently been amenable to scrutiny, and much progress has been made in establishing better ideas on how these morphologies form, and what is their impact on performance. A particularly important, long-standing question concerning surface roughness is its contribution to diffusive transport via, for example, increased surface area contacting the polyamide film and the feed solution. Conflicting trends reported for the correlation between roughness and permeance (e.g., [49,165–167], see Fig. 9A) have made it clear that the quantification of the top surface area of the film is a better proxy than the more commonly-used, AFM-based RMS roughness [113,168]. Even then, simply quantifying the surface area is insufficient if the internal structure of the film and, most importantly, its connection with the permeate space are unknown [169].

Notably, recent advances in imaging have made it clear that these roughness features can enclose significant porous structures – voids, which are liquid-filled under operating conditions. The volume fraction of these voids has been assessed using a variety of techniques, including imaging in 2 and 3 dimensions using various forms of electron microscopy [110,111,113,140,144,146,170], as well as complementary methods such as ellipsometry and water uptake measurements using QCM [140]. These have shown void fractions of up to ~30%, but a much smaller void volume fraction, <1%, was later argued to be more representative of the enclosed void volume fraction, as opposed to voids that communicate directly with the feed-side of the membrane [113]. It was further argued that compression during operation also plays a role in the ultimate volume of these voids, though this seems to be mostly relevant to seawater RO membranes, subjected to pressures as high as 7 MPa. Furthermore, a main question is the connectivity of the voids – specifically those truly separated from the feed side – to the permeate side. Without such connectivity the transport enhancement, due to roughness-increased surface area, is lost [169] (see further discussion in Section 3.4.2).

Are the voids bubbles? The exact mechanism leading to the formation of the nodular voids is not fully understood, and it is likely connected to the instabilities that transform a smooth film into a crumpled one (as outlined in Section 2.5 and Fig. 7). One interesting pathway to their formation may be due to the nucleation of nano-bubbles/droplets, which become incorporated into the forming polyamide film. Bubble-like structures evolving during IP have been observed *in-situ*, first by Yuan et al. [124] and, more recently, by Ukrainsky and Ramon [39].

In both cases, the bubble-like features were observed using optical microscopy at resolutions of several micrometers [39] to tens of micrometers [124] (see Fig. 8C and D), and were obtained for an IP process occurring at a free surface and for distinctly different amine chemistries (the reaction monitored by Yuan et al. [124] is considerably slower, while Ukrainsky and Ramon [39] used typical RO chemistry).

The formation of these bubbles has primarily been linked to either: (i) the temperature increase in the reaction zone during the highly exothermic polymerization reaction [39,58], which can lead to release of dissolved gas or possibly solvent boiling (see Fig. 8B), or (ii) the coalescence, into droplets within the organic phase, of water carried into the reaction zone by the diffusing amine [82,124,171]. It is interesting to note that the latter route to a porous film was already mentioned nearly 30 years ago and shown theoretically by Ji et al. [79], some 20 years ago, but has since received very little attention.

In contrast, the currently prevailing hypothesis of heat-driven bubble formation has received much attention in recent years. Most notably, with the idea that bubble formation is primarily due to release of dissolved CO_2 from the aqueous phase, a series of papers has systematically used carbonate chemistry to probe its influence on the morphology of polyamide films [58,71,168]. Several key findings may be highlighted from these papers: first, it was shown that degassing the aqueous solution resulted in reduced (though still substantial) surface roughness, with nearly complete elimination of 'ridge and valley' features [58]. Furthermore, it was shown that varying the initial pH of the amine solution led to progressively larger nodules, which then evolved into extended structures, overlaying the bottom, nodular voids [71,168]. These finding provide some support of the dissolved gas-bubble hypothesis – since CO_2 solubility is strongly influenced by both temperature and pH of the solution, which increase and decrease, respectively, during IP, potentially promoting gas release. We note, however, that the presence of carbonate may simply act as a buffer, much like 'acid scavengers', whose effect is explainable in the context of film growth intensity and associated instabilities, which can cause crumpling regardless of bubble formation. Another possible drawback of the gas bubble hypothesis lies in the fact that these bubbles are likely formed in the aqueous solution, whereas ultimately the voids are found within the film, formed within the organic phase. So, the bubbles formed in the aqueous phase must somehow migrate into the reaction zone, as the film is being formed, to become entrained in the final film. Due to density differences, the aqueous phase is normally underneath the organic phase, which suggests that bubbles form will tend to rise. It is, however, highly unlikely that gravitational orientation would provide a sufficient driving force for nano-bubble protrusion into the organic phase, therefore, another mechanism might be at play (see Section 2.5).

Configurational impacts on morphology: support membrane and spraying As a final consideration, and following the discussion on bubble formation, we look at recent studies that have shown how roughness may be altered and even eliminated by performing IP at a free surface (or a high surface area support) [60,61,125]. These studies added important insight on links between synthesis conditions and emerging morphologies. For example, under identical conditions, the presence of a support shifted the morphology from a smooth to a rough morphology [61] (see Fig. 9B). Similarly, with a relatively 'free interface', increasing monomer concentrations and reaction time likewise shifted the morphology from smooth to rough [60] (see Fig. 9C). Finally, changes in pH, controlled via carbonate chemistry, have been demonstrated as a route to creating varying degrees of roughness [71] (see Fig. 9E). These observations offer a clear indication pointing at the presence of interfacial instabilities, as described earlier (see Section 2.5).

Another feature, with important implications on transport, are the perforations observed in the support-facing, back side of the resulting film, which are mostly absent in a smooth film formed at a free interface [172] (see Fig. 9D). The presence of a support also relates to the question of bubble formation and entrainment, which may be partially explained based on the experiments of Song et al. [125], whereby the bubbles, once formed, are confined by the presence of the support and so grow toward the organic phase. The deformation due to this growth is thus a possible mechanism for creating crumpled morphologies that are highly connected to the permeate space. Switching the orientation, i.e., having the organic phase within the porous support, changes the morphology of the resulting film, while an unsupported membrane has virtually no prominent roughness features (under the same synthesis conditions in terms of monomer concentration). An interesting point to consider is that the confinement is equally absent in the

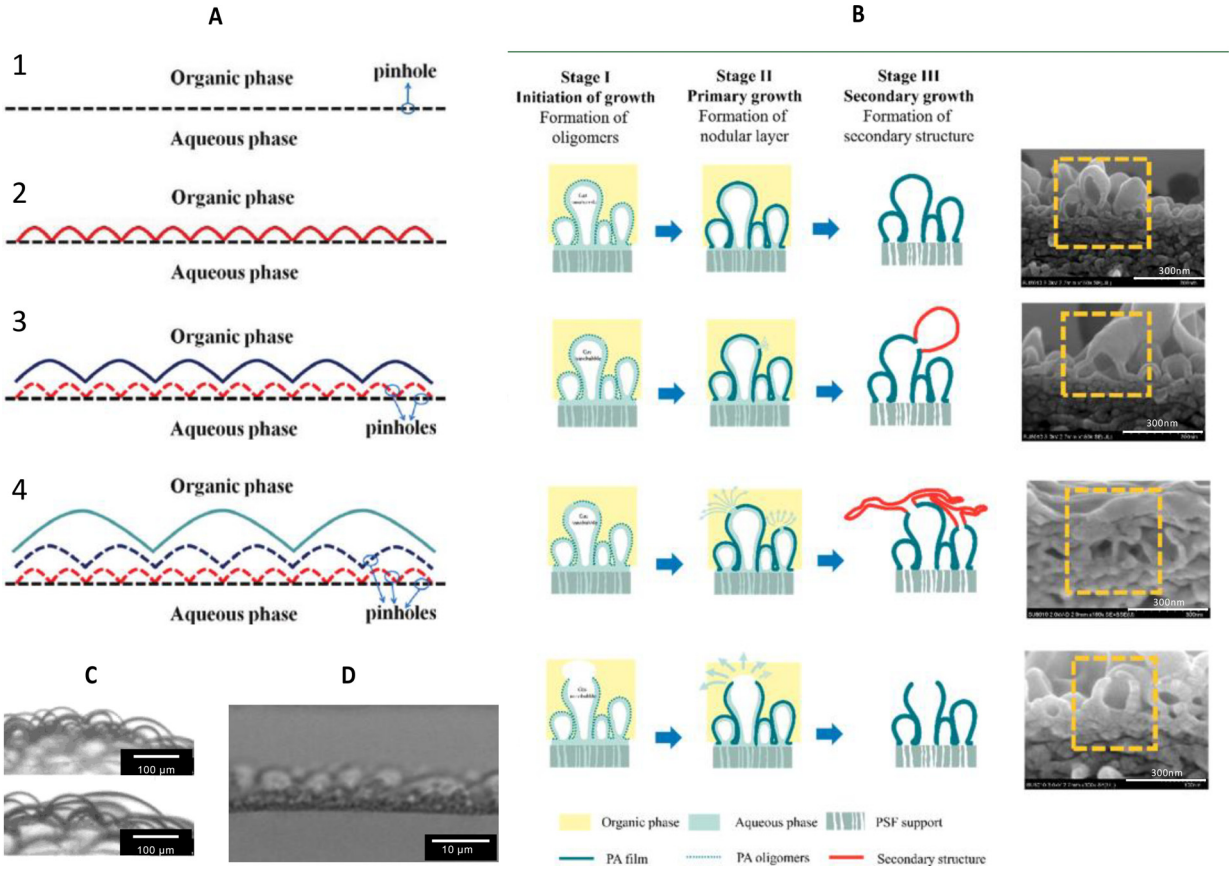

Fig. 8. *Possible pathways for generation of 'bubble-like' morphologies during IP, as well as 'self-healing of film rupture. A) Pinhole gaps and 'defects' in the initial film create sites for initiation of new, rapid growth, which creates hierarchical structures of subsequent polyamide layers.* [124]*, Copyright 2012. Reproduced with permission from the American Chemical Society. B) Gas bubbles, formed due to increased temperature in the reaction zone, lead to nodular structures. The resultant film may burst, creating defects which either remain or are capped by a secondary layer formed, on top.* [112]*, Copyright 2018. Reproduced with permission from the American Chemical Society. C) 'Bubbly' morphologies observed on the scale of 100's of microns.* [124]*, Copyright 2012. Reproduced with permission from the American Chemical Society. D) Bubble-like features observed, on the scale of under 10 microns.* [39]*, Copyright 2018. Reproduced with permission from Elsevier Science Ltd.*

'flipped' IP and the free-IP configurations, which would mean that film deformation due to bubble-induced deflection should be similar (in both cases, the organic phase is above the aqueous phase). The difference between the two cases, if indeed caused solely due to bubbling, is likely due to different rates of bubble formation and, primarily, different bubble size. Curiously, a similar study of 'flipped' IP [111] revealed a much smoother surface, with many holes; however, this may be due to incomplete support impregnation with the organic phase, or some other preparation difference between the two studies.

The configurational change offered by support-less IP may also be achieved using a hydrogel layer as the MPD reservoir [173], creating a continuous, relatively homogenous interface. Under these conditions, however, the MPD transport is significantly slower than the corresponding reaction at a 'free' surface. In contrast, when a heterogenous hydrogel was used, with a typical mesh size much larger than that of a conventional support membrane, the reaction proceeded faster and a thicker film was formed. The morphologies observed at short reaction times were quite different for the two systems, with the homogenous gel producing a seemingly smooth (though with creases that are likely due to experimental artefacts), while the heterogeneous gel produced morphologies more akin to those observed during standard, supported IP.

As a further means of controlling film roughness, spray-assisted IP has been used, in two different ways; either by spraying the organic phase over a conventionally MPD-soaked support membrane [174], or as a dual-spray combining droplets of both phases, simultaneously applied onto a support [175,176]. In the former case, a spray coating is first applied (droplet size on the order of tens of microns), followed by a 'conventional' immersion into the organic phase. The obtained morphology was a typical ridge and valley structure, where the first, spray-generated layer had small nodular features, while the second layer created larger roughness features. The second step was necessary in order to provide a continuous film, while the duration of the first step allowed some degree of optimization through control of the amount of initial polyamide formed. In particular, it is likely that, due to the lag-time between the two steps, the polyamide layer was equilibrated with the amine solution, providing a good starting point for the second step. In contrast, the more recent work by Chowdhury et al [175] and Ma et al. [176] used an electrospray system that applied the organic and aqueous phases simultaneously, presumably resulting in a very large initial surface area for reaction and, hence, good mass transfer properties. The method is able to produce smooth films with variable thickness, which depends on the number of coating cycles applied. The membranes produced in these two studies, while producing similar morphological features, achieved different performance, with the membranes fabricated by Chowdhuri et al. [175] on par with the commercial benchmark. While the monomer concentrations and support material varied between the two studies, it is highly likely that the different electro-spraying conditions are the crucial element here; the droplet size reported by Ma et al. [176] was on the order of 100 microns, while Chowdhury et al. [175] estimated a droplet size on the order of microns (this, how-

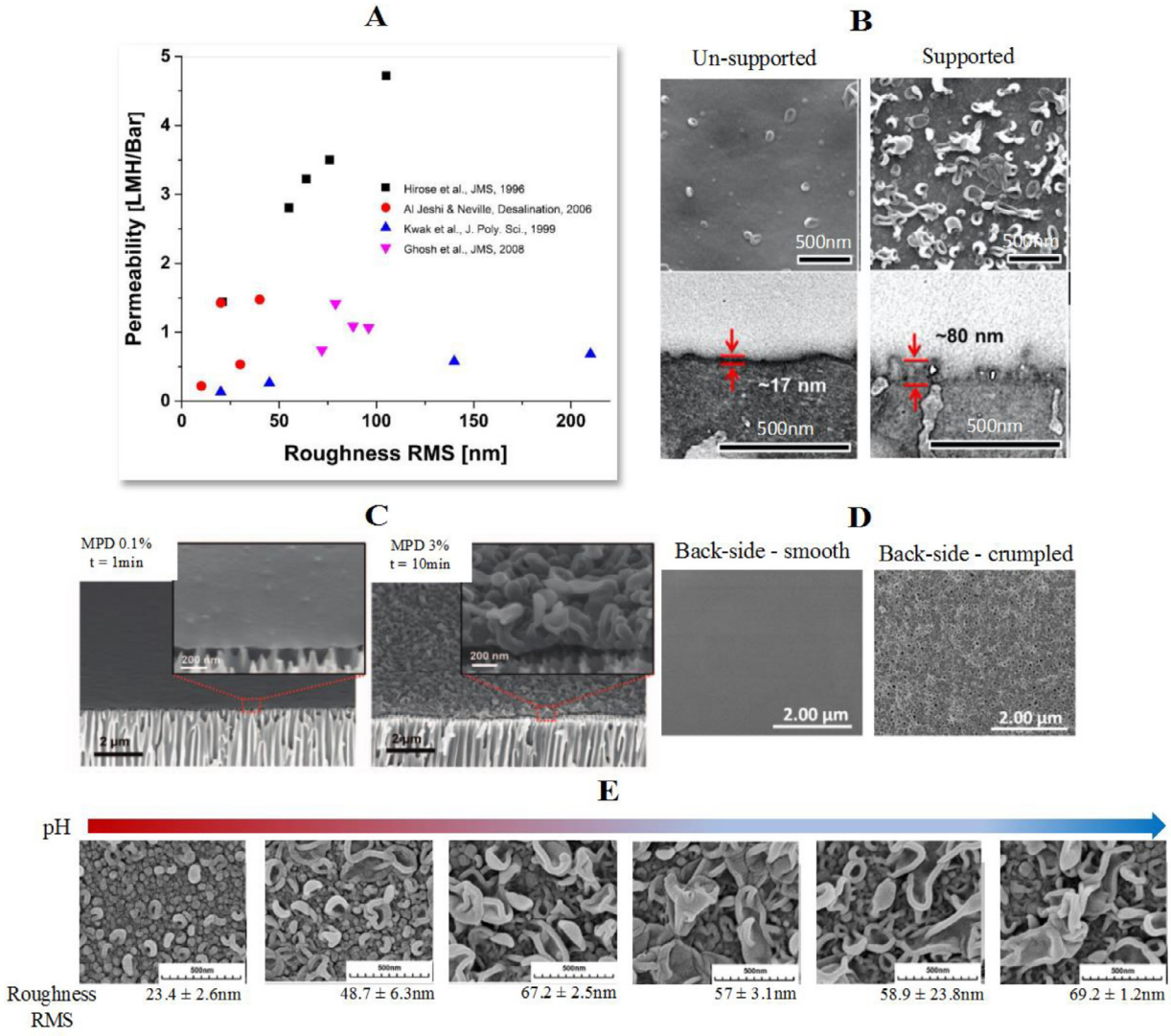

Fig. 9. *Morphology variations of polyamide thin films. (A) Collection of literature data showing attaempts to correlate roughness with permeance. Adopted from* [39] *(data from refs* [49,165–167]*. Copyright 2018. Reproduced with permission from Elsevier Science Ltd. (B) Transition from smooth (left) to 'crumpled' (right) morphology, due to the presence of the support. Scale bars are 500nm.* [61]*, Copyright 2017. Reproduced with permission from Elsevier Science Ltd. (C) Transition from smooth (left) to 'crumpled' (right) morphology due to variation of MPD concentration and reaction time.* [60]*, Copyright 2015. Reproduced with permission from American Association for the Advancement of Science. (D) View of the thin-film 'back', facing the support, for a smooth (left) and crumpled (right) morphology, showing the perforation accompanying 'crumpling'.* [172]*, Copyright 2017. Reproduced with permission from Elsevier Science Ltd. (E) Evolution of morphology with pH of the aquous phase, from a pH of 4.7 (far left) to 12.5 (far right).* [71]*, Copyright 2018. Reproduced with permission from the American Chemical Society.*

ever, was not measured). Droplet size is likely to be a crucial factor in establishing rapid reaction conditions, while maintaining a thin layer associated with each coating step. It is also notable that in this approach, especially, for finer droplet sizes, the rate of polymerization is controlled by the rate of electro-spraying rather than monomer diffusion into the reaction zone. On the one hand, it offers a better control and eliminates instabilities inherent of IP reaction, on the other hand, it no more features spontaneous self-healing of defects thereby transport and selectivity of such films may not be fully equivalent to films made via IP. The promising results of this technique then warrant a closer scrutiny of the mechanisms involved in a droplet-based process.

3.2. Physico-chemical characteristics

Along with geometric parameters that control membrane permeance, (e.g., thickness, area, and porosity), the inherent permeability and, to a greater extent, selectivity, are critically dependent on the physico-chemical characteristics of the polymer, such as polarity, fixed charge content, degree of cross-linking, and water content (swelling). Quantifying these characteristics has been crucial not only for optimizing the IP process and separation performance, but equally for understanding salt rejection and selectivity in general, which is still incompletely understood and not amenable to predictive modeling. Compared with morphological characterization, measuring the relevant physicochemical properties often requires the quantification of species representing only a small fraction of the polymer, which entails techniques with unique sensitivity and depth resolution. Methods that proved the most beneficial and insightful, along with key findings, are summarized below.

3.2.1. Cross-linking, charge density, and ionization behavior

Polyamide films produced by IP always contain some unreacted carboxylic and amine groups, which act as fixed charges that may enhance salt rejection [177]. It was also realized early on that, given the overall stoichiometry of the polyamidation reaction, fixed charge is also complementary to the degree of cross-linking, since a reactive group of a monomer is ultimately converted to a fixed

charge whenever it fails to form a polyamide bond, i.e., a cross-link [104,161,178]. Fixed charges are also believed to be a significant factor in fouling and biofouling [179–181], in which case the focus is on the surface charges rather than within the film [151,182,183]. Surface charges may also serve as anchoring points for modifying the surface properties via grafting [184–188]. For this reason, quantifying charge, its distribution and ways to manipulate it has been the focus of many studies.

The challenge of measuring the fixed charge of polyamide is due to the fact that results obtainable by different techniques are not directly comparable and three types of data are distinguishable, namely,

- Bulk charge density, i.e., the content of fixed charged groups per unit amount (mass or volume) of polyamide; this parameter is directly related to the Donnan ion exclusion mechanism and, therefore, salt rejection [177].
- Areal charge density, i.e., the total amount of ionizable groups within the polyamide layer per membrane area; in order to be relatable to performance metrics such as salt rejection, it requires additional information, e.g., membrane thickness, as explained below.
- Surface or bulk charge density, evaluated from transport or electro-kinetic measurements, such as streaming potential or electrical conductivity (impedance) measurements. These represent only a fraction of the total membrane charge involved in the relevant transport or electrokinetic phenomenon.

The first type of charge density is measurable by methods that analyze overall atom- or chemical group-composition such as XPS or RBS, which possess a depth resolution commensurate with the film thickness, i.e., less than about a micron. A few years following the discovery of aromatic polyamide membranes, Koo et al. presented an XPS study showing that 28% of the TMC units at the membrane surface contain an unreacted carboxylic group, i.e., lack one cross-link, which corresponds to a ~1.1 M charge density, assuming a polyamide density of 1.24 g/cm^3 [178]. Since the penetration depth of XPS is around 5 nm [135,149], this charge content is more representative of the surface characteristics, which left the open question whether this is representative of the average charge of the entire film.

Two decades later, Cahill and co-workers pioneered the use of RBS, another atom-counting spectroscopic technique with a much larger penetration depth, to obtain the overall fraction of charged groups across the entire thickness of polyamide, along with film thickness and other characteristics [148,149,161,163,189,190]. The accuracy was greatly improved by binding easy-to-count heavy ions to the fixed charges, thus enabling measurement of fixed charge at different pH so as to quantify dissociation behavior [149,150,163]. This showed that polyamide typically contains about 0.3–0.6 M of carboxylic groups, corresponding to 94–96% crosslinking, i.e., 8–15% TMC units missing a crosslink. Due to competition with proton binding at lower pH, the fixed charges become fully dissociated only at pH > 9, while at lower pH charges get protonated and lose part of their total ion-binding capacity. The majority of membranes show two pK_a values at around pH 5-6 and 8-9, assigned to different types of pores and, correspondingly, different local environments within the polyamide, as suggested previously by Kwak et al. based on PALS measurements of polyamide porosity [66] (see Section 3.1.1). The higher pK_a ~ 8-9 was assigned to the smaller, <0.25 nm, "network" pores within the dense polyamide. Conversely, the lower value of pK_a ~ 5–6 was assigned to larger >0.35 nm "aggregate" pores, formed during IP in interstices between the aggregated clusters of denser polymer. The smaller network pores constitute a significantly less polarizable, water-lean environment, leading to the higher pK_a, as common for low-dielectric media.

The second type of measurements is typically produced by binding suitable ions to the fixed charges and subsequently quantifying their total areal content directly or after leaching. Schaep and Vandecasteele employed Cs^+ ions that were bound and subsequently leached out, such that their content in the leachate could be accurately determined [191]. The areal charge density measured in this fashion for semi-aromatic membranes was of the order 10^{-5} mole/m^2 or ~10 charges per nm^2. This approach was improved and elaborated by binding cationic dyes to the surface, which can be directly quantified spectroscopically, and Ag^+ ions that could be analyzed after leaching; these methods produced areal densities commensurate with earlier estimates [192,193]. The resulting areal density can be converted to bulk charge density and degree of cross-linking, when the volume or mass thickness is known (see Section 3.1.1). Inverting such a relation, i.e., comparing the bulk and areal charge to estimate thickness may provide an estimated areal mass, i.e., mass thickness. For example, the bulk values reported by Coronell et al, 0.3–0.6 M per volume of dense polyamide (1.24 g/cm^3) [149,163], and the areal charge density 6-20 nm^{-2} found by Chen et al. [193] for SWRO membranes, indicate a film mass of ~10–100 mg/m^2, roughly equivalent to 10–100 nm thickness of dense polymer. Although the uncertainty range is fairly large, this agrees well with other estimates of the thickness and areal mass (e.g., [143,150]). The two types of measurement produce fairly consistent results for the overall charge, when combined with film mass.

Given the very different penetration depth of XPS (a few nanometers) and RBS (over a micron), Coronell et al. [193] applied both methods to analyze the difference between surface and overall charge density, i.e., the possible charge heterogeneity, for several commercial membranes. For a few membranes, XPS showed a somewhat larger charge, as might be expected for an IP process, where the outer surface faces a large stoichiometric excess of the acidic monomer TMC. However, surprisingly, about half of the examined membranes yielded nearly identical results via both methods, indicating that the charge density was fairly uniform across the polyamide layer. One reason could be that excessively acidic and therefore less cross-linked polymer at the surface was removed during sample preparation. Indeed, it was found that the areal charge drops after isolating polyamide films from commercial membrane and thus exposing them to organic solvents, which indicates that solvent treatment removes some loose and most charged fraction [193]. On the other hand, elemental profiling by electron energy loss spectroscopy STEM (STEM-EELS), particularly of N atoms, showed that both supported films in genuine composite membranes and free-standing films prepared in a controlled manner between two free liquid layers, have a fairly uniform elemental composition [6,147].

Apparently, without ruling out options such as the presence of a distinct coating layer, the charge distribution may depend on the preparation time and conditions that manufacturers may use to tune the chemistry of each specific type of membrane. For instance, the kinetic mechanisms outlined in Section 2.3 suggests that the incipient films are likely to be less charged, yet the subsequent diffusion-limited growth may tend to increase the surface charge. This is since the reaction zone, in which incipient film forms, inherently contains a stoichiometric ratio of monomers, however, subsequently, amine monomer diffusing across the film has to react with a large excess of TMC [22,43]. That could also explain the results of the early XPS study by Koo et al. [179] who reported a much larger surface charge and smaller crosslinking than all later estimates. Nonetheless, another likely reason for the relative chemical uniformity of polyamide layer is that, in many cases, it constitutes a structure composed of a crumpled or highly folded nascent film, only 10–20 nm thick. Thereby, surface or bulk analyses, even as surface-sensitive as XPS, nearly randomly sam-

ple various parts of the ultrathin nascent film or simultaneously probe several folded layers, essentially yielding average characteristics, also produced by RBS.

Recently, Ritt el al compared the areal charge density of commercial semi-aromatic polyamide NF270 membrane with several chemically identical but thicker non-porous membranes prepared via a layer-by-layer approach [164]. Similar to fully-aromatic RO polyamide layer, the semi-aromatic films featured two types of carboxylic charges with two pKa values. However, the amount of charges with the lower $pK_a \sim$ 4-5 was nearly constant and independent of thickness, while those with the higher $pK_a \sim 9$ correlated well with thickness. Given that all examined films were dense, this indicates that the more readily dissociated groups are manly located on the surface, where they face a more polar aqueous environment facilitating dissociation, while the inner bulk charges all have a higher pK_a. Based on this result, the same conclusion may apply to RO membranes, i.e., carboxylic groups with lower pKa belong to the surface of the folded nascent film rather than the aggregate pores or, alternatively, such pores are in fact meso- or nanoscopic voids. The main implication of this conclusion is that, since water and salt permeation is controlled by the inner properties of the dense nascent film (cf. MD results by Kolev and Freger [100]), low-pK_a charges are irrelevant for transport, while high-pKa charges would be inactive in the operational pH range. Indeed, a recent impedance study by Stolov and Freger demonstrated that in mid-pH range, where low-pK_a charges should come into play, the ion permeability of fully-aromatic polyamide films only weakly correlated with their nominal content, as measured by RBS [194].

The latter results suggests that the data, based on ion transport characteristics or surface electro-kinetics, may have a more direct relation to membrane performance or, particularly, fouling propensity, since the relations between charge and ion transport in membranes are still poorly understood and much of the nominal charge may be associated and inactive [177,194]. Converting such data to an *effective* charge density using available models may lead to major inconsistencies. For example, Schaep and Vandecasteele [191] evaluated the areal charge density using titration and streaming potential and bulk charge density using membrane potential measurements for several NF membranes. Taking as an example their data for semi-aromatic NF40 membrane and assuming a 50 nm-thick polyamide layer as representative for this membrane type and a permeability of 4 LMH/bar, the reported data translates to the largely disparate equivalent bulk charge densities of 0.6 M, 0.001 M, and 0.0004 mM for titration, streaming potential and membrane potential, respectively. Clearly, only the first number agrees with later RBS or XPS measurements. The obtained discrepancy indicates that the effective charge that controls transport is very different from the nominal, chemical composition-based RBS values. Most likely, the standard ion rejection mechanism, i.e., relation of rejection to nominal charge, calls for a thorough reassessment [177]. Comparing different types of charge measurements will be crucial for developing better models that can guide future membrane design.

3.2.2. Water uptake and swelling

The water-swollen state of polyamide films most closely represents their working conditions. As a small molecule, water readily fills voids within the polyamide (aggregate pores) as well as most free volume (smaller network pores). Therefore, the water content of polyamide membranes plays the role of porosity and, as such, is expected to correlate with water permeability (cf. Eq. 6). Water-filled pores are also pathways for transport of small solutes and, in addition, the water fraction has a strong effect on exclusion of ions, membrane affinity towards various solutes and their convective drag (if significant) by permeating water. Water uptake, or swelling, is therefore critical for understanding the selectivity and permeability of polyamide membranes.

Before the advent of modern ultrasensitive techniques, Arthur [27] measured the water uptake by aromatic polyamide by weighing aromatic polyamide powder, dry and exposed to near-saturated vapor, which showed a water content of about 40% at saturation. Later, more accurate measurements of water uptake using films isolated from commercial membranes or synthesized *in situ* and exposed to saturated or near-saturated vapor, produced generally smaller values. For instance, using a QCM, Liu et al reported ~30% water uptake by isolated commercial films [195]. Microgravimetric measurements of the entire vapor adsorption isotherm for both *in situ*-prepared and isolated commercial films reported by a Lee at al. [196] showed a somewhat smaller but comparable uptake that extrapolated to about 18–25% at saturation. These numbers agree with MD studies that indicated a content of 23–30% in water-equilibrated polyamide [92,98,99,197].

However, measurements of volume expansion (swelling) by the AFM-based scratch method [45,109] andmore accurate deflection measurements by Zhang et al. [198] demonstrated that the polymer volume expansion upon swelling in water is much smaller, on the order of 3–12%. The MD study of a dry and water-equilibrated polymer by Kolev and Freger [99] supplied possible clues explaining these discrepancies. The simulations show that water readily fills the nano- and mesoscopic voids within the polyamide layer (Fig. 3B), which significantly increases the overall polyamide mass yet produces only small volumetric expansion of the dense and rigid matrix surrounding the voids and forming the structural skeleton of the film. The polyamide may then gain much weight but exhibits only slight dimensional changes. If the voids do not form a contiguous network across the entire film, water within voids would have little effect on permeability and selectivity. Recent high-resolution imaging and elemental mapping (see Section 3.1) indeed shows that this is apparently the case, as the dense polymer appears to encase most observed small voids in tight RO membranes. On the other hand, in 'open' membrane types, more voids correlate with a larger permeability. These observations are consistent with the mechanism of IP, which terminates or slows down significantly only after a dense film is formed and blocks monomer permeation (see Section 2.3). When this 'blocking' sublayer increases in resistance, the relative contribution of the nano-voids surrounding the blocking part to the overall resistance and selectivity drops progressively. This is expected to be even more prominent for larger voids, formed when the film gets crumpled in the process (Section 2.5). The ultimate conclusion is, again, that the effective thickness of the polyamide is equivalent to a dense film, whose thickness is only a small fraction of the total superficial thickness. This point was perhaps most convincingly demonstrated by Jiang et al. who prepared ultrathin sub-10 nm films and showed that their water permeability was similar to much thicker polyamide layers of commercial membranes [33].

The above results also suggest that the water fraction pertinent to transport must be that of the dense polymer, rather than the overall water mass uptake. Accordingly, the volumetric expansion or swelling, e.g., as measured by AFM, rather than the much larger mass gain, should be the more appropriate measure of water uptake. Indeed, Dražević et al. found that that swelling of isolated polyamide films measured by AFM led to a reasonable correlation between swelling (water fraction) and intrinsic thickness-normalized water permeability, in agreement with earlier data [45,109]. To address the membrane porosity, this study employed two methods to evaluate thickness: ATR-FTIR spectroscopy quantified the polyamide areal mass and AFM measured superficial thickness as the height of a narrow strip. The combination of the two measurements also evaluated the film poros-

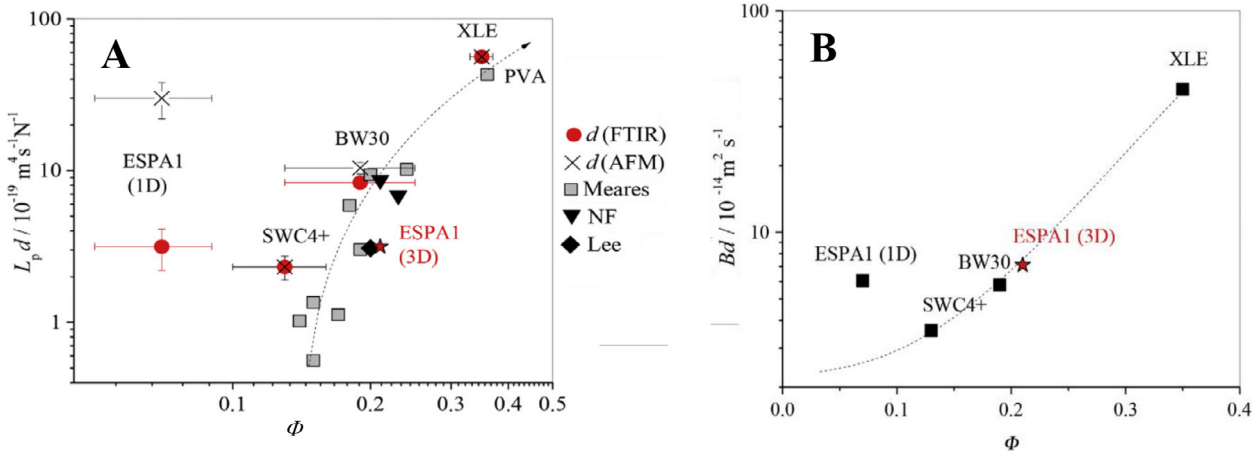

Fig. 10. *(A) General correlation between intrinsic water permeability $L_p d$ and water volume fraction Φ in polyamide for different RO membranes. Water fraction Φ was evaluated as the difference between dry and wet thickness of isolated films on a solid substrate was measured by AFM and normalized by the wet thickness d. The crosses and red circles represent permeabilities normalized by d taken as AFM-based wet thickness and FTIR-based spectroscopic thickness, respectively. The previous data for semi-aromatic NF films [45], fully aromatic polyamide film reported by Lee at al. [196], and for homogeneous cellulose acetate and poly (vinyl alcohol) films reported by Meares [199] are shown for comparison. (B) Correlation between intrinsic salt permeability Bd and water fraction Φ, d being spectroscopic thickness for different RO membranes. In both plots the star is the results for the ESPA1 membrane based on spectroscopic thickness and water fraction tripled (3D swelling). The dotted lines indicate the general trends. [109], Copyright 2014. Reproduced with permission from Elsevier Science Ltd.*

ity, which could differ by as much as an order of magnitude, being largest for the more permeable BW membranes and smallest for tightest SW membranes, in agreement with TEM tomography reported by Pacheco that visualize voids and void fraction in different membranes [144]. Dražević et al. concluded that the most appropriate thickness, δ, for converting water permeance, L_p, to intrinsic water permeability, δL_p, for correlating permeability with swelling was the "spectroscopic", mass-based thickness evaluated using FTIR rather than the larger superficial (volume) thickness measured by AFM [109]. Fig. 10A summarizes the resulting permeability-swelling "master" correlation for different RO membranes, which agrees well with results for homogeneous cellulose acetate films compiled by Meares [199]. Curiously, the most permeable and porous ESPA1 membrane strongly deviated even from such corrected "master" relation. Given the particularly large, >90% porosity of this membrane, as indicated by a 10-fold difference between the volume (AFM) and spectroscopic (FTIR) mass thicknesses, a highly folded polyamide film may swell in a different manner compared to other, denser membranes, exhibiting equal expansion in all dimensions. In this case, expansion in thickness would only represent ~1/3 of the total swelling; indeed, multiplying AFM-based swelling by a factor of 3, ESPA1 results move well within the general trend shown in Fig. 10A. In addition, the difference could also be partly related to the crumpling and increased surface area of the polyamide layer of ESPA1, significantly exceeding the footprint area used to normalize L_p (see Sections 2.5 and 3.2.1).

The fact that different films follow a general correlation between intrinsic permeability and swelling suggests that the effect of swelling on permeation of water molecules is mainly geometric. Essentially, a lower water fraction appears to mainly reduce the permeable area and increase the tortuosity of the percolation paths, while the mobility of water molecules remains bulk-like even in smallest pores and down to small degrees of swelling. MD simulations [90,92–94,98,99] and water mobility probed by advanced techniques such as QENS [200–202] reveal subtle differences in mobility for different states of water and co-existence of several water diffusion regimes within polyamide structure. Yet, overall, they collectively produce an average mobility reasonably close to that of bulk water within typical uncertainties of measured permeability and estimates of effective thickness.

3.3. Nanomechanics of polyamide films

Mechanical properties of polyamide layer are of interest in several contexts. First, in relation to functioning as a semipermeable barrier, the rigidity of the polyamide controls its swelling (water uptake) and thus permeability and selectivity. Mechanical properties also impact membrane robustness when packed into modules, stability during operation and cleaning, sensitivity to presence of chemicals or particulates in the feed flow, and membrane longevity in general.

Khare et al. [35] adapted, for mechanical measurements, the pendant-drop setup used earlier by Chai and Krantz for real-time tensiometry-based monitoring of IP kinetics [36]. In these experiments, a film was first formed around a pendant drop and, subsequently, was strained by injecting a predetermined liquid volume into the drop volume and monitoring stress changes or observing film rupture. Such experiments allowed measuring the elastic modulus, rupture strength and relaxation behavior. This approach was also employed by Roh et al., who found that for films thicker than ~100 nm, formed after 2 min of reaction at monomer concentrations exceeding 0.0025% TMC and 0.01% MPD), the film rupture pressure was linearly dependent on the superficial thickness, measured by profilometry. This translates to a roughly constant rupture modulus of 37 MPa, representing in-plane rigidity. Notably, the modulus is about an order of magnitude smaller than the yield strength of Nomex (~300 MPa [203]), a linear analogue of the MPD-TMC-based polyamide; the much lower rupture strength is likely indicative of a significant film porosity and amorphous structure lacking crystallinity of Nomex. Such a constant thickness-normalized rupture modulus suggests that films thicker than 100 nm had uniform mechanical characteristics and, hence, likely similar porosity. In contrast, the flux and selectivity of these films exhibited a weak dependence on the measured thickness, i.e., in terms of transport resistance, the films had about the same effective thickness, consistent with the conclusion (see next section) that a small fraction of the layer, or a crumpled thin film, determines its transport properties. On the other hand, films thinner than 100 nm, prepared using lower monomer concentrations, showed a progressively lower thickness-normalized rupture modulus, along with lower salt rejection. Based on the model of Section 2.3, these results seem to manifest the reciprocal relation between the monomer concentration and the time t_0 required to

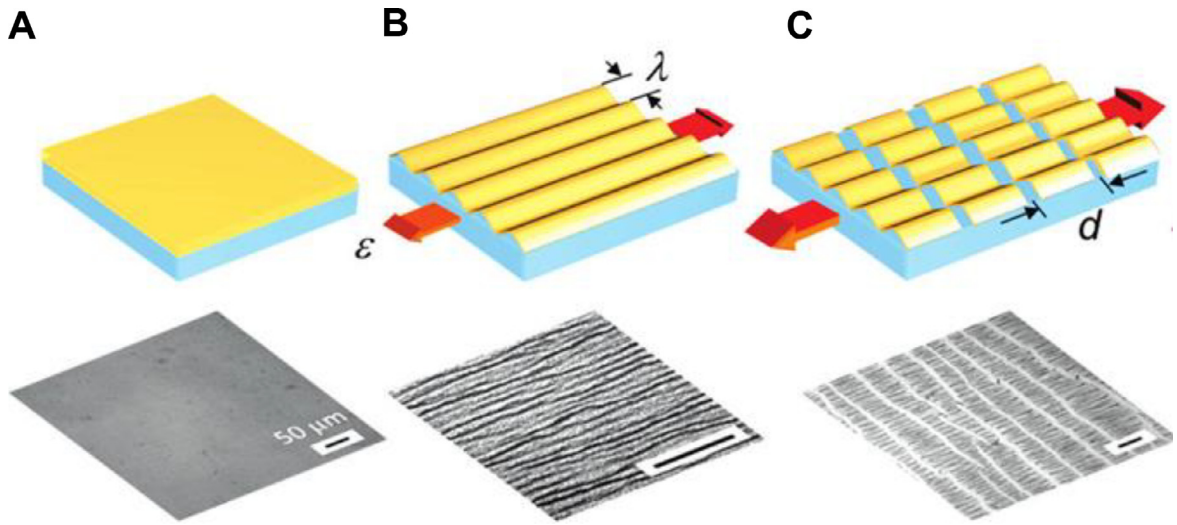

Fig. 11. *Overview of the combined wrinkling-cracking method: (A) a thin rigid membrane on a soft elastic substrate; (B) longitudinal wrinkles induced by uniaxial stretching generating a strain ε, characterized by a wavelength λ; (C) transversal cracks, of length d, developed when the applied strain exceeded failure strain. The bottom row represents an optical microscope images of the aromatic polyamide layer of a reverse osmosis membrane on a poly(dimethylsiloxane) substrate. Scale bars are 50 μm.* [204], *Copyright 2011. Adopted with permission from American Chemical Society.*

complete the initial dense barrier formation. Since Roh et al. fixed the reaction time at 2 min, the thicker films contained a well-formed dense barrier and the growth could proceed well in to the second stage, resulting in a thicker and perhaps more crumpled (i.e., multilayer) film of relatively uniform porosity and mechanical characteristics. Conversely, at lower monomer concentrations, the reaction rate was apparently terminated before the polymer density and crosslinking could reach the maximum, resulting in a mechanically weaker, thinner and less selective layer.

An elegant alternative technique, termed surface wrinkling, particularly suitable for measuring both stiffness and rupture strength of rigid ultrathin films such as polyamide films, was developed by Stafford and co-workers [204]. In this method, a free-standing film is fixed on top of a soft elastic PDMS substrate and, thereafter, substrate stretching causes formation of longitudinal wrinkles, whose spacing as a function of applied strain is uniquely related to the film stiffness (Fig. 11A). Furthermore, when longitudinal strain exceeds the rupture strain, transversal cracks emerge and grow denser as applied strain increases. Extrapolation of applied strain vs. crack spacing then yields the rupture characteristics (Fig. 11B). This approach yielded a rupture strength, for the polyamide layer of a SWC4+ membrane, of ~65 MPa, which is reasonably close to the pedant drop results, given inevitable uncertainties of estimated thickness and porosity [34,35]. It also confirmed that chlorine attack causes stiffening and reduced rupture strength of polyamide. Notably, the strain that marks onset of rupture, ca. 14%, is significantly larger than the yield strain of Nomex fibers, ~2-3% [203]. Since crosslinked polyamide is expected to be less ductile than linear and semicrystalline Nomex, the failure of the former, i.e. appearance of cracks, at a much larger strains may be due to partial unfolding of the crumpled film, which involves disruption of much fewer bonds or weaker adhesive forces, before the crumpled film straightens up and ultimately ruptures.

More recently, the wrinkling method was employed by Karan et al. to investigate the changes occurring in polyamide films during IP synthesis, including the changes over time, not addressed in Roh et al.'s pendant drop study [60]. Most notably, it was observed that when the time of IP reaction (for 0.1% MPD in water and 0.005% TMC in hexane), yielding a planar non-crumpled film, increased from 1 to 10 min, the superficial film thickness increases only slightly, from 7.5 to 8.4 nm. However, film stiffness evaluated by surface wrinkling increases 3-fold, from 0.9 to 2.7 GPa, which is also consistent with a 3-fold increase in areal mass measured by QCM. This is equivalent to the estimated film density increasing from 0.56 to about 1.4 g/cm^3, comparable with the density of the chemically similar but non-porous linear polyamide Nomex, 1.38 g/cm^3. According to the model of Section 3.2, this growth may be understood as densification and thickening of the thin barrier *within* the nascent film, in which polyamide initially constituted only a fraction of the film, but after 10 min filled its entire volume.

3.4. Transport characteristics

3.4.1. Barrier properties towards water and salts

The use of polyamide as the selective barrier in desalination membranes is based on two key characteristics, namely, a high water permeability and a low permeability to salt. The two are usually expressed as respective permeances, A and B [205]. These coefficients are normally deducible from standard filtration tests based on the measured water flux and salt rejection at a given applied pressure. Since they both inversely depend on the membrane thickness, the corresponding intrinsic permeabilities, genuine material characteristics, are obtained by multiplying A and B with δ, the effective membrane thickness. The ratio A/B or its dimensionless counterpart, $(A/B)RT/V_w$, where V_w is the molar volume of water, is a material property as well. It quantifies the selectivity, with the dimensionless ratio currently reaching about 10^5 for the tightest seawater membranes [205].

Measurements of barrier properties A and B, under different conditions, help clarify the mechanisms governing transport and selectivity and understand the physical basis of the outstanding performance of fully aromatic polyamide membranes. However, such measurements may also shed much light on the membrane structure due to the sensitivity of barrier properties to fine structural and morphological details that may elude even the highest-resolution microscopic and spectroscopic methods.

Different studies have generally agreed that transport of water molecules within polyamide occurs mainly by molecular diffusion. Since water is a small molecule and polyamide is abundant in hydrophilic sites, transport of water molecules within polyamide does not encounter kinetic barriers significantly different from self-

diffusion in bulk water. The mobility of water in polyamide is then mainly controlled by geometry, i.e., porosity and tortuosity of the space occupied by water, both of which correlate with polymer swelling (see Section 3.2.2).

Compared to water transport, the mechanism of salt transport is inherently more complex and shows a larger sensitivity to fine structural details. At present, the mechanism of salt transport and rejection is still actively debated and extensively researched [205,206]. It is complicated by the existence of at least three possible physical mechanisms of ion exclusion and the fact that salt transport involves coupled permeation of at least two ionic species, namely, the anion and cation [177]. Salt transport is also noticeably dependent on solution composition, which requires more elaborate measurements and more involved modeling [207–211]. Nevertheless, there is a strong physical basis and sufficient evidence that the dielectric and steric mechanisms are the main contributions responsible for ion rejection in RO [137,205,212–214]. Both critically depend on the pore size and are greatly enhanced when the pore size approaches the ion size [212,215], which is most closely realized in dense, rigid and weakly hydrated polymers. Although it has been long believed that fixed charges within the polymer play a large role (Donnan exclusion), recent analysis of the dependence of salt permeability and conductivity on the fixed charge indicates that this effect is fairly moderate in RO membranes [194], though it is apparently stronger in NF membranes [216,217].

Since exclusion and permeation of all ions is coupled through electroneutrality, the value of salt permeance B lumps cation and anion permeances B_+ and B_-, e.g., for monovalent salts such as NaCl, $B = 2(B_+^{-1} + B_-^{-1})^{-1}$, and it alone supplies incomplete information. However, decomposition of B to B_+ and B_- is possible through complementary measurements of ionic conductivity. Such measurements are best performed using impedance spectroscopy of free-standing films supported on a solid electrode and immersed in an appropriate salt solution [153,194,218,219]. The measured areal conductivity G is proportional to the sum $B_+ + B_-$ and, similar to B, must show an inversely relation to the effective thickness, similar to the water permeance. Indeed, the measured conductivities of high-flux ESPA1 and tight SWC1 membranes differed by about the same factor as their A values, as expected for films of the same polymer differing only in the effective thickness and/or area [155].

Although conductivity, G, or salt permeance, B, of different membranes may be useful as a relative measure of effective thickness, these still cannot reflect the absolute effective thickness, i.e., equivalent thickness of a hypothetic dense polymer, without a representative reference material. As an appropriate reference, Fridman-Bishop and Freger considered chemically similar poly(m-phenylene isophthalamide), known as Nomex, that may be cast as dense films of a well-packed non-porous structure resembling the densest polyamide fragments within RO membranes (see Section 2.4) [32]. Remarkably, the conductivity of Nomex up to NaCl concentrations $C \sim 1$ M at pH < 6 showed unusual dependence and scales as $C^{1/2}$ (see Fig. 12). This was explained by the $\sim 10^3$ times larger affinity of polyamide to H^+ compared with Na^+, whereby the polymer takes up Cl^- anions along with H^+, rather than Na^+ [220]. Fig. 12 shows that the SWC4 RO membrane exhibited a $C^{1/2}$ dependence as well, however, its conductivity was two orders of magnitude higher than that of Nomex films of commensurate thickness (~100 nm). Although the intrinsic conductivity of the polyamide layer in RO membranes, even in its densest part, may still be somewhat higher than in well-packed, dense, and semicrystalline Nomex, this result suggests that the barrier properties of RO membranes are equivalent to a few nanometers-thick film of a dense and nearly neutral polyamide. This conclusion again agrees well with the polyamide layer being essentially a crumpled or folded ultrathin 10–20 nm films (see Sections 2.5 and 3.1).

It is important to note that the characteristics of the ultrathin barrier films are not necessarily identical and may somewhat vary between membranes. Indeed, films having different thicknesses, i.e., permeance A, but identical intrinsic properties, are expected to show the same selectivity A/B. However, Fig. 3B, summarizing the permeability-selectivity relation for many commercial polyamide membranes shows that selectivity varies widely. The primary reasons may be widely different defect rates or the effects of the supporting layer or varying degrees of nascent film folding, i.e., surface area (see next). Yet, different RO membranes may also vary in swelling, thereby more swollen, i.e., more “open” (and, hence, more permeable) membranes also have a larger salt permeance B and so are inherently less selective [45,109]. For example, Fig. 10B presents the results by Drazevic et al [109], showing a strong dependence of the thickness-normalized salt permeability, $B\delta$, (based on spectroscopic mass thickness) and membrane swelling, complementary to the similar correlation for water permeability in Fig. 10A. The differences may arise from adjustments to the IP process introduced by manufacturers, increasing permeability at the expense of selectivity. For example, large variations of the reaction time may modify the intrinsic barrier characteristics of polyamide. As explained in Section 2.3, initial formation of the dense barrier is followed by diffusion-limited growth that increases its thickness. During the latter stage, diffusing and reacting monomers may keep densifying the barrier by filling and blocking the residual interstitial free volume. Such blocking will tend to first eliminate the most accessible, larger pores, and this will progressively reduce both the average and maximum pore sizes. This will tend to more greatly affect B, which is more sensitive to the pore size than A. A similar result may be obtained by a post-treatment that blocks the pores or modifies the intrinsic properties of the polymer [221,222]. The effect of post-treatment may also be opposite as well; for instance, depending on the conditions and time, chlorination may either increase or decrease hydrophobicity of polyamide and thus increase or decrease its selectivity [194,223].

3.4.2. Impact of nanostructure on transport

In the ‘traditional’ view of membrane transport, the membrane is viewed as a homogenous, smooth, contiguous film. The reality of polyamide films is far from this ideal image. It is long known that these films can be extremely uneven and roughness features may have an amplitude that is far greater than the apparent average thickness of the film. Furthermore, recent evidence from the past 5 years has shown that the ‘effective’ film is in fact a ‘crumpled’ and/or nodular structure of a much thinner polyamide film (as discussed extensively in previous Sections 2.5 and 3.1.2). With much improved resolution and careful use of electron microscopy imaging techniques (both SEM and TEM) it has been shown that the structure of aromatic polyamide membranes contains distinctive voids (see, for example, [110,113,144,146,170,224]). More importantly, these voids have been found to be in direct connection with the permeate space via holes easily detectable upon examination of the polyamide layer facing the support (see schematic in Fig. 13a). While it is not clear yet to what extent this connectivity persists and what controls it, experiments have demonstrated that these holes lead into closed cavities – when tracers were introduced into the membrane from the support side, they were captured within the voids (seen by TEM, Fig. 13b), thus proving that the voids were connected to the permeate space [112,225].

The impact of this morphology on transport, traditionally modeled as that through a homogenous layer, is yet to be fully scrutinized theoretically. Two reported attempts at modeling transport through composite membranes, including the presence of voids, were published by Wong et al. [169] and Lin et al. [226]. In these, voids were considered to be as regions within the film, in which

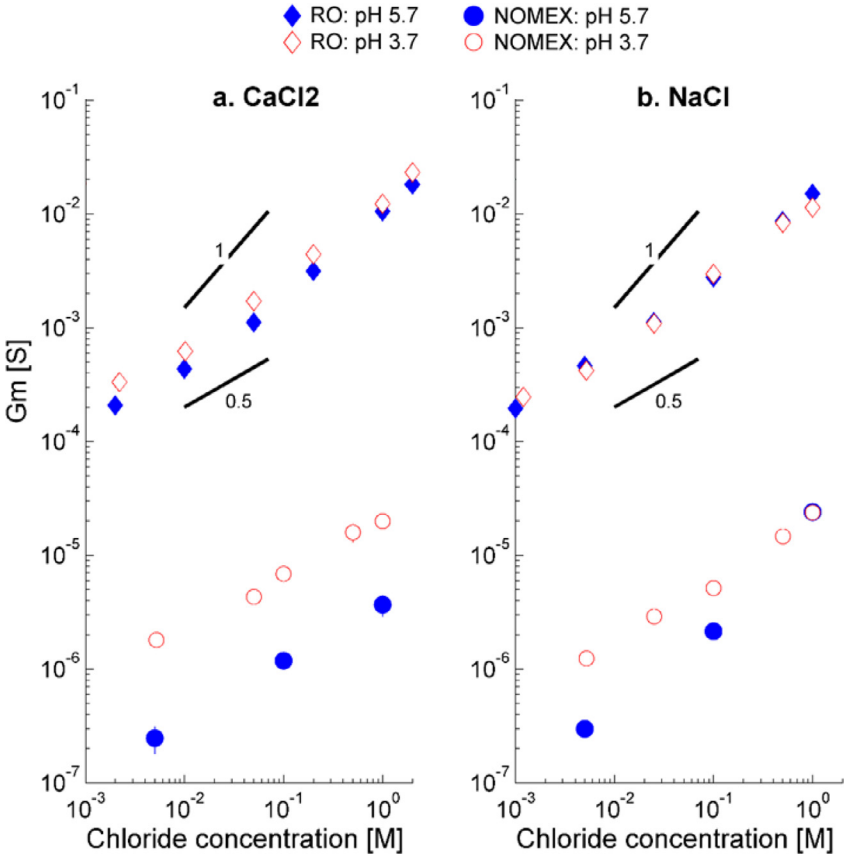

Fig. 12. *Conductance G_m of polyamide films on a solid electrode vs. salt (chloride) solution concentration in $CaCl_2$ and NaCl solutions at pH 3.7 (0.2 mM HCl added) and 5.7 (no HCl added). The RO film was isolated from a SWC5 membrane (Hydranautics) and Nomex film was cast on the electrode from a Nomex solution. Membrane area 0.071 cm^2.* [32],*Copyright 2017. Adopted with permission from Elsevier Science Ltd.*

the diffusivity is large compared with that of the surrounding material, and accounting for the void fraction within the film. Wong et al. [169] also considered the presence of support pores and their locations relative to an undulating, void-containing film. The support layer has been shown to strongly affect the observed transport characteristics of composite membranes (see, for example [227–230,234–240]). The results obtained by Lin et al. [226] led to the conclusion that the intrinsic transport properties of the film (i.e., the actual diffusivity of the permeating species within the polymer) dominated over partitioning or morphological features of the film. Nevertheless, these results indicate that converting membrane footprint area-normalized permeances such as A (L_p) or B to intrinsic characteristics, e.g., estimating r_p from L_p and Eq. (6), has to account for correct morphology corrections, i.e., true rather than superficial thickness and permeation area.

The model framework, however, did not consider void connectivity, position within the film and, most importantly, their communication with the permeate space. When these are considered, it was shown by Wong et al. [169] that film permeance may be substantially affected by morphology. Specifically, a 'crumpled' structure with a voids open to the permeate space (as seen in images of the perforated back-face of the polyamide film, see Fig. 9d) exhibits a positive correlation with film roughness, due to increased contact area with the feed solution [169] - a long-debated issue in the literature, where inconsistent impact of roughness on permeance has often been reported. These calculations show that when interconnectivity results in a greater effective surface area for transport, this quite intuitively leads to enhanced permeance (see Fig. 13c). In contrast, when no connectivity exists roughness has a weak effect on permeance. Further, a similar modeling framework had previously shown that, treated as a continuous film, roughness will only reduce permeance [232]. This serves as an illustration that creating such morphologies, in a controllable manner, is a desirable strategy for making more permeable membranes.

4. Putting the puzzle together

4.1. What makes a perfect membrane: combining chemistry, morphology and mechanics

The quest for the best performing membrane - highly permeable, selective, and robust - has not always been driven by solid, theory-driven rationales and has undergone many trials and errors. Nevertheless, extensive research and insight developed over the last few decades enable the formulation of key criteria that, when combined, could define the best membrane. First, a high *selectivity*, i.e., a low ratio of salt and water permeabilities, is a prerequisite. Mechanisms such as steric and Donnan exclusion have been long believed to control selectivity. However, as recently clarified, the dielectric mechanism, i.e., the high energetic cost of ion dehydration un-compensated by solvation within the membrane, is apparently key to achieving the required level of selectivity for SWRO membranes (currently $\sim 10^{-5}$) [205]. Common past misinterpretations may have stemmed from the fact that the dielectric and Donnan exclusion may show a similar dependence on ion charge [207,212], while the dielectric and steric mechanism share a sensitivity to pore size [215,233].

Maximizing dielectric exclusion sets two main requirements: low polarity of the polymer and the smallest possible 'pore' size.

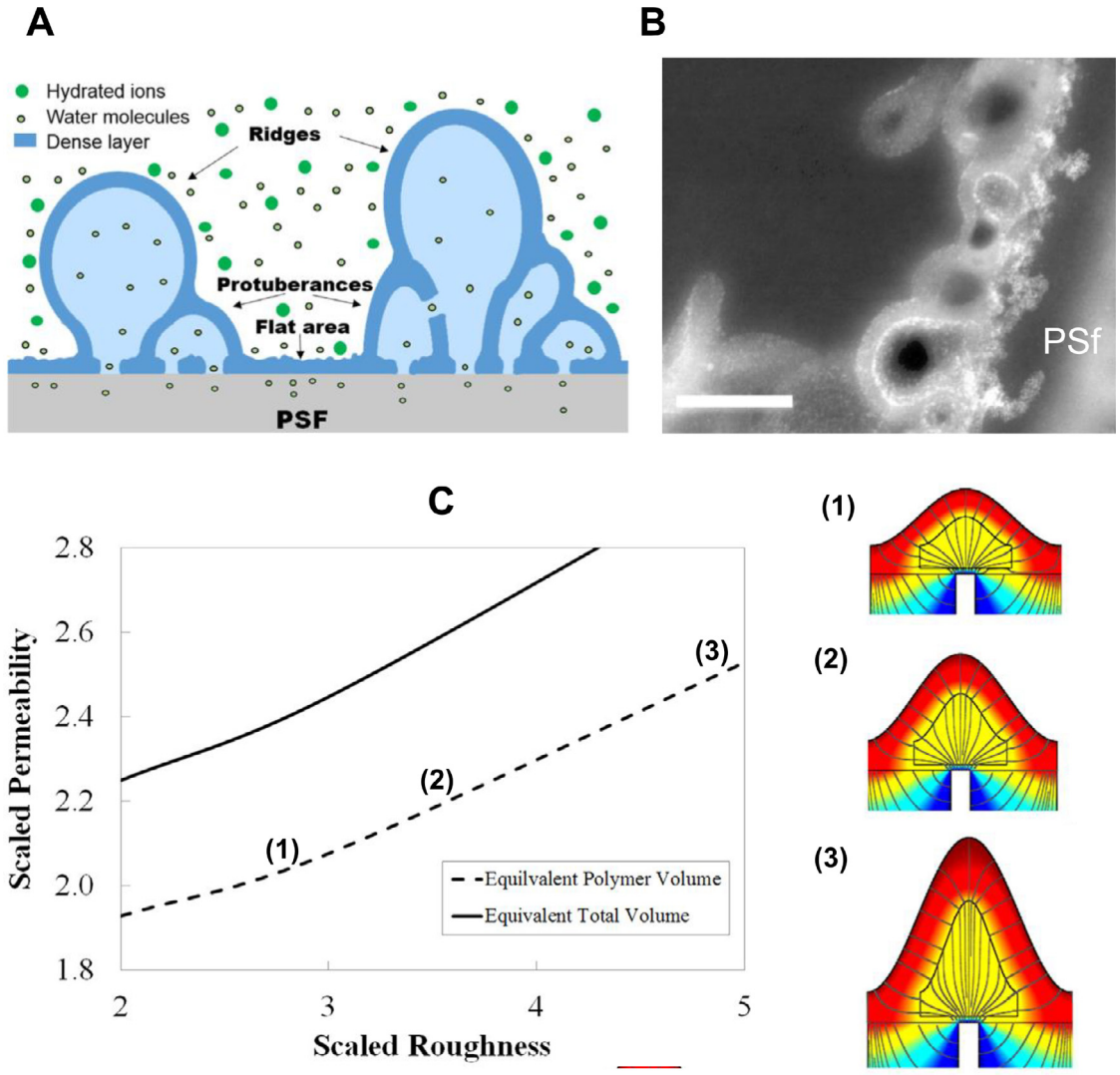

Fig. 13. *Effect of polyamide morphology on transport. (a) Schematic representation of the 'voids' within the crumpled structure of a polyamide thin film, highlighting the potential connectivity between the inner volume of the voids and the permeate space. [111], Copyright 2015. Reproduced with permission from Elsevier Science Ltd. (b) Electron microscopy visualization of flow-path connectivity. Nanoparticles are shown, deposited on the inner surface of the voids while been filtered with the flow coming from the support side into the feed. [225], Copyright 2017. Reproduced with permission from Elsevier Science Ltd. (c) Positive correlation between roughness and permeance, based on model calculations of transport through a film containing voids with good connectivity with the permeate space. [169], Copyright 2016. Reproduced with permission from Elsevier Science Ltd. Marked points on the figure refer structures appearing on the right, showing the calculated transport pathways and concentration field. [231], Copyright 2019. Reproduced with permission from Elsevier Science Ltd.*

These requirements are interrelated, to some extent, since both overall polarity and effective pore size are controlled by water entering the polymer when it swells. As water tends to cluster and form molecular channels, these clusters play the role of a pore network or transport pathways for both water and ions. However, additional factors, such as polymer rigidity, usually controlled by backbone stiffness and crosslinking, may reduce the propensity for clustering and partly decouple it from the degree of swelling. As early as 1977, Strathmann and Michaels [234] noted that reduced water uptake is beneficial for selectivity, however, polymers with similar water uptake may still significantly differ in selectivity, which correlated well with differences in clustering. Excessive clustering is analogous to an increased pore size; within larger water-filled pores, significantly exceeding the size of salt ions, dielectric and steric exclusion would be significantly weakened [212,233]. Suppressing overall swelling and reducing average cluster (pore) size is, then, essential for maximizing selectivity. A dense and rigid matrix that effectively prevents both swelling and clustering of water will be most beneficial for increasing selectivity. However, in a matrix that is too hydrophobic and totally lacks hydrophilic sites, water uptake may be so low that water will be unable to form a connected, percolating network, which will lead to impractically low *water permeability*. Therefore, the best combination seems to be a dense matrix that is *both* rich in mildly hydrophilic groups, capable of binding water molecules, *and* possesses a highly rigid structure that prevents excessive hydration and clustering. This requirement should be fulfilled by selecting the appropriate chemistry, inherent polymer rigidity and degree of crosslinking.

The downside of increasing polymer density and rigidity is that suppressed swelling also reduces water permeability, though not as much as salt permeability (cf. increased selectivity). To a certain degree, the drop in permeability may be offset by reduced *membrane thickness,* so as to keep the permeance within practical limits. However, conventional (non-IP) coating technology sets the lowest possible coating thickness around 100 nm or somewhat below. Thinner films prepared by regular solution-based coating are increasingly likely to contain defects and may lack mechanical robustness required for packing membranes into modules and sta-

ble operation for extended time including periodic cleaning. Novel coating approaches such as layer-by-layer (L-b-L) deposition or polymer grafting may yield thinner films, yet the technology has not matured yet to yield RO-level selectivity [235] or is limited to polyamide films for research [219]. The optimal polymer density and rigidity would then be the maximal one that still allows a reasonable water permeability for ca. 100 nm film, which also imposes an upper limit on selectivity. Nevertheless, a significant reduction in film thickness, without sacrificing robustness, would permit keeping reasonable permeability yet use a denser polymer and thus increase selectivity. This combination appears to be the main factor behind the superiority of aromatic polyamide membranes, as elaborated next.

4.2. Why fully aromatic polyamides are unrivaled: structural hierarchy

The vast literature on the chemistry, morphology, mechanics and barrier properties of polyamide films, reviewed in the preceding sections, suggests that the superior properties of aromatic polyamide membranes rely on two key features:

(a) high density and low swelling of the polymer, ensuring excellent salt rejection; and
(b) very small effective thickness that provides good water permeance.

The former apparently results from the exceptionally high rigidity of the fully aromatic network and tight packing of its flat structural units (see Section 2.4). These features help prevent excessive swelling and keep the film moderately hydrophobic. The planar structure formed in the reaction of aromatic, planar and symmetric TMC and MPD monomers, lacking inherent bends and twists, is likely to be a key factor in producing an exceptionally dense and rigid polymer. Indeed, seemingly minor changes of structural units, e.g., replacement of MPD with the aliphatic, non-planar piperazine, promotes packing defects that increase network flexibility, reduce its density and increase free volume. Packing imperfection also increases the size of free-volume cavities, ultimately resulting in a looser network that takes up much more water (despite the fact that piperazine amide is nominally more hydrophobic than MPD), while larger cavities may facilitate clustering. This is consistent with the drastically lower selectivity observed for semi-aromatic piperazine-based membranes and other membranes, in which MPD is substituted with alternative diamines.

The small effective thickness, established by comparing barrier properties to uniform films of a dense polymer, high-resolution imaging or, more directly, by analyzing planar ultrathin films prepared via modified IP procedures (cf. ssections 3.1 and 3.4.2), may be a fortuitous feature obtained with IP of fully aromatic polyamide. However, we believe that it is likely to be a direct outcome of its inherently high density and selectivity and low permeability. The combination of selectivity and thinness is, therefore, *not coincidental* and follows naturally from the IP mechanism outlined in Section 2.3, which predicts that a polymer of lower permeability will produce a thinner barrier (cf. Eq. 4). The exceptionally low intrinsic permeability may then yield particularly thin and selective films.

The overall view on the evolution and resulting structural hierarchy of fully aromatic polyamide films, spanning molecular to about a micron scale, is conceptually depicted in Fig. 14. Under realistic conditions and relatively high monomer concentrations employed in preparation of composite membranes, very thin films are expected (cf. inverse relation between concentration and incipient thickness, as predicted by Eqs. (2) and (4)). However, during their synthesis, such ultrathin films are prone to instabilities of various nature, e.g., thermal, mechanical, interfacial etc. (Section 2.5), leading to folding, crumpling, and, possibly, rupture of the initially formed first-generation film and formation of transient defects. When formed, the defects will, however, immediately become new preferential reaction sites and will be rapidly healed by next-generation films. Notably, the latter will not form exactly at the defect site but, rather, at some distance (cf. the first-generation film forming at some distance from the interface), forming a dome- or cap-like patch over the defect site. Repeated events of destabilization - crumpling, rupture and patching, occurring in multiple locations all over the forming film, will result in a hierarchical, multi-generation structure, whose morphology will most closely resemble a well-drained foam with voids formed by folds and patches. The resulting polyamide layer should have a significant void fraction but an effective thickness commensurate with that of the first-generation films, containing much smaller molecular and sub-nanometer pores. The films surroundings the voids and responsible for barrier properties of the entire polyamide layer will then be embedded and protected in a thicker, porous film, featuring a mechanically robust “composite” hiding inside and protecting the ultrathin selective barriers. Remarkably, all of its three key features - selectivity, thinness (permeability), and mechanical strength - apparently originate from the unique density and rigidity of the fully aromatic polymer network.

5. Open questions and current challenges

5.1. Barrier properties towards neutral solutes and enhancement via surface grafting and molecular plugs

Polyamide membranes have, generally speaking, been optimized for removal of salts. Governed by the dielectric exclusion mechanism (ion solvation), the mild hydrophobicity of polyamides turns out to be very beneficial for high water-salt selectivity and water permeability. Unfortunately, this feature is far from optimal when it comes to neutral solutes, for which the dielectric and Donnan mechanisms are absent. Rejection of neutral permeants must therefore rely on weaker steric exclusion and physically different solvation within the membrane, which often favors a preferential uptake of neutral, especially organic, molecules from water rather than exclusion. Most notable examples of chemical species, whose rejection by polyamide membranes is unsatisfactory, are boric acid in the context of seawater desalination [236,237] and, in drinking water purification, arsenic and organic micropollutants of emerging concern such as bisphenol-A (BPA) [238–240]. Boric acid is present in seawater at concentrations of 5–7 ppm and must be reduced to under 0.3–0.5 ppm in the permeate. Since it is uncharged at neutral pH, its rejection is typically only around 85–90% for the tightest SWRO and the required removal cannot be achieved in a single pass, necessitating a more sophisticated and costlier multi-pass process design [241]. Although boric acid has no particular affinity to polyamide, its small size and strong H-bonding with water within the polyamide enable it to pass the membrane along with water. Essentially the same factors reduce removal of arsenic, often present in drinking water sources as arsenite, small and uncharged at neutral pH [242,243]. On the other hand, the reason for the low rejection of aromatic molecules such as BPA and similar phenolic compounds is quite different. While their size may be large enough for a steric retention, their high affinity to polyamide results in preferential uptake, enhancing their transport through the membrane [143,240,244–246]. The rejection may be insufficient, 50–90%, even for ‘tight’, fully aromatic membranes, and becomes totally unacceptable for more ‘open’ NF membranes, which would otherwise be the primary choice for drinking water purification.

Since there is no viable alternative for polyamide membranes at present, adjusting their selectivity for neutral molecules, without sacrificing other beneficial characteristics, presents an attrac-

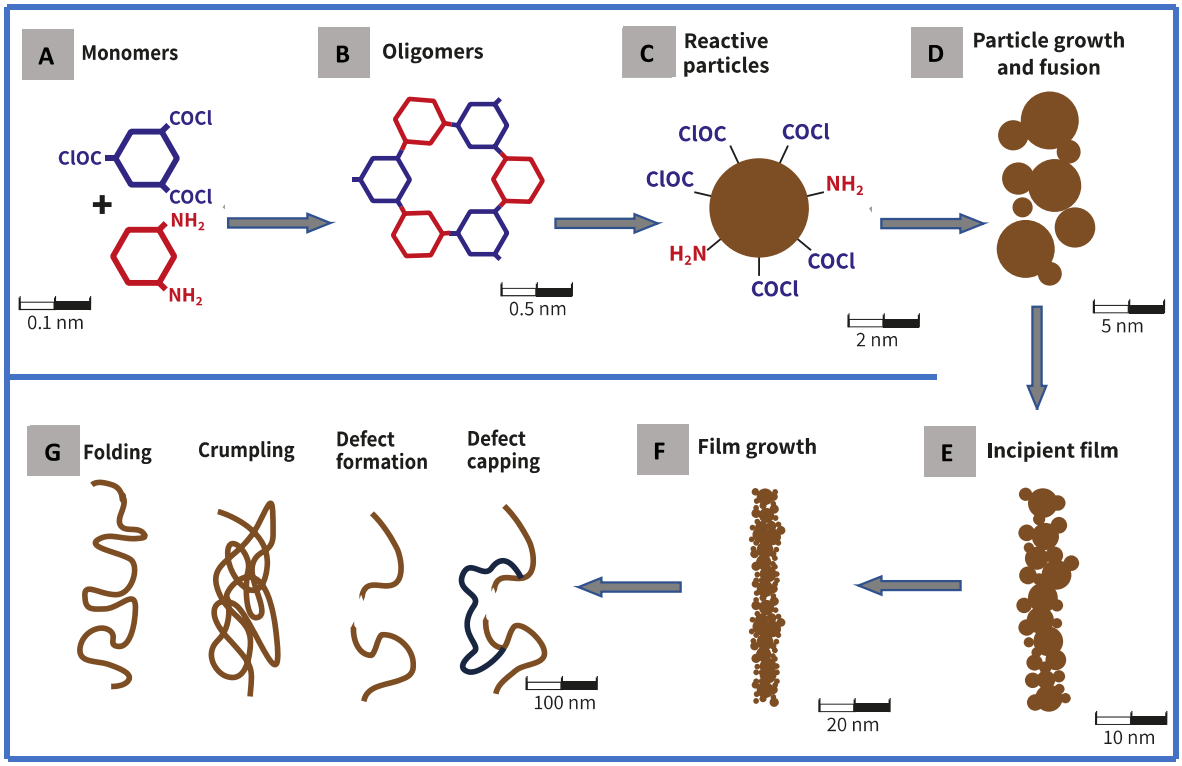

Fig. 14. Conceptualization of the formation and structural hierarchy of the polyamide thin film, along with representative spatial scales. (A) Monomers. (B) Oligomers forming planar structures. (C) 'Reactive particles' formed from oligomers. (D) Aggregation and clustering of reactive particles into progressively larger particles. (E) formation of an incipient film out of polymer particles. (F) increased film growth (G) film destabilization and transition from smooth to rough morphologies, including possible rupture (defect formation) followed by capping.

tive, though challenging, option. One simple approach pursued by a few groups is to add another layer on top of the polyamide, whose rejection characteristics have been optimized for the problematic solutes [182,183,188,247–251]. For instance, it was concluded that hydrophobic polymers should have a low affinity to boric acid and increase its rejection [180,183]. Conversely, charged or hydrophilic non-aromatic coatings could help reject organic pollutants [188,247,249,250]. Curiously, it turns out that such coatings improve selectivity, not so much due to their own properties, but rather by maximizing the selectivity of the polyamide layer itself [183,247]. As highlighted in previous sections, polyamide films, especially fully aromatic ones, possess a highly irregular structure, whose overall selectivity may be controlled by a few 'leaky' spots, through which solutes pass at an increased rate. This was perhaps most explicitly demonstrated recently by measuring gas permeability of reverse osmosis membranes [251]. These leaky sites may either be inherently present in the polyamide layer or may be the result of minor damage during handling and packing of the membranes into modules. A sufficiently selective and well-adhering coating may block leaky spots and reduce their contribution to water, solute and gas permeation, which would bring the overall selectivity closer to the one representing the average of the entire film rather than the few leakiest spots. Indeed, it has been shown that a very thin coating, able to block most of these spots, is sufficient for a significant improvement, while further increasing the coating thickness usually shows only a minor effect [183,247]. This result highlights the fact that there could still be a significant potential for increasing polyamide selectivity through improving uniformity, increasing robustness, and reducing the defect rate.

Another attractive approach could be to tune rejection properties of the polyamide layer through uptake or binding of molecules that may tighten its inner structure and modify its chemistry or polarity [221]. In the early days of polyamide membranes, it was noted that treatment with tannic acid, a natural polyphenol, may dramatically improve salt rejection [3]. Similar to other phenols, tannic acid should have a high affinity to polyamide and adsorb onto the polyamide surface, acting as an ultrathin coating blocking the leakiest sites. However, its relatively small size, ~1700 Da, suggests that it might also penetrate the largest pores in the polyamide, modifying its inner structure and effectively reducing the pore size, which should enhance rejection. A similar concept was recently examined by Shultz et al. [221,252] who found that moderately long alkyl amines act as "molecular plugs", taken up by the polyamide, capable of increasing the rejection of boric acid up to 98%. The rationale behind the choice of alkyl amines is that positively charged amine groups can serve as an anchor, binding the alkyl chain to negative charges within polyamide, while bulky and hydrophobic alkyl chain fill the pores, reducing both their size and polarity, which is known to increase boron rejection. Decyl amine was found to produce the largest effect, reflecting the optimal balance between amine hydrophobicity, which increases with the alkyl group size, and the ability to fit in pores that control boric acid permeation. Other studies explored this concept further, using other types of plug molecules. For example, a flexible chain polymer, polyisobutylene (PIB), was added to the organic phase during IP and thus incorporated within the PA film, hypothesized to interpenetrate the film structure and, as mentioned above, reduce larger spaces within the network and increase size exclusion [253]. A recent study showed a similar effect imparted by uptake of 4-nitrobenenesulfonyl, reaching a boron rejection of 93.1% [222].

Finally, we briefly mention what is perhaps the most widely-explored approach to modifying polyamide membranes – incorporation of nanoparticles within the active layer, creating thin-film nanocomposites (TFN). While mostly studied in the context of improving permeance and salt rejection [254], there have also been

several studies aimed at targeting improved selectivity towards boron and micropollutants. A large array of possible filler materials has been tested, with some interesting approaches demonstrated based on functionalized nano materials such as silica [255], carbon nanotubes [256] and metal-oragnic-frameworks [257]. The interested reader is referred to the recent review [258] on TFN membranes.

5.2. Alternative materials

While our focus here is on the superior performance of polyamide films, the discussion would not be complete without mention of possible future alternatives to polyamide. Notable examples are briefly discussed, with references made to relevant studies, for the interested reader.

Biomimetic approaches, such as artificial water channels, attempt to replicate the functionality of cell-membrane proteins (Aquaporins). These artificial water channels have been successful in exhibiting extremely fast transport while maintaining high selectivity [259–261]. Challenges remain, however, in scale-up capability and process adaptations, including, for example, the choices made with respect to the matrix in which the channels are embedded [260,262]. Other promising approaches are based on nanomaterials such as nanotubes and nanosheets, mostly carbon-based [263–266]. Here, again, fast water transport has been observed both theoretically and experimentally, particularly for the case of carbon nanotubes [267–269]. Layered nanosheets, particularly graphene and graphene-oxide, have also been the focus of several studies, but uncertainties remain with respect to the actual transport mechanisms and properties, primarily due to the unknown morphology of constructed layers, and their response to solution characteristics [270].

To place in a more general perspective, three contexts may be considered as the motivation for replacing polyamide; (i) increased permeance, (ii) increased selectivity and (iii) sustainability. The latter is an important prospect for future development of membrane materials and fabrication, based on sustainable practices and green chemistry [263]. Increased permeance, possibly the most commonly encountered motivation for studying various next-generation materials over the years, is usually considered as a possible route to reduced energy consumption. However, it would appear that improvements to energy efficiency is unlikely to result from alternative materials without significant process-based enhancement [206]. Finally, improved selectivity appears to provide a strong motivation for future material development [13,271]. In particular, tuning selectivity holds great promise in targeting specific separation requirements, for example the removal of boron from seawater and micropollutants from wastewater (see previous section). Nanochannel-based approaches may prove a vital component for the success of future membranes incorporating such materials [272–275].

6. Summary and outlook

The current state of desalination and water purification is much indebted to the advent of polymeric, thin-film composite membranes, based on interfacially-polymerized polyamide. It will likely remain the material of choice in the foreseeable future. Here, we have strived to provide a wide overview of various features that contributed to this success. These include various synthesis conditions used, fundamental experimental and theoretical aspects of interfacial polymerization, characterization methods and, in particular, insight into the unique nano-scale structure of the polyamide, both in terms of its molecular packing as well as its arrangement as a continuous film. A combination of improved characterization methods and tailored experimental visualization of polyamide structure, has enabled distinctive conclusions to be made with respect to the impact on transport. At the molecular scale, a balance between water uptake, facilitating the formation of pathways, and maintenance of high confinement, conspire to produce good selectivity. Most importantly, the defining feature of the interfacial polymerization process is an intrinsically thin film, essential as compensation for the relatively 'tight' structure.

Despite major advances in understanding, as outlined herein, there remain several gaps which, if successfully bridged, could lead to better control over membrane properties and result in improved membranes, geared towards specific separations. Furthermore, such level of control would be crucial on the path to use of more sustainable chemistries and production practices. These mostly revolve around a better fundamental understanding of the morphological evolution of polyamide under various interfacial polymerization conditions, consisting of insight gained through advanced modeling, *in-situ* visualization and high-resolution post-fabrication characterization.

A main conclusion presented herein is the importance of the morphological features of the polyamide layer and its role in establishing the 'structural hierarchy' (Fig. 13), deemed crucial in creating the correct balance between permeability and selectivity. While several possible mechanisms may be identified as involved in the structural evolution of the thin-film as it forms, these are mostly speculative at this point, and require further future study. However, a main point is the implication of heat release during IP, inherent irregularities present in the configuration, such as the support membrane, and the ensuing instabilities that may consequently arise. In particular, new configurations used for the fabrication process, such as electro-spraying or layer-by-layer synthesis, offer new degrees of freedom with respect to control of the polymerization, particularly in terms of heat and mass transfer and, hence, the resulting 'bulk' morphology of the film.

While outside the scope of the current paper, it is worth noting another aspect related to the morphology of the polyamide thin film – the propensity for fouling. Indeed, the rough morphology of the polyamide active layer has long been associated with increased fouling propensity. Theoretically, it has been shown that if roughness creates significant heterogeneity in the distribution of permeance along the membrane surface, this can translate to fouling 'hot-spots' [232]. Further, for particles with sizes on the same scale as the roughness, modification of colloidal interfacial interactions can also enhance adhesion [276]. On the other hand, a recent study showed that smooth and crumpled membranes showed little difference in their fouling propensity [277]. Theoretical considerations suggest that it may be more likely that the porous support and its distributed pores impact the variability of the local permeance more so than the thin film itself, and this may again translate into increased fouling propensity [169,227].

Future work should be aimed at establishing a better degree of control over the resulting morphology, utilizing this property to further tune membrane performance. A strong emphasis should be placed on studying fundamental aspects of the polymerization process, as affected by the configuration used and synthesis parameters. In particular, identifying and understanding the various instability mechanisms leading to film crumpling, rupture and general structural properties, may play a key role in establishing improved control over the polymerization process. Linking multi-scale, model-based insight with advanced *in-situ* observation and post-reaction characterization has recently been employed to gain large leaps in understanding, though the link between model and experiment requires significant improvement. These approaches must be further utilized and developed, not only in pursuit of better polyamide membranes, but also for providing the guidelines to membrane fabrication from sustainable materials.

A unique feature of interfacial polymerization is that it offers a playground for independently varying, over a wide range, three key membrane characteristics: thickness, permeation area and roughness. That being said, actual control over the features is still not complete and the large parameter space probed experimentally over the years is often muddled by conflicting effects. Better understanding of the physics underlying the process, as affected by synthesis conditions, is essential for future developments of membranes with well-designed morphologies. The choice of which characteristic to focus on varies with specific applications and developments that affect the relative importance of different factors. For example, it appears that surface roughness may not be as detrimental as was initially thought and post-coating with low-fouling materials could be an easy means to mitigate its negative impact on performance. The overall trend over the past decades has been primarily on increasing permeability by modifying the process in empirical ways that affected the membrane thickness and permeation area. Likely, the potential for pursuing this direction further, without concurrent increase in selectivity, may be limited by other factors, such as concentration polarization, and result in minor benefits in terms of process efficiency and energy consumption. In this respect, we presume that future efforts need to focus on enhancing selectivity, dictated by the intrinsic properties of polyamide. This includes both its inherent physicochemical characteristics and molecular-scale defects formed within the polyamide network during polymerization. Deep understanding and control of interfacial polymerization and, especially, evolution of the complex, aggregated morphology down to molecular scale, are key to achieving this goal, while continuing to rely on the classical "winner" chemistries. Another potentially beneficial approach could be in boosting the selectivity of the classical systems by judiciously modifying their chemistry or filling network defects, e.g., using post-coatings or by incorporation of other moieties ("molecular plugs") during or post-polymerization. This approach may be particularly beneficial for applications, where the intrinsic selectivity of polyamide has thus far been insufficient, such as boron or arsenic removal, or in new rapidly growing fields, such as organic-solvent NF/RO.

Declaration of Competing Interest

The authors declare that they have no known competing financial interests or personal relationships that could have appeared to influence the work reported in this paper.

CRediT authorship contribution statement

Viatcheslav Freger: Conceptualization, Visualization, Writing – original draft, Writing – review & editing. **Guy Z. Ramon:** Conceptualization, Visualization, Writing – original draft, Writing – review & editing.

References

[1] Cadotte JE, Petersen RJ, Larson RE, Erickson EE. A new thin-film composite seawater reverse osmosis membrane. Desalination 1980;32:25–31. doi:10.1016/S0011-9164(00)86003-8.

[2] Cadotte JE, Lloyd D. Evolution of composite reverse osmosis membranes. In: Materials science of synthetic membranes. American Chemical Society; 1985. p. 273–94. vol. 269. doi:10.1021/bk-1985-0269.ch012.

[3] Petersen RJ. Composite reverse osmosis and nanofiltration membranes. J Membr Sci 1993;83:81–150.

[4] Mulder MHV. Basic principles of membrane technology. Netherlands: Dordrecht: Kluwer Academic; 1996.

[5] Lee KP, Arnot TC, Mattia D. A review of reverse osmosis membrane materials for desalination—development to date and future potential. J Membr Sci 2011;370:1–22.

[6] Kurihara M, Sasaki T. The pursuits of ultimate membrane technology including low pressure seawater reverse osmosis membrane developed by "mega–ton water system" project. J Membr Sci Res 2017;3:157–73.

[7] Marchetti P, Jimenez Solomon MF, Szekely G, Livingston AG. Molecular separation with organic solvent nanofiltration: a critical review. Chem Rev 2014;114:10735–806. doi:10.1021/cr500006j.

[8] Thompson KA, Mathias R, Kim D, Kim J, Rangnekar N, Johnson JR, et al. N - aryl-linked spirocyclic polymers for membrane separations of complex hydrocarbon mixtures. Science 2020;369(80):310–15. doi:10.1126/science.aba9806.

[9] Poloncarzova M, Vejrazka J, Vesely V, Izak P. Effective purification of biogas by a condensing-liquid membrane. Angew Chem Int Ed 2011;50:669–71.

[10] Pacheco FA, Pinnau I, Reinhard M, Leckie JO. Characterization of isolated polyamide thin films of RO and NF membranes using novel TEM techniques. J Membr Sci 2010;358:51–9. doi:10.1016/j.memsci.2010.04.032.

[11] Schaefer A, Fane AG, Waite TD. Nanofiltration: principles and applications. Elsevier; 2005.

[12] Kedem O, Freger V. Determination of concentration-dependent transport coefficients in nanofiltration: defining an optimal set of coefficients. J Membr Sci 2008;310:586–93.

[13] Werber JR, Deshmukh A, Elimelech M. The critical need for increased selectivity, not increased water permeability, for desalination membranes. Environ Sci Technol Lett 2016;3:112–20. doi:10.1021/acs.estlett.6b00050.

[14] Yang Z, Guo H, Tang CY. The upper bound of thin-film composite (TFC) polyamide membranes for desalination. J Membr Sci 2019;590:117297. doi:10.1016/j.memsci.2019.117297.

[15] Morgan PW. Interfacial polymerization. Encycl Polym Sci Technol 2011. doi:10.1002/0471440264.pst168.

[16] Morgan PW, Kwolek SL. Interfacial polycondensation. II. Fundamentals of polymer formation at liquid interfaces. J Polym Sci 1959;40:299–327. doi:10.1002/pola.1996.816.

[17] Millich F, Carraher CE. Interfacial synthesis: polymer applications and technology. New York: Marcel Dekker Inc; 1977.

[18] Raaijmakers MJT, Benes NE. Current trends in interfacial polymerization chemistry. Prog Polym Sci 2016;63:86–142. doi:10.1016/j.progpolymsci.2016.06.004.

[19] Lim F. Biomedical applications of microencapsulation. Boca Raton: CRC press; 2019.

[20] Ozkan G, Franco P, De Marco I, Xiao J, Capanoglu E. A review of microencapsulation methods for food antioxidants: principles, advantages, drawbacks and applications. Food Chem 2019;272:494–506.

[21] Liu Y, McCrory CCL. Modulating the mechanism of electrocatalytic CO_2 reduction by cobalt phthalocyanine through polymer coordination and encapsulation. Nat Commun 2019;10:1–10.

[22] Freger V. Kinetics of film formation by interfacial polycondensation. Langmuir 2005;21:1884–94. doi:10.1021/la048085v.

[23] Linder C, Kedem O, Schäfer AI, Fane AG. History of nanofiltration membranes 1960 to 1990. In: Nanofiltration: principles, applications, and new materials. Wiley-VCH; 2021. p. 35–40.

[24] Bartels CR, Kreuz KL, Wachtel A. Structure-performance relationships of composite membranes: porous support densification. J Membr Sci 1987;32:291–312.

[25] Kwak SY, Kim CK, Kim JJ. Effects of bisphenol monomer structure on the surface morphology and reverse osmosis (RO) performance of thin-film-composite membranes composed of polyphenyl esters. J Polym Sci Part B Polym Phys 1996;34:2201–8. doi:10.1002/(SICI)1099-0488(19960930)34:13⟨2201::AID-POLB9⟩3.0.CO;2-Y.

[26] Sundet SA, Arthur SD, Campos D, Eckman TJ, Brown RG. Aromatic/cycloaliphatic polyamide membrane. Desalination 1987;64:259–69.

[27] Arthur SD. Structure-property relationship in a thin film composite reverse osmosis membrane. J Membr Sci 1989;46:243–60.

[28] Hirose M, Minamizaki Y, Kamiyama Y. The relationship between polymer molecular structure of RO membrane skin layers and their RO performances. J Membr Sci 1997;123:151–6.

[29] Gerard R, Hachisuka H, Hirose M. New membrane developments expanding the horizon for the application of reverse osmosis technology. Desalination 1998;119:47–55.

[30] Cadotte JE. Interfacially synthesized reverse osmosis membrane. U.S. Patent 4,277,344, issued July;7 1981.

[31] Tang CY, Kwon YN, Leckie JO. Probing the nano- and micro-scales of reverse osmosis membranes—a comprehensive characterization of physiochemical properties of uncoated and coated membranes by XPS, TEM, ATR-FTIR, and streaming potential measurements. J Membr Sci 2007;287:146–56. doi:10.1016/j.memsci.2006.10.038.

[32] Fridman-Bishop N, Freger V. What makes aromatic polyamide membranes superior: new insights into ion transport and membrane structure. J Membr Sci 2017;540. doi:10.1016/j.memsci.2017.06.035.

[33] Jiang Z, Karan S, Livingston AG. Water transport through ultrathin polyamide nanofilms used for reverse osmosis. Adv Mater 2018;30:1–7. doi:10.1002/adma.201705973.

[34] Soice NP, Greenberg AR, Krantz WB, Norman AD. Studies of oxidative degradation in polyamide RO membrane barrier layers using pendant drop mechanical analysis. J Membr Sci 2004;243:345–55. doi:10.1016/j.memsci.2004.06.039.

[35] Khare VP, Greenberg AR, Krantz WB. Development of pendant drop mechanical analysis as a technique for determining the stress-relaxation and water-permeation properties of interfacially polymerized barrier layers. J Appl Polym Sci 2003;90:2618–28. doi:10.1002/app.12892.

[36] Chai GY, Krantz WB. Formation and characterization of polyamide membranes via interfacial polymerization. J Membr Sci 1994;93:175–92.

[37] Matthews TD, Yan H, Cahill DG, Coronell O, Mariñas BJ. Growth dynamics of interfacially polymerized polyamide layers by diffuse reflectance spectroscopy and Rutherford backscattering spectrometry. J Membr Sci 2013;429:71–80. doi:10.1016/j.memsci.2012.11.040.
[38] Nowbahar A, Mansard V, Mecca JM, Paul M, Arrowood T, Squires TM. Measuring interfacial polymerization kinetics using microfluidic interferometry. J Am Chem Soc 2018;140:3173–6. doi:10.1021/jacs.7b12121.
[39] Ukrainsky B, Ramon GZ. Temperature measurement of the reaction zone during polyamide film formation by interfacial polymerization. J Membr Sci 2018;566:329–35. doi:10.1016/j.memsci.2018.09.011.
[40] Toubeli A, Kiparissides C. Synthesis and characterization of polyterephthalamide membranes for encapsulation use: effect of the amine type and composition on the membrane permeability. J Membr Sci 1998;146:15–29.
[41] Chu LY. Smart membrane materials and systems: from flat membranes to microcapsule membranes. Berlin, Hedelberg: Springer Science & Business Media; 2011.
[42] Zhang Y, Rochefort D. Characterisation and applications of microcapsules obtained by interfacial polycondensation. J Microencapsul 2012;29:636–49.
[43] Freger V, Srebnik S. Mathematical model of charge and density distributions in interfacial polymerization of thin films. J Appl Polym Sci 2003;88:1162–9. doi:10.1002/app.11716.
[44] Jiang Z, Miao J, He Y, Tu K, Chen S, Zhang R, et al. A novel positively charged composite nanofiltration membrane based on polyethyleneimine with a tunable active layer structure developed via interfacial polymerization. RSC Adv 2019;9:10796–806.
[45] Freger V. Swelling and morphology of the skin layer of polyamide composite membranes: an atomic force microscopy study. Environ Sci Technol 2004;38:3168–75. doi:10.1021/es034815u.
[46] Nikonov VZ, Savinov VM, Millich F, Carraher CRJ. Polyamides. In: Interfacial synth. New York: Marcel Dekker; 1977. p. 157–207. vol. 2.
[47] Kwak SY, Jung SG, Kim SH. Structure-motion-performance relationship of flux-enhanced reverse osmosis (RO) membranes composed of aromatic polyamide thin films. Environ Sci Technol 2001;35:4334–40.
[48] Kong C, Shintani T, Kamada T, Freger V, Tsuru T. Co-solvent-mediated synthesis of thin polyamide membranes. J Membr Sci 2011;384. doi:10.1016/j.memsci.2011.08.055.
[49] Ghosh AK, Jeong BH, Huang X, Hoek EMV. Impacts of reaction and curing conditions on polyamide composite reverse osmosis membrane properties. J Membr Sci 2008;311:34–45. doi:10.1016/j.memsci.2007.11.038.
[50] Mo Y, Tiraferri A, Yip NY, Adout A, Huang X, Elimelech M. Improved antifouling properties of polyamide nanofiltration membranes by reducing the density of surface carboxyl groups. Environ Sci Technol 2012;46:13253–61.
[51] Inoue T. Reverse osmosis membrane. Sen'i Gakkaishi 2004;60. doi:10.2115/fiber.60.P_295.
[52] Li L, Zhang S, Zhang X, Zheng G. Polyamide thin film composite membranes prepared from isomeric biphenyl tetraacyl chloride and m-phenylenediamine. J Membr Sci 2008;315:20–7. doi:10.1016/j.memsci.2008.02.022.
[53] Wang H, Zhang Q, Zhang S. Positively charged nanofiltration membrane formed by interfacial polymerization of 3,3',5,5'-biphenyl tetraacyl chloride and piperazine on a poly(acrylonitrile) (PAN) support. J Membr Sci 2011;378:243–9. doi:10.1016/j.memsci.2011.05.015.
[54] Xie W, Geise GM, Freeman BD, Lee HSS, Byun G, McGrath JE. Polyamide interfacial composite membranes prepared from m-phenylene diamine, trimesoyl chloride and a new disulfonated diamine. J Membr Sci 2012;403-404:152–61. doi:10.1016/j.memsci.2012.02.038.
[55] Yu S, Liu M, Liu X, Gao C. Performance enhancement in interfacially synthesized thin-film composite polyamide-urethane reverse osmosis membrane for seawater desalination. J Membr Sci 2009;342:313–20. doi:10.1016/j.memsci.2009.07.003.
[56] Liu M, Zheng Y, Shuai S, Zhou Q, Yu S, Gao C. Thin-film composite membrane formed by interfacial polymerization of polyvinylamine (PVAm) and trimesoyl chloride (TMC) for nanofiltration. Desalination 2012;288:98–107. doi:10.1016/j.desal.2011.12.018.
[57] Zhang R, Yu S, Shi W, Wang W, Wang X, Zhang Z, et al. A novel polyesteramide thin film composite nanofiltration membrane prepared by interfacial polymerization of serinol and trimesoyl chloride (TMC) catalyzed by 4–dimethylaminopyridine (DMAP). J Membr Sci 2017;542:68–80. doi:10.1016/j.memsci.2017.07.054.
[58] Ma XH, Yao ZK, Yang Z, Guo H, Xu ZL, Tang CY, et al. Nanofoaming of polyamide desalination membranes to tune permeability and selectivity. Environ Sci Technol Lett 2018;5:123–30. doi:10.1021/acs.estlett.8b00016.
[59] Yao Y, Zhang P, Jiang C, DuChanois RM, Zhang X, Elimelech M. High performance polyester reverse osmosis desalination membrane with chlorine resistance. Nat Sustain 2020;4:138–46. doi:10.1038/s41893-020-00619-w.
[60] Karan S, Jiang Z, Livingston AG. Sub-10 nm polyamide nanofilms with ultrafast solvent transport for molecular separation. Science 2015;348(80):1347–51. doi:10.1126/science.aaa5058.
[61] Park SJ, Choi W, Nam SE, Hong S, Lee JS, Lee JH. Fabrication of polyamide thin film composite reverse osmosis membranes via support-free interfacial polymerization. J Membr Sci 2017;526:52–9. doi:10.1016/j.memsci.2016.12.027.
[62] Kim IC, Jeong BR, Kim SJ, Lee KH. Preparation of high flux thin film composite polyamide membrane: the effect of alkyl phosphate additives during interfacial polymerization. Desalination 2013;308:111–14. doi:10.1016/j.desal.2012.08.001.
[63] Khorshidi B, Thundat T, Pernitsky D, Sadrzadeh M. A parametric study on the synergistic impacts of chemical additives on permeation properties of thin film composite polyamide membrane. J Membr Sci 2017;535:248–57. doi:10.1016/j.memsci.2017.04.052.
[64] Yan W, Wang Z, Zhao S, Wang J, Zhang P, Cao X. Combining co-solvent-optimized interfacial polymerization and protective coating-controlled chlorination for highly permeable reverse osmosis membranes with high rejection. J Membr Sci 2019;572:61–72. doi:10.1016/j.memsci.2018.10.084.
[65] Lee J, Wang R, Bae TH. A comprehensive understanding of co-solvent effects on interfacial polymerization: interaction with trimesoyl chloride. J Membr Sci 2019;583:70–80. doi:10.1016/j.memsci.2019.04.038.
[66] Kim SHO, Kwak SY, Suzuki T. Positron annihilation spectroscopic evidence to demonstrate the flux-enhancement mechanism in morphology-controlled thin-film-composite (TFC) membrane. Environ Sci Technol 2005;39:1764–70. doi:10.1021/es049453k.
[67] Kamada T, Ohara T, Shintani T, Tsuru T. Controlled surface morphology of polyamide membranes via the addition of co-solvent for improved permeate flux. J Membr Sci 2014;467:303–12. doi:10.1016/j.memsci.2014.03.072.
[68] Mansourpanah Y, Alizadeh K, Madaeni SS, Rahimpour A, Soltani Afarani H. Using different surfactants for changing the properties of poly(piperazineamide) TFC nanofiltration membranes. Desalination 2011;271:169–77. doi:10.1016/j.desal.2010.12.026.
[69] Fang W, Shi L, Wang R. Interfacially polymerized composite nanofiltration hollow fiber membranes for low-pressure water softening. J Membr Sci 2013;430:129–39. doi:10.1016/j.memsci.2012.12.011.
[70] Mansourpanah Y, Madaeni SS, Rahimpour A. Fabrication and development of interfacial polymerized thin-film composite nanofiltration membrane using different surfactants in organic phase; study of morphology and performance. J Membr Sci 2009;343:219–28. doi:10.1016/j.memsci.2009.07.033.
[71] Peng LE, Yao Z, Liu X, Deng B, Guo H, Tang CY. Tailoring polyamide rejection layer with aqueous carbonate chemistry for enhanced membrane separation: mechanistic insights, chemistry-structure-property relationship, and environmental implications. Environ Sci Technol 2019;53:9764–70. doi:10.1021/acs.est.9b03210.
[72] Hermans S, Bernstein R, Volodin A, Vankelecom IFJ. Study of synthesis parameters and active layer morphology of interfacially polymerized polyamide-polysulfone membranes. React Funct Polym 2015;86:199–208. doi:10.1016/j.reactfunctpolym.2014.09.013.
[73] Tan Z, Chen S, Peng X, Zhang L, Gao C. Polyamide membranes with nanoscale Turing structures for water purification. Science 2018;360(80):518–21. doi:10.1126/science.aar6308.
[74] Wang Z, Liang S, Jin Y, Zhao L, Hu L. Controlling structure and properties of polyamide nanofilms by varying amines diffusivity in organic phase. J Membr Sci 2019;574:1–9. doi:10.1016/j.memsci.2018.12.036.
[75] Yuan S, Zhang G, Zhu J, Mamrol N, Liu S, Mai Z, et al. Hydrogel assisted interfacial polymerization for advanced nanofiltration membranes. J Mater Chem A 2020;8:3238–45. doi:10.1039/c9ta12984g.
[76] Enkelmann V, Wegner G. Mechanism of interfacial polycondensation and the direct synthesis of polyamide membranes. Appl Polym Symp 1975;3189:365–72.
[77] Zhang Y, Benes NE, Lammertink RGH. Visualization and characterization of interfacial polymerization layer formation. Lab Chip 2015;15:575–80. doi:10.1039/c4lc01046a.
[78] Li W, Liu X, Li Z, Fane AG, Deng B. Unraveling the film-formation kinetics of interfacial polymerization via low coherence interferometry. AIChE J 2019:8–10. doi:10.1002/aic.16863.
[79] Ji J, Dickson JM, Childs RF, McCarry BE. Mathematical model for the formation of thin-film composite membranes by interfacial polymerization: porous and dense films. Macromolecules 2000;33:624–33.
[80] Yang X. Monitoring the interfacial polymerization of piperazine and trimesoyl chloride with hydrophilic interlayer or macromolecular additive by *in situ* FT-IR spectroscopy. Membranes 2020;10:12 (Basel). doi:10.3390/membranes10010012.
[81] Berezkin AV, Khokhlov AR. Mathematical modeling of interfacial polycondensation. J Polym Sci Part B Polym Phys 2006;44:2698–724.
[82] Janssen L, Te Nijenhuis K. Encapsulation by interfacial polycondensation. I. The capsule production and a model for wall growth. J Membr Sci 1992;65:59–68.
[83] Karode SK, Kulkarni SS, Suresh AK, Mashelkar RA. Molecular weight distribution in interfacial polymerization—model development and verification. Chem Eng Sci 1997;52:3243–55.
[84] Yashin VV, Balazs AC. Theoretical model of interfacial polymerization. J Chem Phys 2004;121:11440–54.
[85] Dhumal SS, Suresh AK. A comprehensive model for kinetics and development of film structure in interfacial polycondensation. Polymer 2009;50:5851–64 (Guildf).
[86] Freger V. Nanoscale heterogeneity of polyamide membranes formed by interfacial polymerization. Langmuir 2003;19:4791–7. doi:10.1021/la020920q.
[87] Berezkin AV, Kudryavtsev YV. Linear interfacial polymerization: theory and simulations with dissipative particle dynamics. J Chem Phys 2014;141:194906.
[88] de Gennes PG, Hervet H. Statistics of «starburst» polymers. J Phys Lett 1983;44:351–60.
[89] Bosman AW, Janssen HM, Meijer EW. About dendrimers: structure, physical properties, and applications. Chem Rev 1999;99:1665–88.
[90] Kotelyanskii MJ, Wagner NJ, Paulaitis ME. Molecular dynamics simulation study of the mechanisms of water diffusion in a hydrated, amorphous polyamide. Comput Theor Polym Sci 1999;9:301–6.

[91] Kotelyanskii MJ, Wagner NJ, Paulaitis ME. Atomistic simulation of water and salt transport in the reverse osmosis membrane FT-30. J Membr Sci 1998;139:1–16.
[92] Hughes ZE, Gale JD. A computational investigation of the properties of a reverse osmosis membrane. J Mater Chem 2010;20:7788–99.
[93] Luo Y, Harder E, Faibish RS, Roux B. Computer simulations of water flux and salt permeability of the reverse osmosis FT-30 aromatic polyamide membrane. J Membr Sci 2011;384:1–9. doi:10.1016/j.memsci.2011.08.057.
[94] Ding M, Szymczyk A, Goujon F, Soldera A, Ghoufi A. Structure and dynamics of water confined in a polyamide reverse-osmosis membrane: a molecular-simulation study. J Membr Sci 2014;458:236–44.
[95] Ridgway HF, Orbell J, Gray S. Molecular simulations of polyamide membrane materials used in desalination and water reuse applications: Recent developments and future prospects. J Membr Sci 2017;524:436–48.
[96] Ghoufi A, Dražević E, Szymczyk A. Interactions of organics within hydrated selective layer of reverse osmosis desalination membrane: a combined experimental and computational study. Environ Sci Technol 2017;51:2714–2719.
[97] Song Y, Xu F, Wei M, Wang Y. Water flow inside polamide reverse osmosis membranes: a non-equilibrium molecular dynamics study. J Phys Chem B 2017;121:1715–22.
[98] Harder E, Walters DE, Bodnar YD, Faibish RS, Roux B. Molecular dynamics study of a polymeric reverse osmosis membrane. J Phys Chem B 2009;113:10177–82. doi:10.1021/jp902715f.
[99] Kolev V, Freger V. Hydration, porosity and water dynamics in the polyamide layer of reverse osmosis membranes: a molecular dynamics study. Polym 2014;55:1420–6 (United Kingdom). doi:10.1016/j.polymer.2013.12.045.
[100] Kolev V, Freger V. Molecular dynamics investigation of ion sorption and permeation in desalination membranes. J Phys Chem B 2015;119:14168–79. doi:10.1021/acs.jpcb.5b06566.
[101] Wei T, Zhang L, Zhao H, Ma H, Sajib MSJ, Jiang H, et al. Aromatic polyamide reverse-osmosis membrane: an atomistic molecular dynamics simulation. J Phys Chem B 2016;120:10311–18.
[102] Shen M, Keten S, Lueptow RM. Dynamics of water and solute transport in polymeric reverse osmosis membranes via molecular dynamics simulations. J Membr Sci 2016;506:95–108. doi:10.1016/j.memsci.2016.01.051.
[103] Berezkin AV, Kudryavtsev YV. Effect of cross-linking on the structure and growth of polymer films prepared by interfacial polymerization. Langmuir 2015;31:12279–90.
[104] Coronell O, Mariñas BJ, Zhang X, Cahill DG. Quantification of functional groups and modeling of their ionization behavior in the active layer of FT30 reverse osmosis membrane. Environ Sci Technol 2008;42:5260–6.
[105] Coronell O, Marinas BJ, Cahill DG. Accessibility and ion exchange stoichiometry of ionized carboxylic groups in the active layer of FT30 reverse osmosis membrane. Environ Sci Technol 2009;43:5042–8.
[106] Dražević E, Košutić K, Kolev V, Freger V. Does hindered transport theory apply to desalination membranes? Environ Sci Technol 2014;48:11471–8. doi:10.1021/es502085p.
[107] Ambegaokar V, Halperin BI, Langer JS. Hopping conductivity in disordered systems. Phys Rev B 1971;4:2612.
[108] Torquato S. Random heterogeneous materials: microstructure and macroscopic properties. New York: Springer-Verlag; 2002.
[109] Dražević E, Košutić K, Freger V. Permeability and selectivity of reverse osmosis membranes: correlation to swelling revisited. Water Res 2014;49:444–52.
[110] Song X, Smith JW, Kim J, Zaluzec NJ, Chen W, An H, et al. Unraveling the morphology-function relationships of polyamide membranes using quantitative electron tomography. ACS Appl Mater Interfaces 2019;11:8517–26. doi:10.1021/acsami.8b20826.
[111] Yan H, Miao X, Xu J, Pan G, Zhang Y, Shi Y, et al. The porous structure of the fully-aromatic polyamide film in reverse osmosis membranes. J Membr Sci 2015;475:504–10. doi:10.1016/j.memsci.2014.10.052.
[112] Song X, Gan B, Qi S, Guo H, Tang CY, Zhou Y, et al. Intrinsic nanoscale structure of thin film composite polyamide membranes: connectivity, defects, and structure-property correlation. Environ Sci Technol 2020;54:3559–69. doi:10.1021/acs.est.9b05892.
[113] Culp TE, Shen Y, Geitner M, Paul M, Roy A, Behr MJ, et al. Electron tomography reveals details of the internal microstructure of desalination membranes. Proc Natl Acad Sci 2018;115:201804708. doi:10.1073/pnas.1804708115.
[114] Nakouzi E, Steinbock O. Self-organization in precipitation reactions far from the equilibrium. Sci Adv 2016;2:e1601144. doi:10.1126/sciadv.1601144.
[115] Turing AM. The chemical basis of morphogenesis. Bull Math Biol 1990;52:153–97. doi:10.1007/BF02459572.
[116] Ouyang Q, Swinney HL. Transition from a uniform state to hexagonal and striped Turing patterns. Nature 1991;352:610–12. doi:10.1038/352610a0.
[117] Epstein IR, Xu B. Reaction-diffusion processes at the nano- and microscales. Nat Nanotechnol 2016;11:312–19. doi:10.1038/nnano.2016.41.
[118] Eckert K, Grahn A. Plume and finger regimes driven by an exothermic interfacial reaction. Phys Rev Lett 1999;82:4436–9. doi:10.1103/PhysRevLett.82.4436.
[119] Eckert K, Acker M, Shi Y. Chemical pattern formation driven by a neutralization reaction. I. Mechanism and basic features. Phys Fluids 2004;16:385–99. doi:10.1063/1.1636160.
[120] Kabova YO, Alexeev A, Gambaryan-Roisman T, Stephan P. Marangoni-induced deformation and rupture of a liquid film on a heated microstructured wall. Phys Fluids 2006;18:012104. doi:10.1063/1.2166642.
[121] Pearson JRA. On convection cells induced by surface tension. J Fluid Mech 1958;4:489–500. doi:10.1017/S0022112058000616.
[122] Diewald M, Matthiessen K, Müller SC, Brand HR. Oscillatory hydrodynamic flow due to concentration dependence of surface tension. Phys Rev Lett 1996;77:4466–9. doi:10.1103/PhysRevLett.77.4466.
[123] Bratsun DA, De Wit A. On marangoni convective patterns driven by an exothermic chemical reaction in two-layer systems. Phys Fluids 2004;16:1082–96. doi:10.1063/1.1648641.
[124] Yuan F, Wang Z, Yu X, Wei Z, Li S, Wang J, et al. Visualization of the formation of interfacially polymerized film by an optical contact angle measuring device. J Phys Chem C 2012;116:11496–506. doi:10.1021/jp210209v.
[125] Song X, Gan B, Yang Z, Tang CY, Gao C. Confined nanobubbles shape the surface roughness structures of thin film composite polyamide desalination membranes. J Membr Sci 2019;582:342–9. doi:10.1016/j.memsci.2019.04.027.
[126] Kumaran V, Fredrickson GH, Pincus P. Flow induced instability of the interface between a fluid and a gel at low Reynolds number. J Phys II 1994. doi:10.1051/jp2:1994173.
[127] Shankar V, Kumar L. Stability of two-layer Newtonian plane couette flow past a deformable solid layer. Phys Fluids 2004;16:4426–42. doi:10.1063/1.1808772.
[128] Patne R, Ramon GZ. Stability of fluid flows coupled by a deformable solid layer. J Fluid Mech 2020.
[129] Chatterjee S, McDonald C, Niu J, Velankar SS, Wang P, Huang R. Wrinkling and folding of thin films by viscous stress. Soft Matter 2015;11:1814–27. doi:10.1039/c4sm02501f.
[130] Mei H, Huang R, Chung JY, Stafford CM, Yu HH. Buckling modes of elastic thin films on elastic substrates. Appl Phys Lett 2007;90:1–3. doi:10.1063/1.2720759.
[131] Box F, O'Kiely D, Kodio O, Inizan M, Castrejón-Pita AA, Vella D. Dynamics of wrinkling in ultrathin elastic sheets. Proc Natl Acad Sci U S A 2019;116:20875–80. doi:10.1073/pnas.1905755116.
[132] Chen W, Gui X, Yang L, Zhu H, Tang Z. Wrinkling of two-dimensional materials: methods, properties and applications. Nanoscale Horiz 2019;4:291–320. doi:10.1039/c8nh00112j.
[133] Huang Z, Suo R, Huang R, Suo Z. Wrinkling of a compressed elastic film on a viscous layer. J Appl Phys 2002;91:1791–802 J Appl Phys J Appl Phys J Appl Phys J Appl Phys. doi:10.1063/1.1427407.
[134] Evans AA, Cheung E, Nyberg KD, Rowat AC. Wrinkling of milk skin is mediated by evaporation. Soft Matter 2017;13:1056–62. doi:10.1039/c6sm02102f.
[135] Bernstein R, Kaufman Y, Freger V, Hoek EMV, Tarabara VV. Membrane characterization. Encyclopedia of membrane science and technology editors, Hoboken: John Wiley and Sons, Inc; 2013. vol. 2.
[136] Culp TE, Khara B, Brickey KP, Geitner M, Zimudzi TJ, Wilbur JD, et al. Nanoscale control of internal inhomogeneity enhances water transport in desalination membranes. Science 2021;371 (80-)72 LP - 75. doi:10.1126/science.abb8518.
[137] Bason S, Kaufman Y, Freger V. Analysis of ion transport in nanofiltration using phenomenological coefficients and structural characteristics. J Phys Chem B 2010:114. doi:10.1021/jp911615n.
[138] Bartels CR. A surface science investigation of composite membranes. J Membr Sci 1989;45:225–45. doi:10.1016/S0376-7388(00)80516-5.
[139] Bass M, Freger V. Facile evaluation of coating thickness on membranes using ATR-FTIR. J Membr Sci 2015. doi:10.1016/j.memsci.2015.05.059.
[140] Lin L, Lopez R, Ramon GZ, Coronell O. Investigating the void structure of the polyamide active layers of thin-film composite membranes. J Membr Sci 2016;497:365–76. doi:10.1016/j.memsci.2015.09.020.
[141] Tang CY, Kwon YN, Leckie JO. Fouling of reverse osmosis and nanofiltration membranes by humic acid:€"effects of solution composition and hydrodynamic conditions. J Membr Sci 2007;290:86–94.
[142] Roh IJ. Influence of rupture strength of interfacially polymerized thin-film structure on the performance of polyamide composite membranes. J Membr Sci 2002;198:63–74.
[143] Ben-David A, Bason S, Jopp J, Oren Y, Freger V. Partitioning of organic solutes between water and polyamide layer of RO and NF membranes: correlation to rejection. J Membr Sci 2006;281. doi:10.1016/j.memsci.2006.04.017.
[144] Pacheco F, Sougrat R, Reinhard M, Leckie JO. Pinnau I. 3D visualization of the internal nanostructure of polyamide thin films in RO membranes. J Membr Sci 2015;501:33–44. doi:10.1016/j.memsci.2015.10.061.
[145] Tang CY, Yang Z, Hilal N, Ismail AF, Matsuura TORD. Transmission electron microscopy (TEM). In: Membership character. Elsevier; 2017. p. 145–59.
[146] Kłosowski MM, McGilvery CM, Li Y, Abellan P, Ramasse Q, Cabral JT, et al. Micro-to nano-scale characterisation of polyamide structures of the SW30HR RO membrane using advanced electron microscopy and stain tracers. J Membr Sci 2016;520:465–76. doi:10.1016/j.memsci.2016.07.063.
[147] McGilvery CM, Abellan P, Kłosowski MM, Livingston AG, Cabral JT, Ramasse QM, et al. Nanoscale chemical heterogeneity in aromatic polyamide membranes for reverse osmosis applications. ACS Appl Mater Interfaces 2020;12:19890–902.
[148] Mi BX, Coronell O, Marinas BJ, Watanabe F, Cahill DG, Petrov I. Physico–chemical characterization of NF/RO membrane active layers by Rutherford backscattering spectrometry. J Membr Sci 2006;282:71–81.
[149] Coronell O, Mariñas BJ, Cahill DG. Depth heterogeneity of fully aromatic polyamide active layers in reverse osmosis and nanofiltration membranes. Environ Sci Technol 2011;45:4513–20. doi:10.1021/es200007h.
[150] Perry LA, Reliable CO. bench-top measurements of charge density in the active layers of thin-film composite and nanocomposite membranes using quartz crystal microbalance technology. J Membr Sci 2013;429:23–33. doi:10.1016/j.memsci.2012.11.023.

[151] Baransi-Karkaby K, Bass M, Levchenko S, Eitan S, Freger V. Facile modification of reverse osmosis membranes by surfactant-assisted acrylate grafting for enhanced selectivity. Environ Sci Technol 2017;51:2347–54. doi:10.1021/acs.est.6b05260.

[152] Ben-David A, Oren Y, Freger V. Thermodynamic factors in partitioning and rejection of organic compounds by polyamide composite membranes. Environ Sci Technol 2006;40:7023–8.

[153] Bason S, Oren Y, Freger V. Ion transport in the polyamide layer of RO membranes: composite membranes and free-standing films. J Membr Sci 2011;367. doi:10.1016/j.memsci.2010.10.048.

[154] Bason S, Ben-David A, Oren Y, Freger V. Characterization of ion transport in the active layer of RO and NF polyamide membranes. Desalination 2006;199:31–3.

[155] Bason S, Oren Y, Freger V. Characterization of ion transport in thin films using electrochemical impedance spectroscopy II: examination of the polyamide layer of RO membranes. J Membr Sci 2007;302:10–19.

[156] Bason S, Kedem O, Freger V. Determination of concentration-dependent transport coefficients in nanofiltration: experimental evaluation of coefficients. J Membr Sci 2009;326:197–204. doi:10.1016/j.memsci.2008.09.054.

[157] Kosutic K, Dolar D, Kunst B. On experimental parameters characterizing the reverse osmosis and nanofiltration membranes' active layer. J Membr Sci 2006;282:109–14.

[158] Deon S, Dutournie P, Bourseau P. Modeling nanofiltration with Nernst-Planck approach and polarization layer. AIChE J 2007;53:1952–69.

[159] Van der Bruggen B, Schaep J, Wilms D, Vandecasteele C. Influence of molecular size, polarity and charge on the retention of organic molecules by nanofiltration. J Membr Sci 1999;156:29–41.

[160] Albo J, Hagiwara H, Yanagishita H, Ito K, Tsuru T. Structural characterization of thin-film polyamide reverse osmosis membranes. Ind Eng Chem Res 2014;53:1442–51. doi:10.1021/ie403411w.

[161] Cahill DG, Freger V, Kwak SY. Microscopy and microanalysis of reverse-osmosis and nanofiltration membranes. MRS Bull 2008;33:27–32. doi:10.1557/mrs2008.11.

[162] Nadler R, Srebnik S. Molecular simulation of polyamide synthesis by interfacial polymerization. J Membr Sci 2008;315:100–5.

[163] Coronell O, González MI, Mariñas BJ, Cahill DG. Ionization behavior, stoichiometry of association, and accessibility of functional groups in the active layers of reverse osmosis and nanofiltration membranes. Environ Sci Technol 2010;44:6808–14. doi:10.1021/es100891r.

[164] Ritt CL, Werber JR, Wang M, Yang Z, Zhao Y, Kulik HJ, et al. Ionization behavior of nanoporous polyamide membranes. Proc Natl Acad Sci U S A 2020;117:30191–200. doi:10.1073/pnas.2008421117.

[165] Hirose M, Ito H, Kamiyama Y. Effect of skin layer surface structures on the flux behavior of RO membranes. J Membr Sci 1996;121:209–15. doi:10.1016/S0376-7388(96)00181-0.

[166] Kwak SY, Jung SG, Yoon YS, Ihm DW. Details of surface features in aromatic polyamide reverse osmosis membranes characterized by scanning electron and atomic force microscopy. J Polym Sci Part B Polym Phys 1999;37:1429–40. doi:10.1002/(SICI)1099-0488(19990701)37:13⟨1429::AID-POLB9⟩3.0.CO;2-B.

[167] Al-Jeshi S, Neville A. An investigation into the relationship between flux and roughness on RO membranes using scanning probe microscopy. Desalination 2006;189:221–8. doi:10.1016/j.desal.2005.08.001.

[168] Ma X, Yang Z, Yao Z, Guo H, Xu Z, Tang CY. Tuning roughness features of thin film composite polyamide membranes for simultaneously enhanced permeability, selectivity and anti-fouling performance. J Colloid Interface Sci 2019;540:382–8. doi:10.1016/j.jcis.2019.01.033.

[169] Wong MCY, Lin L, Coronell O, Hoek EMV, Ramon GZ. Impact of liquid-filled voids within the active layer on transport through thin-film composite membranes. J Membr Sci 2016;500:124–35. doi:10.1016/j.memsci.2015.11.033.

[170] Lu X, Nejati S, Choo Y, Osuji CO, Ma J, Elimelech M. Elements provide a clue: nanoscale characterization of thin-film composite polyamide membranes. ACS Appl Mater Interfaces 2015;7:16917–22. doi:10.1021/acsami.5b05478.

[171] Ji J, Mehta M. Mathematical model for the formation of thin-film composite hollow fiber and tubular membranes by interfacial polymerization. J Membr Sci 2001;192:41–54.

[172] Xu J, Yan H, Zhang Y, Pan G, Liu Y. The morphology of fully-aromatic polyamide separation layer and its relationship with separation performance of TFC membranes. J Membr Sci 2017;541:174–88. doi:10.1016/j.memsci.2017.06.057.

[173] Wang M, Stafford CM, Cox LM, Blevins AK, Aghajani M, Killgore JP, et al. Controlled growth of polyamide films atop homogenous and heterogeneous hydrogels using gel-liquid interfacial polymerization. Macromol Chem Phys 2019;220:1–11. doi:10.1002/macp.201900100.

[174] Tsuru T, Sasaki S, Kamada T, Shintani T, Ohara T, Nagasawa H, et al. Multilayered polyamide membranes by spray-assisted 2-step interfacial polymerization for increased performance of trimesoyl chloride (TMC)/m-phenylenediamine (MPD)-derived polyamide membranes. J Membr Sci 2013;446:504–12. doi:10.1016/j.memsci.2013.07.031.

[175] Chowdhury MR, Steffes J, Huey BD, McCutcheon JR. 3D printed polyamide membranes for desalination. Science 2018;361(80):682–6. doi:10.1126/science.aar2122.

[176] Ma XHH, Yang Z, Yao ZKK, Guo H, Xu ZLL, Tang CY. Interfacial polymerization with electrosprayed microdroplets: toward controllable and ultrathin polyamide membranes. Environ Sci Technol Lett 2018;5:117–22. doi:10.1021/acs.estlett.7b00566.

[177] Freger V. Ion partitioning and permeation in charged low-T* membranes. Adv Colloid Interface Sci 2020;277:102107.

[178] Koo JY, Petersen RJ, Cadotte JE. ESCA study on chlorine degradation of FT30 membrane. ACS Polym Polym Prepr (Am Chem Soc Div Polym Chem) 1986;27:391–2.

[179] Childress AE, Elimelech M. Effect of solution chemistry on the surface charge of polymeric reverse osmosis and nanofiltration membranes. J Membr Sci 1996;119:253–68.

[180] Bernstein R, Belfer S, Freger V. Bacterial attachment to RO membranes surface-modified by concentration-polarization-enhanced graft polymerization. Environ Sci Technol 2011;45:5973–80. doi:10.1021/es1043694.

[181] Bernstein R, Freger V, Lee JH, Kim YG, Lee J, Herzberg M. 'Should I stay or should I go?' Bacterial attachment vs biofilm formation on surface-modified membranes. Biofouling 2014;30:367–76. doi:10.1080/08927014.2013.876011.

[182] Bernstein R, Belfer S, Freger V. Toward improved boron removal in RO by membrane modification: feasibility and challenges. Environ Sci Technol 2011;45. doi:10.1021/es103991u.

[183] Baransi-Karkaby K, Bass M, Freger V. *In situ* modification of reverse osmosis membrane elements for enhanced removal of multiple micropollutants. Membranes 2019;9 (Basel). doi:10.3390/membranes9020028.

[184] Rana D, Matsuura T. Surface modifications for antifouling membranes. Chemical Reviews 2010;110:2448–71.

[185] Choudhury RR, Gohil JM, Mohanty S, Nayak SK. Antifouling, fouling release and antimicrobial materials for surface modification of reverse osmosis and nanofiltration membranes. J Mater Chem A 2018;6:313–33.

[186] Cheng Q, Zheng Y, Yu S, Zhu H, Peng X, Liu J, et al. Surface modification of a commercial thin-film composite polyamide reverse osmosis membrane through graft polymerization of N-isopropylacrylamide followed by acrylic acid. J Membr Sci 2013;447:236–45.

[187] Van Wagner EM, Sagle AC, Sharma MM, La YH, Freeman BD. Surface modification of commercial polyamide desalination membranes using poly (ethylene glycol) diglycidyl ether to enhance membrane fouling resistance. J Membr Sci 2011;367:273–87.

[188] Kim JH, Park PK, Lee CH, Kwon HH. Surface modification of nanofiltration membranes to improve the removal of organic micro-pollutants (EDCs and PhACs) in drinking water treatment: graft polymerization and cross-linking followed by functional group substitution. J Membr Sci 2008;321:190–8.

[189] Zhang XJ, Cahill DG, Coronell O, Marinas BJ. Partitioning of salt ions in FT30 reverse osmosis membranes. Appl Phys Lett 2007;91:181904.

[190] Mi BX, Marinas BJ, Cahill DG. RBS characterization of arsenic(III) partitioning from aqueous phase into the active layers of thin-film composite NF/RO membranes. Environ Sci Technol 2007;41:3290–5.

[191] Schaep J, Vandecasteele C. Evaluating the charge of nanofiltration membranes. J Membr Sci 2001;188:129–36.

[192] Tiraferri A, Elimelech M. Direct quantification of negatively charged functional groups on membrane surfaces. J Membr Sci 2012;389:499–508.

[193] Chen D, Werber JR, Zhao X, Elimelech M. A facile method to quantify the carboxyl group areal density in the active layer of polyamide thin-film composite membranes. J Membr Sci 2017;534:100–8.

[194] Stolov M, Freger V. Membrane charge weakly affects ion transport in reverse osmosis. Environ Sci Technol Lett 2020;7:440–5.

[195] Liu M, Wu D, Yu S, Gao C. Influence of the polyacyl chloride structure on the reverse osmosis performance, surface properties and chlorine stability of the thin-film composite polyamide membranes. J Membr Sci 2009;326:205–14.

[196] Lee J, Doherty CM, Hill AJ, Kentish SE. Water vapor sorption and free volume in the aromatic polyamide layer of reverse osmosis membranes. J Membr Sci 2013;425:217–26.

[197] Gu Q, Li K, Li S, Cui R, Liu L, Yu C, et al. *In silico* study of structure and water dynamics in CNT/polyamide nanocomposite reverse osmosis membranes. Phys Chem Chem Phys 2020;22:22324–31.

[198] Zhang XJ, Cahill DG, Coronell O, Marinas BJ. Absorption of water in the active layer of reverse osmosis membranes. J Membr Sci 2009;331:143–51.

[199] Meares P. The mechanism of water transport in membranes. Philos Trans R Soc Lond B 1977;278:113.

[200] Sharma VK, Singh PS, Gautam S, Mitra S, Mukhopadhyay R. Diffusion of water in nanoporous NF polyamide membrane. Chem Phys Lett 2009;478:56–60.

[201] Chan EP, Frieberg BR, Ito K, Tarver J, Tyagi M, Zhang W, et al. Insights into the water transport mechanism in polymeric membranes from neutron scattering. Macromolecules 2020;53:1443–50.

[202] Foglia F, Livingston A, Cabral J, Team JC. Neutron reflectivity, water dynamics and performance of polyamide nanofilms for water desalination. APS 2018;2018:L60–130.

[203] Raja SN, Basu S, Limaye AM, Anderson TJ, Hyland CM, Lin L, et al. Strain-dependent dynamic mechanical properties of Kevlar to failure: structural correlations and comparisons to other polymers. Mater Today Commun 2015;2:e33–7.

[204] Chung JY, Lee JH, Beers KL, Stafford CM. Stiffness, strength, and ductility of nanoscale thin films and membranes: a combined wrinkling-cracking methodology. Nano Lett 2011;11:3361–5. doi:10.1021/nl201764b.

[205] Freger V. Selectivity and polarization in water channel membranes: lessons learned from polymeric membranes and CNTs. Faraday Discuss 2018;209:371–88.

[206] Patel SK, Ritt CL, Deshmukh A, Wang Z, Qin M, Epsztein R, et al. The relative insignificance of advanced materials in enhancing the energy efficiency of desalination technologies. Energy Environ Sci 2020. doi:10.1039/d0ee00341g.

[207] Yaroshchuk AE. Non-steric mechanisms of nanofiltration: superposition of Donnan and dielectric exclusion. Sep Purif Technol 2001;22-3:143–58.
[208] Nir O, Bishop NF, Lahav O, Freger V. Modeling pH variation in reverse osmosis. Water Res 2015;87:328–35.
[209] Fridman-Bishop N, Tankus KA, Freger V. Permeation mechanism and interplay between ions in nanofiltration. J Membr Sci 2018;548. doi:10.1016/j.memsci.2017.11.050.
[210] Bowen WR, Welfoot JS. Modeling the performance of membrane nanofiltration - critical assessment and model development. Chem Eng Sci 2002;57:1121–37.
[211] Szymczyk A, Labbez C, Fievet P, Vidonne A, Foissy A, Pagetti J. Contribution of convection, diffusion and migration to electrolyte transport through nanofiltration membranes. Adv Colloid Interface Sci 2003;103:77–94.
[212] Yaroshchuk AE. Dielectric exclusion of ions from membranes. Adv Colloid Interface Sci 2000;85:193–230. doi:10.1016/S0001-8686(99)00021-4.
[213] Szymczyk A, Fatin-Rouge N, Fievet P, Ramseyer C, Vidonne A. Identification of dielectric effects in nanofiltration of metallic salts. J Membr Sci 2007;287:102–10.
[214] Fridman-Bishop N, Nir O, Lahav O, Freger V. Predicting the rejection of major seawater ions by spiral-wound nanofiltration membranes. Environ Sci Technol 2015;49. doi:10.1021/acs.est.5b00336.
[215] Deen WM. Hindered transport of large molecules in liquid-filled pores. AIChE J 1987;33:1409–25. doi:10.1002/aic.690330902.
[216] Levchenko S, Freger V. Breaking the symmetry: mitigating scaling in tertiary treatment of waste effluents using a positively charged nanofiltration membrane. Environ Sci Technol Lett 2016;3. doi:10.1021/acs.estlett.6b00283.
[217] Kaganovich M, Zhang W, Freger V, Bernstein R. Effect of the membrane exclusion mechanism on phosphate scaling during synthetic effluent desalination. Water Res 2019;161:381–91.
[218] Freger V, Bason S. Characterization of ion transport in thin films using electrochemical impedance spectroscopy. I. Principles and theory. J Membr Sci 2007;302:1–9.
[219] Shaffer DL, Feldman KE, Chan EP, Stafford GR, Stafford CM. Characterizing salt permeability in polyamide desalination membranes using electrochemical impedance spectroscopy. J Membr Sci 2019;583:248–57.
[220] Fridman-Bishop N, Freger V. When salt-rejecting polymers meet protons: an electrochemical impedance spectroscopy investigation. Langmuir 2017;33. doi:10.1021/acs.langmuir.6b04263.
[221] Shultz S, Bass M, Semiat R, Freger V. Modification of polyamide membranes by hydrophobic molecular plugs for improved boron rejection. J Membr Sci 2018;546. doi:10.1016/j.memsci.2017.10.003.
[222] Li Y, Wang S, Song X, Zhou Y, Shen H, Cao X, et al. High boron removal polyamide reverse osmosis membranes by swelling induced embedding of a sulfonyl molecular plug. J Membr Sci 2020;597:117716. doi:10.1016/j.memsci.2019.117716.
[223] Tang CY, Reinhard M, Leckie JO. Effects of hypochlorous acid exposure on the rejection of salt, polyethylene glycols, boron and arsenic (V) by nanofiltration and reverse osmosis membranes. Water Res 2012;46:5217–23.
[224] Chen J, Zhang M, Li F, Qian L, Lin H, Yang L, et al. Membrane fouling in a membrane bioreactor: high filtration resistance of gel layer and its underlying mechanism. Water Res 2016;102:82–9. doi:10.1016/j.watres.2016.06.028.
[225] Li Y, Kłosowski MM, McGilvery CM, Porter AE, Livingston AG, Cabral JT. Probing flow activity in polyamide layer of reverse osmosis membrane with nanoparticle tracers. J Membr Sci 2017;534:9–17. doi:10.1016/j.memsci.2017.04.005.
[226] Lin L, Weigand TM, Farthing MW, Jutaporn P, Miller CT, Coronell O. Relative importance of geometrical and intrinsic water transport properties of active layers in the water permeability of polyamide thin-film composite membranes. J Membr Sci 2018;564:935–44. doi:10.1016/j.memsci.2018.08.002.
[227] Ramon GZ, Wong MCY, Hoek EMV. Transport through composite membrane, part 1: is there an optimal support membrane? J Membr Sci 2012;415-416:298–305. doi:10.1016/j.memsci.2012.05.013.
[228] Bruna M, Chapman SJ, Ramon GZ. The effective flux through a thin-film composite membrane. EPL (Europhys Lett) 2015;110:40005. doi:10.1209/0295-5075/110/40005.
[229] Wijmans JG, Hao P. Influence of the porous support on diffusion in composite membranes. J Membr Sci 2015;494:78–85. doi:10.1016/j.memsci.2015.07.047.
[230] Zhu L, Jia W, Kattula M, Ponnuru K, Furlani EP, Lin H. Effect of porous supports on the permeance of thin film composite membranes: part I. Track-etched polycarbonate supports. J Membr Sci 2016;514:684–95. doi:10.1016/j.memsci.2015.11.043.
[231] Mondal S, Griffiths IM, Ramon GZ. Forefronts in structure-performance models of separation membranes. J Membr Sci 2019;588:117166. doi:10.1016/j.memsci.2019.06.006.
[232] Ramon GZ, Hoek EMV. Transport through composite membranes, part 2: impacts of roughness on permeability and fouling. J Membr Sci 2013. doi:10.1016/j.memsci.2012.08.004.
[233] Anderson JE, Pusch W. The membrane/water partition coefficients of ions: electrostatic calculations of dielectric heterogeneity. Berichte Der Bunsenges Für Phys Chem. 1976;80:846–9.
[234] Strathmann H, Michaels AS. Polymer-water interaction and its relation to reverse osmosis desalination efficiency. Desalination 1977;21:195–202.
[235] Bruening ML, Dotzauer DM, Jain P, Ouyang L, Baker GL. Creation of functional membranes using polyelectrolyte multilayers and polymer brushes. Langmuir 2008;24:7663–73.
[236] Freger VS, Shemer H, Sagiv AA, Semiat RR. Boron removal using membranes. Amsterdam: Elsevier, Inc; 2015. doi:101016/B978-0-444-63454-200008-3.
[237] Hilal N, Kim GJ, Somerfield C. Boron removal from saline water: a comprehensive review. Desalination 2011;273:23–35.
[238] Bellona C, Drewes JE, Xu P, Amy G. Factors affecting the rejection of organic solutes during NF/RO treatment - a literature review. Water Res 2004;38:2795–809.
[239] Xu P, Drewes JE, Bellona C, Amy G, Kim T, Adam M, et al. Rejection of emerging organic micropollutants in nanofiltration-reverse osmosis membrane applications. Water Environ Res 2005;77:40–8.
[240] Schäfer AI, Akanyeti I, Semião AJC. Micropollutant sorption to membrane polymers: a review of mechanisms for estrogens. Adv Colloid Interface Sci 2011;164:100–17.
[241] Faigon M, Hefer D. Boron rejection in SWRO at high pH conditions versus cascade design. Desalination 2008;223:10–16.
[242] Teychene B, Collet G, Gallard H, Croue JP. A comparative study of boron and arsenic (III) rejection from brackish water by reverse osmosis membranes. Desalination 2013;310:109–14.
[243] Xu P, Capito M, Cath TY. Selective removal of arsenic and monovalent ions from brackish water reverse osmosis concentrate. J Hazard Mater 2013;260:885–91.
[244] Verliefde ARD, Cornelissen ER, Heijman SGJ, Hoek EMV, Amy GL, der BBV, et al. Influence of solute– membrane affinity on rejection of uncharged organic solutes by nanofiltration membranes. Environ Sci Technol 2009;43:2400–6.
[245] Drazevic E, Bason S, Kosutic K, Freger V. Enhanced partitioning and transport of phenolic micropollutants within polyamide composite membranes. Environ Sci Technol 2012;46:3377–83. doi:10.1021/es204188j.
[246] Nghiem LD, Schafer AI, Elimelech M. Pharmaceutical retention mechanisms by nanofiltration membranes. Environ Sci Technol 2005;39:7698–705.
[247] Ben-David A, Bernstein R, Oren Y, Belfer S, Dosoretz C, Freger V. Facile surface modification of nanofiltration membranes to target the removal of endocrine-disrupting compounds. J Membr Sci 2010;357:152–9.
[248] Bernstein R, Belfer S, Freger V. Improving performance of spiral wound RO elements by *in situ* concentration polarization-enhanced radical graft polymerization. J Membr Sci 2012:405–6. doi:10.1016/j.memsci.2012.02.046.
[249] Guo H, Deng Y, Tao Z, Yao Z, Wang J, Lin C, et al. Does hydrophilic polydopamine coating enhance membrane rejection of hydrophobic endocrine-disrupting compounds? Environ Sci Technol Lett 2016;3:332–8.
[250] Guo H, Deng Y, Yao Z, Yang Z, Wang J, Lin C, et al. A highly selective surface coating for enhanced membrane rejection of endocrine disrupting compounds: mechanistic insights and implications. Water Res 2017;121:197–203.
[251] Park J, Yoon HW, Paul DR, Freeman BD. Gas transport properties of PDMS–coated reverse osmosis membranes. J Membr Sci 2020;604:118009.
[252] Shultz S, Freger V. *In situ* modification of membrane elements for improved boron rejection in RO desalination. Desalination 2018;431:66–72. doi:10.1016/j.desal.2017.08.021.
[253] Wang S, Zhou Y, Gao C. Novel high boron removal polyamide reverse osmosis membranes. J Membr Sci 2018;554:244–52. doi:10.1016/j.memsci.2018.03.014.
[254] Jeong BH, Hoek EMV, Yan Y, Subramani A, Huang X, Hurwitz G, et al. Interfacial polymerization of thin film nanocomposites: a new concept for reverse osmosis membranes. J Membr Sci 2007;294:1–7. doi:10.1016/j.memsci.2007.02.025.
[255] Wu B, Wang S, Wang J, Song X, Zhou Y, Gao C. Facile fabrication of high-performance thin film nanocomposite desalination membranes imbedded with alkyl group-capped silica nanoparticles. Polymers 2020;12:1415 (Basel). doi:10.3390/polym12061415.
[256] Ng ZC, Chong CY, Lau WJ, Karaman M, Ismail AF. Boron removal and antifouling properties of thin-film nanocomposite membrane incorporating PECVD-modified titanate nanotubes. J Chem Technol Biotechnol 2019;94:2772–82. doi:10.1002/jctb.6044.
[257] Liu L, Xie X, Qi S, Li R, Zhang X, Song X, et al. Thin film nanocomposite reverse osmosis membrane incorporated with UiO-66 nanoparticles for enhanced boron removal. J Membr Sci 2019;580:101–9. doi:10.1016/j.memsci.2019.02.072.
[258] Zhao DL, Japip S, Zhang Y, Weber M, Maletzko C, Chung TS. Emerging thin-film nanocomposite (TFN) membranes for reverse osmosis: a review. Water Res 2020;173:115557. doi:10.1016/j.watres.2020.115557.
[259] Song W, Joshi H, Chowdhury R, Najem JS, Shen Y, Lang C, et al. Artificial water channels enable fast and selective water permeation through water-wire networks. Nat Nanotechnol 2019;15:73–9. doi:10.1038/s41565-019-0586-8.
[260] Song W, Tu YM, Oh H, Samineni L, Kumar M. Hierarchical optimization of high-performance biomimetic and bioinspired membranes. Langmuir 2019;35:589–607. doi:10.1021/acs.langmuir.8b03655.
[261] Song W, Kumar M. Artificial water channels: toward and beyond desalination. Curr Opin Chem Eng 2019;25:9–17. doi:10.1016/j.coche.2019.06.007.
[262] Werber JR, Elimelech M. Permselectivity limits of biomimetic desalination membranes. Sci Adv 2018;4:eaar8266. doi:10.1126/sciadv.aar8266.
[263] Nunes SP, Culfaz-emecen PZ, Ramon GZ, Visser T, Henk G, Jin W, et al. Thinking the future of membranes : perspectives for advanced and new membrane materials and manufacturing processes. J Membr Sci 2020;598:117761. doi:10.1016/j.memsci.2019.117761.
[264] Hu M, Mi B. Enabling graphene oxide nanosheets as water separation membranes. Environ Sci Technol 2013;47:3715–23. doi:10.1021/es400571g.

[265] Boretti A, Al-Zubaidy S, Vaclavikova M, Al-Abri M, Castelletto S, Mikhalovsky S. Outlook for graphene-based desalination membranes. npj Clean Water 2018;1:1–11. doi:10.1038/s41545-018-0004-z.
[266] Chong J, Wang B, Li K. Graphene oxide membranes in fluid separations. Curr Opin Chem Eng 2016;12:98–105. doi:10.1016/j.coche.2016.04.002.
[267] Zhang X, Zhou W, Xu F, Wei M, Wang Y. Resistance of water transport in carbon nanotube membranes. Nanoscale 2018;10:13242–9. doi:10.1039/C8NR03116A.
[268] Mattia D, Calabrò F. Explaining high flow rate of water in carbon nanotubes via solid-liquid molecular interactions. Microfluid Nanofluidics 2012;13:125–30. doi:10.1007/s10404-012-0949-z.
[269] Falk K, Sedlmeier F, Joly L, Netz RR, Bocquet L. Molecular origin of fast water transport in carbon nanotube membranes: superlubricity versus curvature dependent friction. Nano Lett 2010;10:4067–73. doi:10.1021/nl1021046.
[270] Chong JY, Wang B, Mattevi C, Li K. Dynamic microstructure of graphene oxide membranes and the permeation flux. J Membr Sci 2018;549:385–92. doi:10.1016/j.memsci.2017.12.018.
[271] Park HB, Kamcev J, Robeson LM, Elimelech M, Freeman BD. Maximizing the right stuff: the trade-off between membrane permeability and selectivity. Science 2017;356(80):1138–48. doi:10.1126/science.aab0530.
[272] Epsztein R, DuChanois RM, Ritt CL, Noy A, Elimelech M. Towards single-species selectivity of membranes with subnanometre pores. Nat Nanotechnol 2020;15:426–36. doi:10.1038/s41565-020-0713-6.
[273] Vlassiouk I, Smirnov S, Siwyt Z. Ionic selectivity of single nanochannels. Nano Lett 2008;8:1978–85. doi:10.1021/nl800949k.
[274] Kim WK, Kanduč M, Roa R, Dzubiella J. Tuning the permeability of dense membranes by shaping nanoscale potentials. Phys Rev Lett 2019;122:1–6. doi:10.1103/PhysRevLett.122.108001.
[275] Bocquet L. Nanofluidics coming of age. Nat Mater 2020;19:254–6. doi:10.1038/s41563-020-0625-8.
[276] Hoek EM, Bhattacharjee S, Elimelech M. Effect of membrane surface roughness on colloid– membrane DLVO interactions. Langmuir 2003;19:4836–47.
[277] Jiang Z, Karan S, Livingston AG. Membrane fouling: does microscale roughness matter? Ind Eng Chem Res 2020;59:5424–31. doi:10.1021/acs.iecr.9b04798.